STOCHASTIC MODELING OF EXPANSION AND SHRINKAGE PHENOMENA IN STARCH BASED MELTS DURING EXTRUSION

by

ANUBHA GARG

B.Tech, Indian Institute of Technology, Kharagpur, 2011

A THESIS

submitted in partial fulfillment of the requirements for the degree

MASTER OF SCIENCE

Department of Grain Science and Industry
College of Agriculture

KANSAS STATE UNIVERSITY
Manhattan, Kansas

2013

Approved by:

Major Professor
Dr. Sajid Alavi

Copyright

Abstract

Extrusion is a popular technology for production of expanded products. However, variability in multiple input parameters can lead to significant variations in the end product which becomes a concern for process control and efficiency in industries. This study was focused on understanding the uncertainty in input parameters during extrusion and their impact on variability in output.

A mechanistic model was developed for bubble growth dynamics in starch based melts at microscopic and macroscopic levels using heat, mass and momentum transfer equations. This model was used for uncertainty simulations using the Monte-Carlo method by integrating it with a stochastic interface for input of randomly generated process data based on experimentally obtained distributions and output of simulated distributions of end-product properties such as expansion ratio (ER).

A pilot-scale twin screw extruder was used for processing of corn-based expanded products, which was used as a model system for experimental validation of the mathematical model. A 4x2 factorial design was used with different in-barrel moisture contents (19, 23, 28 and 33% dry basis) and extruder screw speeds (250 and 350 rpm) to measure process data (such as moisture injection rate and T_{die}) and product characteristics (such as ER). Average experimental ER ranged from 2.33-10.88 and simulated ER ranged from 1.16-12.86, where both had similar trends with respect to in-barrel moisture (MC) and die temperature (T_{die} = 108.8-145.4˚C) although conditions for optimum expansion differed possibly due to non-correspondence of material properties. Experimental coefficient of variation (CV) for MC (0.6-1.6%) and T_{die} (0.29-0.91%) and an assumed CV of 2% for a material constant (k_f) that controls the consistency index of starch-based melt were used for simulations. The stochastic model was used to carry out

sensitivity analysis for CV of ER with respect to CV of MC, T_{die} and k_f. Variability in ER was impacted the most by variation in $T_{die,}$ followed by MC with k_f having relatively lower impact on it. Since there are fundamental flaws in modeling approach as reflected by the thermodynamically infeasible parameter dynamics, the results from these mechanistic or stochastic simulations cannot be used as a basis for scientific analysis.

Table of Contents

List of Figures

List of Tables

Acknowledgements

I am thankful to my major professor, Dr. Sajid Alavi for giving me this opportunity and imparting his knowledge to me over the course of my MS program.

I want to thank my committee member: Dr. Hulya Dogan, Dr. Jon Faubion and Dr. Girish Ganjyal for their consistent guidance and help. A sincere vote of thanks to Eric Maichel, Max Remund and other employees in the extrusion facility at BIVAP for helping me with my experimental runs.

A special mention to Bunge, Atchison, Kansas for their corn meal donation which was helpful for performing experiments for this study. I would also like to thank Wenger Manufacturing Inc. for helping with the technical problems in the extruder.

I am thankful for the consistent help and support received from my lab mates, summer interns in extrusion lab and support staff in department of grain science.

I am extremely grateful for having a wonderful and supporting family and amazing friends.

Chapter 1 - Introduction

1.1 Extrusion cooking

Extrusion cooking is extensively used in the production of varieties of foods and especially expanded products such as breakfast cereal, snack food, pet food etc. Due to its versatility in production of different food categories, it has become increasing popular as a processing technique for product development. Extrusion cooking holds a great potential in overcoming the production challenges while using difficult biomaterials (in terms of processing) such as fiber and also maintaining the organoleptic properties of the food product.

An extruder can be seen as a compilation of different units such as pump, heat exchanger, bio-reactor for transporting, mixing, heating, shearing and transformation of raw materials that are input in the extruder using a feeder (Chiruvella et al., 1996). The high temperature and high pressure conditions inside the extruder result in several phase transitions such as starch gelatinization, melting and defragmentation. Also other changes such as protein denaturation, complex formation between amylose and lipids take place (Lai and Kokini, 1991). The extruded products are referred to as cooked (in case of snacks, ready-to-eat foods) or partially cooked (in case of pasta, 3G snacks etc.) based on the level of starch gelatinization taking place inside the cooking zone of the barrel. Gelatinization is generally characterized as swelling of starch granules, loss of crystalline structure and thereby loss of birefringence. There are several tests for determining the level of gelatinization of starch in a processed food, most common being iodine complexing method (Gomez and Aguilera, 1983).

The single screw extruder has a simpler geometry as compared to a twin screw extruder. However, the twin screw extruders because of their complex geometry are more versatile in their

usage as compared to a single screw extruder. The screw profile of a twin screw extruder can generally be divided into different zones such as feeding, melting, mixing, reaction development, devolatilization, pumping and shaping (Vergnes et al., 2006) similar to a single screw extruder but the shear generated is more in case of a twin screw extruder. Also, a twin screw extruder exhibits self-cleaning characteristic if the screws have intermeshing profile.

In the competitive sector of food products, it is of immense importance to keep innovating and providing new options which are healthier, tastier and value for money. The physical as well as the sensory properties of a food commodity largely depend on the processing conditions as well as the ingredients used for production. Extrusion is a complex process and it is essential to understand the dynamics of the process at the fundamental level and to investigate the optimum conditions of operation. Generally trial and error method is used for trying out different processing conditions to find the best one. This leads to unnecessary consumption of time and resources. However, much help can be obtained in this regard from mathematical tools such as modeling (or computer simulation) of extrusion process.

1.2 Mathematical modeling

A mathematical model is a theoretical tool for simulating the outcome of a process without actually performing the experiment (Vergnes, 2006 et al.). It is also an effective tool for obtaining the fundamental understanding of the process. A model for extrusion can take up independent variables as input such as feed rate, screw speed, water and steam input in the extruder and pre-conditioner etc. and utilize fundamental mechanistic equations of heat and mass transfer taking place during the process to predict/estimate the physical characteristics of the extruded product such as expansion ratio, open cell fraction etc.

1.2.1 Modeling of extrusion cooking

The concept of modeling extrusion process dates back to the beginning of 1940s when it was used for analyzing flow of polymers. It is easier to understand the behavior of plastics and other polymers because of the homogeneity in their structure and well characterized physical and rheological properties (Tadmor and Klein, 1978; Tadmor and Gogos, 1979; Karwe and Jaluria, 1990; Gopalakrishna et al., 1992). These polymers have predictable behavior upon carrying out mechanical interactions and thermo-mechanical processing.

However, the modeling of food extrusion is a relatively new concept. It is more complicated than modeling polymers because food materials have heterogeneous properties and their phase transitions are not well defined. The changes upon interactions between bio-molecules and extruder are very complex (Chiruvella et al., 1996). Hence, there is a need for further studies on modeling of extrusion cooking for food products to develop a better understanding of the process and production of healthier and better food items.

Although it is a good practice to obtain the optimum processing conditions with the help of modeling and simulation without actually performing experiments but it should be noted that modeling method is based on several approximations and assumptions. During modeling, for simplicity, the extrusion conditions are generally assumed to be static and isothermal, raw material is assumed to be homogeneous which might result in deviations from the actual result (Vergnes et al., 2006). Hence, it is very important to validate the modeling results experimentally.

1.2.2 Modeling approaches

Vergnes et al. (2006) defined different approaches to modeling based on chemical engineering and continuum mechanics. The first approach based on chemical engineering

estimated the approximate flow conditions by considering the screw profile as a series of chemical reactor units having forward and backward flow. Similarly, energy balance and kinetic equations were calculated. This approach did not lead to accurate results because of oversimplification of the extrusion process while modeling. Also, the parameters such as number and type of chemical reactors had to be adjusted for every process before predicting the flow conditions. Therefore, this approach is not very useful for scaling up either and is not used commonly.

The second approach based on continuum mechanics utilized mass, momentum and energy balance equations to estimate the flow conditions and considered local geometry, kinematics and boundary conditions. This type of approach was based on real conditions, was more flexible and accurate and could be used as a better predictive model. Therefore, generally models are based on continuum mechanics approach. Alavi et al. (2003) modeled the process dynamics of starch based products during supercritical fluid extrusion (with CO_2 as the nucleating agent) using heat, mass and momentum transfer equations which helped in understanding the mechanism of bubble growth and shrinkage process taking place during expansion as the melt exits the extruder die.

Cheng et al. (2010) used Buckingham's pi dimensional analysis method to model the extrudate expansion upon changing the extruder operation parameters. In Buckingham pi dimensional analysis method, the key process parameters are identified and dimensionless groups are formed using them. Then these dimensionless groups are related by a physical equation which can be rearranged to find the dependence of a specific property on other process parameters. Cheng et al. (2010) found a satisfactory correlation between the extrudate expansion

values obtained from the model and the actual experiments. Fan et al. (1994) also used dimensional analysis method and used Runge-Kutta method to solve the equations.

Response surface modeling is another common method to obtain the optimum parameters for processing. A 3- dimensional response surface is created by inserting the experimental values in the model and the tip of the surface represents the maximum or the minimum of the parameter that is being modeled and is usually the optimum point for operation. The response surface is mostly analyzed graphically. Vainionpaa, J. (1993) studied the potential of canonical analysis in solving the response surface equations instead of solving them graphically. In canonical analysis method, a canonical equation is derived from the fitted second-order polynomial curves and the center- point for the equation is determined, also called stationary point, which has the possibility of being the optimum point of operation for the process. Vainionpaa, J. (1993) computed the second order polynomials using statgraphics statistical package (STSC, inc., Rockville, MD) and mathematica 386 program was used for matrix calculations. This method is advantageous, especially in case of large number of independent variables, when it is difficult to represent the data graphically and solve it.

Li (1999) suggested that though 3-D CFD is a powerful modeling tool but considering the complex geometry of an extruder, it can get very complicated and time consuming to use it for finding optimum processing parameters. Instead of 3-D CFD, a 1-D model was used in their study to simulate various characteristics like temperature and pressure profile, shaft power input, fill factor and residence time distribution for different processing parameters.

1.2.3 Modeling parameters

Modeling approaches mentioned in the previous section were selected based on the modeling parameters to be studied. Several studies are available on the modeling of flow

dynamics, rheology of the melt during the extrusion process, residence time distribution, expansion of the extrudate upon exit etc.

Ficarella et al. (2004) modeled the flow dynamics of the material inside the extruder considering the cereal compound to be an isotropic, time-independent, inelastic and incompressible and shear-thinning non-Newtonian liquid. Since, the fluid considered was non-Newtonian, the shear viscosity used in the model was taken from a study by Harper (1978) and it was dependent on the local shear rate, moisture contents, temperature and pressure. The equation was given as follows:

$$\eta = K\gamma^{m-1} \exp\left(\frac{K_n}{T}\right) \exp(-K_m C) \quad (1\text{-}1)$$

In equation (1-1) K, T and C represent the consistency, temperature and moisture content of the fluid. K_n and K_m are constants and m represents the power law index.

Cindio et al. (2001) modeled the rheology of two immiscible non Newtonian fluids for the production of filled snacks by co-extrusion cooking. The behavior of dough was considered as viscoelastic and the filler was represented using a nonlinear viscous model. The rheological properties and the mathematical model were used to design the experiments in a more scientific way. Engmann et al. (2006) also modeled the rheology and microstructural changes in chocolate upon extrusion considering rheological behavior of the chocolate same as those of perfect plastic.

Residence time distribution is another useful factor to be modeled since it is a cumulative result of processing parameters as well as flow and mixing conditions (Kumar et al., 2007). It can be easily measured using tracers and monitoring their concentration in the extrudates at different time intervals. Kumar et al. (2007) modeled the residence time distribution using conceptual flow modeling based on plug flow with finite number of continuously stirred tank reactors which have a dead volume fractions lined in series.

Fan et al. (1994) modeled the expansion of extrudates by studying the growth and shrinkage dynamics of bubbles inside the extrudate. Bubble growth modeling was also carried out by Alavi et al. (2003) in case of supercritical fluid extrusion. In their study, CO_2 was used as the nucleating agent and was majorly responsible for expansion as the melt came out of the die. The impact of extrudate moisture on expansion in their study was observed only when the extrudate was dried in the oven.

1.2.4 Modeling softwares

There are several softwares commercially available for finite element modeling method. In these softwares, the user has the flexibility of defining the geometry, initial and boundary conditions, processing conditions, material properties etc. and the results can be simulated along with visual graphics in some softwares for better understanding. Engmann et al. (2006) used finite element software known as Forge2 (Transvalor S.A., Sophia Antipolis, France) for solving two dimensional elastic-plastic and rigid-plastic deformation problems. Ficarella et al. (2004) used the POLYFLOW software (Fluent Inc., Lebanon, NH) for performing numerical simulations. A simulation code was written using the already existing theoretical models describing the fluid-dynamics and rheology of the fluid. The model was based on finite element velocity-pressure formulation (Forting, 1987). COMSOL Multiphysics is another efficient tool for development of mathematical models based on fundamental equations of heat, mass and momentum transfer to describe the process.

However, in some studies, the mathematical model was developed based on mechanistic equation by writing a code in a particular programing language. Kumar et al. (2007) used MATLAB 7.0 (The Mathworks Inc., Natick, MA, USA) for programming, SAS 8.2 (SAS Institute Inc., Cary, NC, USA) for statistical analysis & development of predictive quadratic

models and Neuroshell 2 (Release 4.0, Ward Systems Groups, Inc., Frederick, MD, USA) to build the neural network model for prediction of parameters. Alavi et al. (2003) used visual basic with EXCEL ™ as interface for modeling process dynamics during expansion of extrudates and product characteristics such as bubble radius, expansion ratio and open cell fraction etc.

In the current study, Visual Basic was used for developing the mechanistic model as well as the stochastic interface for the deterministic model. MS Excel was used as the user interface i.e. for obtaining input from the user and for displaying the output.

1.3 Objectives

The main objective of this study was to develop a mathematical model in context of extrusion processing of directly expanded snacks using a combined approach of deterministic and stochastic model. This model used a distribution of the input parameters in the practically operational range and utilized each set of input parameters to provide the output parameters as a distribution as well. The stochastic component, thus, helped in predicting the impact of variability associated with input parameters and thereby assessing the significance level of different input parameters which can help in making cost efficient changes during the production. The specific objectives of the study were to:

1) Develop a mechanistic model for bubble growth and shrinkage process taking place in starch-based melts during extrusion processing;

2) Characterize and quantify variability in process parameters (moisture injection in the extruder, die temperature, etc.) using data acquisition system and pilot-scale processing trials;

3) Develop a stochastic input interface for the mechanistic model developed in Objective 1, and utilize the data collected in Objective 2 as input parameters to the model.

4) Develop a stochastic output interface for the model, and utilize the integrated stochastic/ mechanistic model to generate outputs related to product characteristics such as expansion ratio;

5) Compare the results obtained from the integrated stochastic/ mechanistic model with experimental results for product characteristics obtained from pilot-scale extrusion trials; and

6) Utilize the model to identify the relative contributions of different processing factors to the end-product variability.

References

Alavi, S.H., Rizvi, S.S.H., & Harriott, P. (2003). Process dynamics of starch-based microcellular foams produced by supercritical fluid extrusion. I: Model development. Food Research International, 36, 309-319.

Cheng, H. & Friis, A. (2010). Modeling extrudates expansion in a twin screw food extrusion cooking process through dimensional analysis methodology. Food and Bioproducts Processing, 88, 188-194.

Chin-Hsien Li (1999). Modelling extrusion cooking. Institution of Chemical Engineers, 77C, 0960-3085.

Chiruvella, R.V., Jaluria, Y., & Karwe, M.V. (1996). Numerical simulation of the extrusion process for food materials in a single screw extruder. Journal of Food Engineering, 30, 449-467.

Cindio, B., Gabriele, D., Pollini, C.M., Peressini, D., & Sensidoni, A. (2001). Filled snack production by co-extrusion cooking:1. Rheological modeling of the process. Journal of Food Engineering, 52, 67-74.

Engmann, J., & Mackley, M.R. (2006). Semi-solid processing of chocolate and cocoa butter, modeling rheology and microstructure changes during extrusion. Food and Bioproducts Processing, 84, 102-108.

Fan, J., Mitchell, J.R., & Blanshard, J.M.V. (1994). A computer simulation of the dynamics of bubble growth and shrinkage during extrudate expansion. Journal of Food Engineering, 23, 337-356.

Ficarella, A., Milanese, M., & Laforgia, D. (2004). Numerical study of the extrusion process in cereals production: Part I. Fluid-dynamic analysis of the extrusion system. Journal of Food Engineering, 73, 103-111.

Forting, M. (1987). Old and new finite elements for incompressible flows. International Journal of Numerical Methods in Fluids I, 347-364.

Gomez, M.H., & Aguilera, J.M. (1983). Changes in the starch fraction during extrusion-cooking of corn. Journal of Food Science, 48, 378-381.

Gopalakrishnan, S., Jaluria, Y., & Karwe, M.V. (1992). Heat and mass transfer in a single-screw extruder for non-Newtonian materials. International Journal of Heat Mass Transfer, 35(1), 221-237.

Harper, J.M. (1978). Extrusion processing of food. Food Technologies, 32(7), 67.

Karwe, M.V., & Jaluria, Y. (1990). Numerical simulation of fluid flow and heat transfer in a single screw extruder for non-Newtonian fluids. Numerical Heat Transfer, Part A. 17, 167-190.

Kumar, A., Ganjyal, G., Jones, D. & Hanna, M. (2007). Modeling resistance time distribution in a twin-screw extruder as a series of ideal steady-state flow reactors. Journal of Food Engineering, 84, 441-448.

Lai, L.S., & Kokini, J.L. (1991). Physicochemical changes and rheological properties of starch during extrusion (A review).Biotechnology Progress, 7, 251-266.

Tadmor, Z., & Gogos, C. (1979). Principles of polymer processing. John Wiley, New York.

Tadmor, Z, & Klein, I. (1978). Engineering principles of plasticating extrusion. Robert E. Krieger publishing company, Malabar, FL.

Vainionpaa, J. (1993). Numerical solution of response surface equations for extrusion cooked cereals. Journal of Food Engineering, 24, 181-196.

Vergnes, B., & Berzin, F. (2006). Modeling of reactive systems in twin screw extrusion: challenges and applications. Comptes Rendus Chimie, 9, 1409-1418.

Chapter 2 - Stochastic modeling of expansion and shrinkage phenomena during extrusion for starch-based melts: I Development of the mechanistic model and stochastic interface

Abstract

Expanded products such as snacks, breakfast cereal etc. are commonly manufactured using extrusion processing. The current study focuses on the fundamental understanding of expansion and shrinkage dynamics taking place during extrusion of starch-based foams at both microscopic level (an individual bubble) as well as macroscopic level (extrudate). The code for the model was written in Microsoft Visual Basic with Excel as interface for input and output of parameters. Mechanistic equations involving heat, mass transfer were incorporated at both microscopic and macroscopic level for simulating the growth dynamics. The mechanistic model developed was later integrated with the stochastic interface for understanding the variability in output parameter such as expansion ratio as a result of variability in input parameters such as in-barrel moisture content, die temperature etc. The results for mechanistic and stochastic model were validated with literature and experimental values and are provided in chapter-3 of this thesis.

2.1 Introduction

Extrusion cooking is extensively used for production of different categories of food including expanded foods such as breakfast cereals, pet food, snacks; semi-cooked foods such as pasta etc. Due to possibility of high temperature and shear conditions inside the extruder, several changes like starch gelatinization, protein denaturation, amylose lipid complex formation etc. take place (Lai and Kokini, 1991). The heat and moisture treatment resulting in gelatinization of

starch leads to cooking of the melt and the product coming out of the die is usually expanded for high starch compositions (Moraru & Kokini, 2003).

Such expanded extruded products have a characteristic cellular architecture depending on the raw material formulation and processing conditions. This microstructure in-turn impacts the sensory attributes of the product. Several studies have been conducted on investigation of the texture and microstructure relationship. Agbisit et al. (2007) studied the microstructure of extrudates formed by corn starch using X-ray microtomography (XMT) which was later related to textural properties of the extrudate (determined using texture analyzer). Cheng et al. (2007) studied the sensory attributes of the extrudates associated with the acoustics upon crushing. They also studied the microstructure of these extrudates formed by corn starch and whey protein isolates in different percentages. Karkle et al. (2012) examined the relationship of mechanical properties with the microstructure of the extrudates formed by using corn flour and apple pomace in different percentages in the formulation. Hence, it is established that the microstructure formed during extrusion is extremely important in terms of the textural and sensory properties of the product. Thereby, a greater understanding of expansion and shrinkage process taking place during extrusion which results in the formation of microstructure is extremely beneficial. This can be done by using imaging techniques or theoretical tools such as a mathematical model.

Mathematical modeling of a processing technique is useful not only for estimating the optimized operating conditions but also for obtaining the fundamental understanding of the entire process. Vergnes et al. (2006) suggested two different approaches towards modeling a process. The first approach was based on chemical engineering and it estimated the flow conditions by considering the screw profile as a series of chemical reactor units having forward and backward flow. Since for predicting the flow conditions, the number and type of reactors had to be adjusted

for every process, this approach was not useful in generalizing the model. The second approach was based on continuum mechanics and utilized mass, momentum and energy balance equations to estimate the flow conditions and considered local geometry, kinematics and boundary conditions for development of the model. This approach is more generalized and hence most models are based on this approach. Chin Hsien Li (1999) used a 1-D computational fluid dynamics (CFD) method for simulating characteristics like temperature and pressure profile, shaft power input; fill factor and residence time distribution etc. for different processing parameters. They suggested that 3-D CFD is a powerful tool for modeling a process like extrusion; however, due to computational complexity and consumption of time, they used 1-D CFD in their study.

In the current study, initially a mathematical model was developed to understand the process of expansion and shrinkage at the most fundamental level with the help of mechanistic equations. Later, this deterministic model was integrated with a stochastic interface. Hence, the objectives of this part of the study were to (1) develop microscopic level of the model for heat and mass transfer taking place in an individual bubble resulting in its growth and shrinkage. (2) develop macroscopic level of the model for the extrudate using heat and mass transfer equations for the bulk. (3) integrate the microscopic and macroscopic models and develop an algorithm for the simultaneous simulation of both the levels (4) introduce the concept of stochastic modeling and develop the algorithm for stochastic interface and integrating it with the mechanistic model developed in objectives (1)-(3).

2.2 Mathematical modeling of expansion and shrinkage phenomena during extrusion

The expansion and shrinkage phenomena observed in an extrudate can be investigated at two levels. The microscopic level accounts for the growth and collapse taking place in an individual bubble. The bubble is assumed to be spherical and is divided into finite number of spherical shells (N) as shown in figure 2-1a. R and L represent the bubble radius and domain radius respectively for an individual bubble. The width of the bubble (W) is given by (L-R).

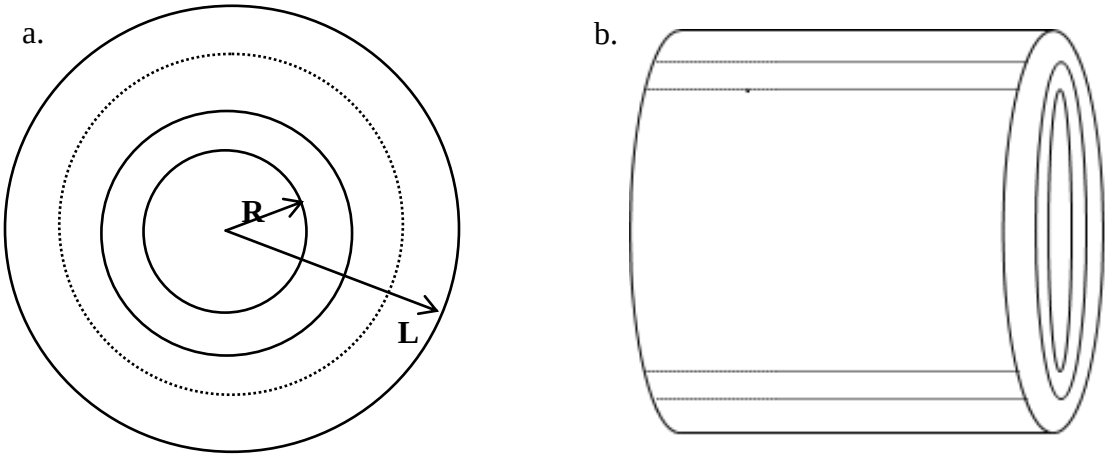

Figure 2-1 a. Spherical shells for the microscopic model. b. Cylindrical shells for the macroscopic model.

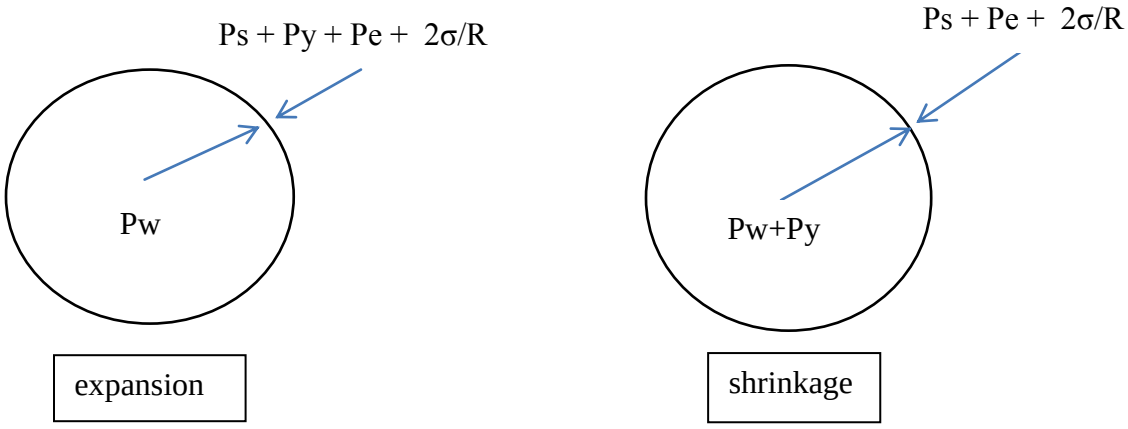

Figure 2-2 Pressure components acting on the individual bubble wall during expansion and shrinkage

The different pressure components (yield stress, elastic stress, surface tension, vapor pressure and atmospheric pressure) act on the wall of an individual bubble and are responsible for the resulting expansion and shrinkage depending on the direction of the resultant pressure (figure 2-2). The macroscopic level accounts for overall expansion that is observed in the extrudate coming out of the die. In the mechanistic model, the extrudate is assumed to have a cylindrical geometry and is also divided into finite number of cylindrical shells (N_b) (figure 2-1b). Heat and mass transfer taking place within the cylindrical shells of the extrudate as well as with the atmosphere is studied at this level.

2.2 Bubble growth dynamics during extrusion

For production of expanded products using an extruder, the flour is fed into the extruder. A more expanded product is obtained usually at a lower moisture content range. This is because lower moisture content increases the viscosity resulting in greater shear in the extruder which leads to higher expansion. At very low moisture content, the starch degrades due to extremely high shear and as a result not enough expansion is obtained (Chinnaswamy et al., 1988). Cheng et al. (2010) modeled the expansion of the extrudate at different operating parameters using Buckingham's pi dimensional analysis method. In this method, dimensionless groups were formed using the key process parameters. Later, these dimensionless groups were related by physical equation which could be rearranged to find the dependence of a specific property on other process parameters. Cheng et al. (2010) found satisfactory correlation between the expansion values obtained by simulation and experimentally.

Due to high pressure present inside the heads of the extruder, the steam formed from the in-barrel moisture content remains in the superheated state inside the extruder and the die. As the material flows out of the die, due to sudden change of pressure, the instability is created and the

steam formation inside these bubbles lead to expansion (Wang et al., 2005). The moisture migrates from the matrix to the inside of the bubble which represents the microscopic level of the model. At the macroscopic level moisture is lost due to evaporation as the product cools down as well as due to convective transfer with the atmosphere. However, in the current study, temperature loss due to evaporation is not considered and for heat transfer at the macroscopic level, conduction between cylindrical shells and convective transfer between outermost layer and the atmosphere is considered.

There are several studies on bubble growth dynamics during extrusion processing conducted both at the microscopic and macroscopic levels. One of the most comprehensive literatures include the puffing process studied by Alavi et al. (2003) for super critical fluid extrusion using carbon-di-oxide as the nucleating agent. They used the popcorn puffing model of Schwartzberg et al. (1995) for modeling the bubble growth at the microscopic level and coupled it with macroscopic level model for extrudate formation. The flow inside the die, moisture loss and temperature reduction in the extrudate were controlled by mass and momentum equations from the literature. The consistency index which affected the viscosity was temperature and moisture dependent and played a significant role in expansion and shrinkage of the extrudate. The expansion of the extruded product largely depended on the magnitude and direction of the difference in pressure (ΔP) acting on the bubble wall. The dynamics of difference in pressure components is explained further in chapter 3.

It is interesting to note that during the puffing process, the bubbles expand and if the cell wall becomes extremely thin, it might lead to coalescence of cell walls or might lead to bursting of bubbles which increases the open cell fraction. Once the cell is open, it loses its ability to expand (Schwartzberg et al., 1995). The entire process of expansion and shrinkage stops as the

temperature drops down below its glass transition temperature range (Tg +30) (Fan et al., 1994; Wang et al., 2005). The glass transition temperature of the extrudate changes depending on the moisture content of the extrudate. The equation used for calculating glass transition temperature (T_g) is given by equation 2-1 (Wang et al., 2005)

$$T_g = \frac{M_1 \Delta C_{p1} T_{g1} + M_2 \Delta C_{p2} T_{g2}}{M_1 \Delta C_{p1} + M_2 \Delta C_{p2}} \quad (2\text{-}1)$$

where

M_1 : mass fractions of moisture, M_2 : mass fraction of solid starch.

ΔC_{p1}: change in specific heat of water at T_{g1}, ΔC_{p2}: change in specific heat of starch at T_{g2}

T_{g1}: Glass transition temperature of water, T_{g2}: glass transition temperature of solid starch

Hence, the expansion at the microscopic level steers the expansion observed in the extrudate at the macroscopic level as the product comes out of the die. The supercritical fluid extrusion carried out by Alavi et al. (2003) was done at high moisture and low temperature because in their study, carbon-di-oxide was majorly responsible for expansion. The water had a dual role of plasticizer and expansion driver but its role in expansion during extrusion was relatively not significant due to low temperature used during extrusion (mostly below 100°C).

In another study conducted by Wang et al. (2005) bubble growth dynamics was investigated during steam extrusion. They also used the heat, mass and momentum transfer equation to study the puffing process during extrusion with steam playing the major role in expansion. In their study, the microscopic and macroscopic models were coupled by reducing the loss in moisture content from the cylindrical macroscopic shells proportionately from the spherical microscopic shells. Lach, L. (2006) developed the model for steam expansion based on the supercritical fluid extrusion model by Alavi et al. (2003) using fluent. In their study, the input

parameters and certain equations such as equation for viscosity was changed to adapt for higher temperature process. The material properties they used were not tested for a material but the values used were to obtain results close to realistic values of bubble growth etc. Fan et al. (2012) developed a bubble growth model for expansion in cornstarch using computation fluid dynamics method. They used William-Landel-Ferry equation (WLF formula) for capturing the impact of moisture as well as temperature (in the range where extrusion is carried out for expanded snacks) on starch viscosity.

These models available in the literature have been validated using experimental results and most of them have shown quantitative coherence with the real time data. However, the input parameters for these models were point estimates. In real-time production, there is a variability associated with these input parameters which could be inherent in the raw material used for extrusion or could be due to minor fluctuations in the processing conditions. Hence, there is a need for a new approach to study the expansion and shrinkage mechanism which can consider more realistic values of input parameters and give a more accurate picture of the output from the simulated results. In the current study, this issue was addressed using an integrated stochastic and mechanistic approach.

2.3 Stochastic modeling

In practical situations, the input parameters such as moisture content, screw speed, temperature and other properties of the material such as viscosity, diffusivity etc., are not fixed values, instead they generally have a probability distribution with a standard deviation. The variability in processing conditions and raw material leads to the variability in product characteristics. These inherent complexities and variability in food materials and their processing conditions can be accounted for using a stochastic model.

Sin et al. (2009) used the example of cultivation of *S. coelicolor* for antibiotic production to explain the uncertainties associated with the biological process and methods to perform the uncertainty and sensitivity analysis on them for development of more reliable models. They classified the uncertainty associated with biological processes into three categories: 1) Stochastic uncertainty which is due to randomness associated with a process such as failure of aeration system in the middle etc. 2) Subjective (or input) uncertainty which addresses the issue of variability associated with the input parameters and their impact on the end results. For example, this could also be a result of variability carried forward from parameter estimation and errors associated with them. Dolan and Mishra (2013) suggested methods for parameter estimation for food processes which could address the issue of uncertainty to an extent. 3) Structural uncertainty which comes from the assumptions made while defining the physical system/process for the purpose of removing complications while model development.

In the past, little work has been done on the uncertainty and sensitivity analysis of the processes involving food materials. Feyissa et al. (2012) studied the uncertainty involved during a contact baking process. They used the Monte Carlo technique for this analysis and the uncertainty in the output was represented using the mean, the 10^{th} and the 90^{th} percentile of the output distribution. For carrying out the sensitivity analysis, they utilized both the scatter plot as well as the standardized regression coefficient method. Taking lead from this model, the stochastic model for extrusion processing was developed in the current study.

In this study, the variation in the input parameters such as moisture injection in the extruder, temperature etc. was recorded using a data acquisition system (DAQ) during the actual extrusion run. This distribution curve was plotted and each value of the distribution was fed into the mechanistic model which resulted in output for the product characteristics in the form of a

distribution as well. Hence a Monte-Carlo simulation approach was utilized to study the sensitivity of different input parameters and their impact on the product characteristics.

2.4 Assumptions of the model

The current model was built based on the fundamental equations of mass and momentum transfer, also considering temperature, moisture dependence of several parameters such as diffusivity, viscosity etc. However, as mentioned before, modeling of biopolymers is a complex process due to their unpredictable behavior. Hence there were several assumptions and approximations included in the model. 1) The material flowing inside the extruder was considered to be homogenous. 2) The die swell is also responsible for expansion which is mostly significant at lower temperatures (Fan et al., 1994). However, in the current model die swell was neglected and the expansion considered was only caused by vapor generated. 3) The complex chemical reactions and degradation of components during the severe extrusion conditions was not considered as it was difficult to account for such reactions for modeling purposes. 4) All the bubbles were considered uniform and spherical for simplification 5) The material was considered incompressible fluid following the power law (k, n) 6) Temperature drop due to evaporation was not considered. 7) The axial expansion of the extrudate was not taken into account and sectional expansion ratio was calculated by taking (2/3) power of the volumetric expansion ratio predicted by the model.

2.5 Microscopic model

The microscopic model comprised of studying the nucleation and bubble growth dynamics during expansion process. During extrusion, as the material flows inside the die, the pressure of the fluid matrix decreases towards the exit. Nucleation of bubbles takes place when

the saturation vapor pressure of the steam is more than the pressure of the melt. The bubble starts growing as a result of pressure difference between saturation vapor pressure and opposing pressure components which include elastic stress, yield stress, tensile stress and fluid pressure. The fluid pressure is the pressure of the melt when the material is inside the die and fluid pressure is equal to atmospheric pressure as the extrudate comes out of the die. As the bubble grows due to conversion of moisture to steam, more moisture moves inside the microscopic shells from the matrix. For finite element modeling method incorporated in this study, each bubble was divided into N number of shells.

2.5.1 Bubble expansion and shrinkage

Bubble expansion and shrinkage takes place depending on the pressure components acting on the wall of an individual bubble. These pressure components include vapor pressure, elastic stress, tensile stress, yield stress and fluid/atmospheric pressure (figure 2-2). If the resultant pressure acts in the outward direction, it leads to expansion of the bubble. However, if the resultant pressure acts in the inward direction, the bubble collapses. Yield stress is defined as the threshold stress that is required for the material to start flowing (Genovese and Rao, 2006). Such materials retain elasticity at low stress values and become viscous when high stress is applied. Genovese and Rao (2006) suggested several methods of measuring yield stress such as stress-relaxation, creep compliance, torsion, uniaxial compression, vane mixer method etc. Schwartzberg et al (1995) measured surface tension (σ) by measuring the rise of starch in a sealed glass tube at popping temperature for popcorn (180-200˚C).

Hence equations for pressure components dependent on moisture content of the bubble, temperature, bubble radius, domain radius etc. were taken from Schwartzberg et al (1995). The rate of bubble growth as a function of pressure difference, material properties such as viscosity,

heat and mass transfer at the microscopic level (equation 2-2 to equation 2-43) were also taken from Schwartzberg et al. (1995) and are given as follows.

Vapor pressure (P_w) of the moisture content in the bubble is given by equation 2-2

$$P_w = P_{wsat} \times a_w \tag{2-2}$$

where P_{wsat} is the saturation vapor pressure (equation 2-3) at a given temperature (T) of the bubble and a_w is the water activity (equation 2-4) at the surface of the cell. X_{wc} in equation 2-4 represents the moisture content at the inner most layer of the bubble. B and C are the coefficients in equation for a_w and F is a term in the equation for a_w given by equations 2-5 to 2-7.

$$P_{wsat} = 1002.2 \times \exp\left[9.43699 - \frac{3867.44}{T - 43.37}\right] KPa \tag{2-3}$$

$$a_w = BX_{wc} + \frac{CX_{wc}}{F + X_{wc}} \tag{2-4}$$

where

$$B = -0.5362 - 0.001394 \times T + \frac{2.0474 \times (468.9 - T)}{477.42 - T} \tag{2-5}$$

$$C = 0.2479 + 0.001216 \times T \tag{2-6}$$

$$F = 0.002004 + 0.3165 \times 10^{-5} T \tag{2-7}$$

Elastic stress (P_e) acting on the cell wall is given by equation 2-8. R_o in equation 2-8 represents the initial bubble radius at the beginning of expansion and R represents the radius of bubble at any time instant. L is the domain radius of the bubble (figure 2-1a)

$$Pe = E\left[\frac{5}{2} - \frac{2R_o}{R} - \frac{1}{2}\left(\frac{R_o}{R}\right)^4\right]\left(\frac{L^3 - R^3}{L^3 + 2R^3}\right) \tag{2-8}$$

where

$$E = E_b \ (X_{wa} \geq 0.15) \tag{2-9}$$

$$E = E_b \exp\left[\beta_f (0.15 - X_{wa})\right] \ (X_{wa} < 0.15) \tag{2-10}$$

$$E_b = E_r \times \exp[\frac{300 - T}{26}] \quad (2\text{-}11)$$

E_r = 10KPa, β_f = 17 (2-12)

Equation 2-11 is an estimated function. In Schwartzberg et al. (1995), the coefficient of the T in the exponential function was taken as 0.1 but in equation 2-11, the coefficient of T was 0.038. Also the constant in the exponential function was 45.32 in the equation provided by Schwartzberg et al. (1995). This estimated function was taken from Alavi et al. (2003). Functions are estimated to make the model stable and obtain values that are closer to the realistic range of different parameters.

Yield stress (ΔP_y) acting on the cell wall is given by equation 2-13 where τ_o is the flow yield stress.

$$\Delta P_y = \pm 3.464 \tau_o \, [1/3 + ln(L/R) \,] \quad (2\text{-}13)$$

where $$\tau_o = \tau_r \; (X_w \geq 0.15) \quad (2\text{-}14)$$

$$\tau_o = \tau_r \exp\left[\beta_f (0.14 - X_w)\right] (X_w < 0.15), \tau_r = 0.1 \; kPa \quad (2\text{-}15)$$

The value for constants taken is assumed. Schwartzberg et al. (1995) used value of τ_r as 2 kPa. Different values for τ_r were tried for simulation in the current study and the value for constant taken was to provide better stability to the model and for prediction of realistic dynamics of different parameters involved during expansion and shrinkage process. Using all these equations for different pressure components given above, the pressure difference and rate of change of bubble radius ($\dot{R}$) is given by equation 2-16. P_s is the fluid pressure which is the pressure of the melt inside the extruder (P_f) and atmospheric pressure as the melt exits the die.

$$P_w - Ps - Pe - \Delta P_y - \frac{2\sigma}{R} = \frac{4\left(2\sqrt{3}\right)^{n-1}}{n} (\frac{\dot{R}}{R})[\xi + k_c - k_s \left(\frac{R}{L}\right)^{3n} + I \quad (2\text{-}16)$$

where $$\xi = \int_R^L \frac{\partial K}{\partial r} (\frac{R}{r})^{3n} dr \quad (2\text{-}17)$$

ξ in equation 2-17 accounts for the variability in consistency index across the different shells of the spherical bubble depending on the radius of the shell. The term I in equation 2-16 represents the inertia of the bubble and it is given by equation 2-19.

Consistency index (k) determines the viscosity of the melt and it is given by equation 2-18. The k_f in the equation is a constant which was useful in varying the value of consistency index in the stochastic model later. This equation is taken from Parker et al. (1989) who derived it for maize starch. The subscripts c and s in equation 2-16 represent the consistency index of the innermost core and outermost surface of the individual bubble respectively.

$$k = k_f \, 0.000672 \times \exp[\frac{4960}{T} - \frac{12.1 \times X_w}{1 + X_w}] \quad (2\text{-}18)$$

The letter I in equation 2-16 denotes the inertial terms which was neglected as its value is small for both small and large values of radius of bubble (Schwartzberg et al., 1995). Its mathematical equation is estimated as given by equation 2-19

$$I = \rho_s \dot{R}^2 \left[\frac{3}{2} - \frac{2R}{L} + \frac{1}{2}\left(\frac{R}{L}\right)^2\right] + \rho_s R\ddot{R}\left[1 - \frac{R}{L}\right] \quad (2\text{-}19)$$

In equation 2-19, ρ_s is the density of the material in microscopic shells, $\dot{R}$ represents the rate of change of bubble radius, and $\ddot{R}$ represents the second derivate of radius with respect to time ($\frac{d^2R}{dt^2}$).

The radius of the outermost layer of the bubble, also referred to as domain radius (L), is mathematically expressed as given in equation 2-20 where R is the radius of the bubble at any given point of time (Schwartzberg et al., 1995).

$$L = [R^3 + \frac{3}{4\pi}\sum_{i=1}^{N}\frac{\Delta M}{\rho_i}]^{1/3} \quad (2\text{-}20)$$

ΔM in equation 2-20 represents the mass in each spherical shell of the bubble and depends on the total number of layers in the bubble. Hence, when number of shells in the microscopic model is changed, it affects ΔM which in turn affects the domain radius as well as the mass transfer taking place in the bubble. ρ_i is the density of the dry matter in i^{th} shell of the individual bubble.

2.5.2. Mass transfer in the bubble

The bubble was divided into N shells and the moisture content of different layers in the bubble is represented in figure 2-3. During bubble expansion, part of the moisture present in the spherical shells of the bubble is slowly converted into steam which is trapped inside the inner most layer of the bubble. As more and more moisture is converted to steam from the inner-most layer of the bubble, diffusion takes place in the spherical shells of the bubble in the inward direction. At the same time, moisture is being lost from the cylindrical macroscopic shells of the extrudate.

In the current study, the average loss in moisture from the extrudate was divided by N spherical shells of the bubble and this moisture content was subtracted from each spherical shell of the bubble along with loss in moisture due to diffusion within the spherical shells. This helped in integrating the microscopic and macroscopic levels of the mechanistic model. Moisture diffusion inside the spherical bubble shells, expressed in numerical form of partial differential equation is given by equation 2-21. ρ_i and r_i represent the density and radius of the ith spherical shell at any instant of time.

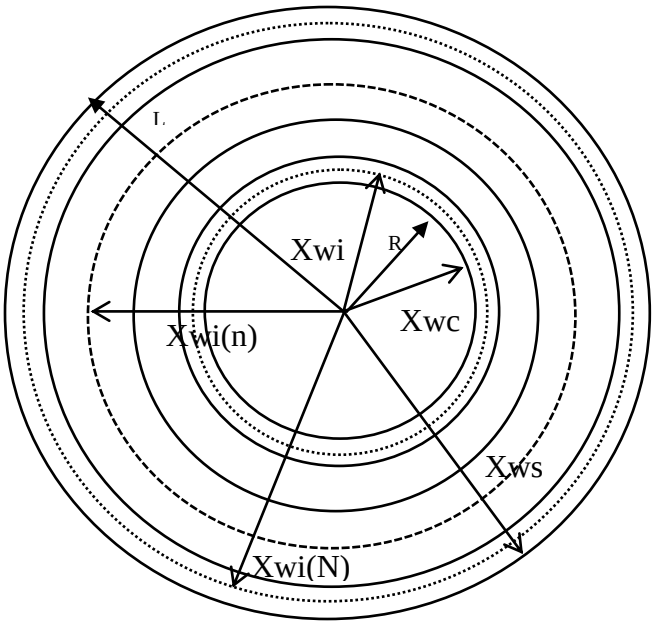

Figure 2-3 Moisture content in the spherical shells of the bubble (Microscopic level)

$$\Delta X_{wi} = \frac{\Delta t}{\Delta M}\left[\frac{D_{i+1/2}A_i(\rho_{i+1}X_{wi+1} - \rho_i X_{wi})}{(r_{i+1} - r_i)} - \frac{D_{i-1/2}A_{i-1}(\rho_i X_{wi} - \rho_{i-1}X_{wi-1})}{(r_i - r_{i-1})}\right] \quad (2\text{-}21)$$

where $$D_{i+1/2} = \frac{D_i + D_{i+1}}{2} \text{ and } D_{i-1/2} = (D_i + D_{i-1})/2 \quad (2\text{-}22)$$

Equation 2-22 helps in calculating the value of diffusivity by taking the average of diffusivity value of the adjacent spherical shells. The diffusivity of moisture in these spherical shells depends on the moisture and temperature of the shells at any instant of time. Diffusivity was calculated using equation 2-23, which was taken from Van der Lijn (1976) who found this relationship for maltose.

$$D = 1.35 \times 10^{-8} \exp\left[\frac{-21.61(548 - T)(1.194 + 3.68X_w)}{T(1 + 18.98X_w)}\right] m^2/s \quad (2\text{-}23)$$

$$A_i = (4\pi)\left[R^3 + \frac{3}{4\pi}\sum_{j=1}^{i}\frac{\Delta M_j}{\rho_j}\right]^{2/3} \quad (2\text{-}24)$$

Equation 2-24 calculates the exposed area for diffusion in i_{th} layer. The summation j =1 to i calculates the volume based on mass and density for all layers up to i_{th} layer.

Moisture diffusion in the outermost spherical shell of the bubble and the outer surface of the bubble is given by equation 2-25 and equation 2-26 respectively.

$$\Delta X_{wN} = \frac{\Delta t}{\Delta M}[A_{N-1}D_{N-1/2}\frac{(\rho_{N-1}X_{wN-1} - \rho_N X_{wN})}{(r_N - r_{N-1})} - A_s D_s \frac{(\rho_N X_{wN} - \rho_s X_{ws})}{(L - r_N)}] \quad (2\text{-}25)$$

$$\Delta X_{ws} = \frac{2D_s(\Delta t)(X_{wN} - X_{ws})}{(L - r_N)^2} \quad (2\text{-}26)$$

The mass of water vapor present in the bubble is given by equation 2-27. It can be seen that the mass of water vapor is dependent on radius of the bubble and the specific volume of water vapor which change during the bubble growth process. Hence, the change in mass of water vapor (ΔQ) in small time step Δt is given by equation 2-28 where υ is the specific volume of vapor in the pore and is given by equation 2-31.

$$Q = \frac{4\pi R^3}{3\upsilon} \quad (2\text{-}27)$$

$$\Delta Q = \frac{4\pi R^2}{3\upsilon}[3(\Delta R) - \alpha(\Delta T) + \zeta(\Delta X_c)] \quad (2\text{-}28)$$

Where

$$\alpha = \frac{GR}{P_w \upsilon}\left[1 - T\frac{d(lnP_{wsat})}{dT} - \frac{T}{a_w}\frac{\partial a_w}{\partial T}\right] \quad (2\text{-}29)$$

And

$$\zeta = \frac{GRT}{P_w \upsilon a_w}\frac{\partial a_w}{\partial X_{wc}} \quad (2\text{-}30)$$

$$\upsilon = \frac{GT}{P_w} - 0.01637\ \frac{m^2}{s} \quad (2\text{-}31)$$

$$G\ = 0.4561\ \frac{m^3 kPa}{kg.K} \quad (2\text{-}32)$$

For the core of the bubble, moisture diffusion (ΔX_{wc}) is given by equation 2-33

$$\kappa \Delta X_{wc} = \frac{D_c(X_{w1} - X_{wc})\Delta t}{(r_1 - R)(\Delta r)} + \alpha(\Delta T)\theta - 3(\Delta R)\theta \quad (2\text{-}33)$$

where

$$\kappa = 1 + \zeta\theta,\ \theta = \frac{1}{3\nu\rho_c}[\frac{1}{\Delta r} - \frac{2}{R}] \quad (2\text{-}34)$$

$$\Delta r = \frac{R}{3} \text{ when } (r_1\text{-}R) > R \text{ and } \Delta r = r_1 - R \text{ when } (r_1\text{-}R) < R \quad (2\text{-}35)$$

Moisture diffusion in the first or the inner most layer of the bubble is expressed differently than other layers and is given by equation 2-36.

$$\Delta X_{w1} = \frac{1}{\Delta M}\left[\frac{D_{3/2} A_1 (\rho_2 X_{w2} - \rho_1 X_{w1})\Delta t}{(r_2 - r_1)} - \Delta Q\right] \quad (2\text{-}36)$$

In the mathematical model, the change in moisture content was calculated over a small time step (Δt) and the values of moisture content in different layers and other parameters including pressure components, temperature and moisture in the cylindrical macroscopic shells were updated with each time step. In finite element modeling method, this time step Δt is small enough to prevent instability during computations in the finite element mathematical model. It is a function of bubble dimensions (radius of the N^{th} shell of bubble and its domain radius) as well as diffusivity of water on the surface of the bubble. If the time step for the process is assumed greater than that, it might not lead to the convergence of different partial differential equations to a particular solution due to their non-linearity (Lach, L., 2006). Hence the minimum time step for encountering instability was obtained by equation 2-37

$$\Delta t_m = \frac{(L - r_N)^2}{2D_s} \quad (2\text{-}37)$$

Based on the instabilities encountered in the model computation, the actual time step was taken as a fraction of Δt_m. 0.7 was chosen by hit and trial as it led to stability in the model for processing conditions with die temperature up to 410K

$$\Delta t = 0.7 \times \Delta t_m \quad (2\text{-}38)$$

Rearranging the pressure equation given by equation 2-16, the change in radius of the bubble (ΔR) is given by equation 2-39.

$$\Delta R = R(\Delta t)[\frac{P_w - P_s - \Delta P_y - \frac{2\sigma}{R}}{\frac{4(2\sqrt{3})^{n-1}}{n}[\xi + K_c - K_s(\frac{R}{L})^{3n}}]^{1/n} \quad (2\text{-}39)$$

2.5.3. Open cell fraction and open pore volume

During bubble growth, if the wall stress acting upon the bubbles exceeds the maximum failure stress of the bubbles, they burst open. After this cell rupture, the bubbles can coalesce with adjacent cells and the radius of individual cell can increase. However, in this model the coalescence phenomenon was not considered. Typically the bubbles that rupture lose their ability to expand further (Schwartzberg et al., 1995). Since all the bubbles don't have same radii in the beginning and the material properties are also not homogenous, not all the bubbles rupture at the same time. Hence the expansion of the bubbles and the extrudate continues. Schwartzberg et al. (1995) represented the distribution of change in number of open cells as a normal distribution with respect to Z where Z is a function of wall stress and failure stress (equation 2-40).

$$Z = \frac{(S_w - S_f)}{2S_f} \quad (2\text{-}40)$$

In equation 2-40, S_w is the wall stress and S_f is the failure stress. At the beginning of expansion S_w is given by equation 2-41 and towards the end of expansion when W (Cell wall thickness) <<R, S_w is given by equation (2-42).

$$Sw = \frac{\Delta P_w R^2}{W^2 + 2RW} \quad (2\text{-}41)$$

$$S_w = \Delta P_w R/2W \quad (2\text{-}42)$$

$$\Delta f_o = \frac{\Delta Z}{\sqrt{2\pi}} \exp[\frac{-Z^2}{\psi}] \quad (2\text{-}43)$$

The change in number of open cells (Δf_o) is given by equation 2-43 where ψ represents the spread of the distribution. In this model value of ψ was taken as 0.75. Fraction of pore volume that is open is given by equation 2-44. It represents the volume of open cells divided by

total volume (volume of open cells + volume of closed cells). The subscripts j and k in equation 2-44 represent the time steps j and k, with time step k being the next time step after j.

$$F_o = \frac{\sum_{j=1}^{k} (\Delta f)_{o\,j} \, {R_j}^3}{(1 - f_o)_k {R_k}^3 + \sum_{j=1}^{k} (\Delta f_o)_j \, {R_j}^3} \tag{2-44}$$

2.6 Macroscopic model

As mentioned earlier, the macroscopic model accounts for the heat and mass transfer that takes place at the extrudate level. Alavi et al. (2003) studied the flow of the melt inside the extruder die and the pressure gradient associated with it. In their study, the pressure drop inside the die was given by the fluid flow equation for laminar flows in non-Newtonian fluids (equation 2-45 to 2-49).

$$\frac{dP_f}{dx} = -\frac{4K}{[d(x)]^{3n+1}} \left(\frac{8m_f}{\pi\rho}\right)^n \left(\frac{3n+1}{n}\right)^n \tag{2-45}$$

where

$$d(x) = d_{en} - \left(\frac{d_{en} - d_{ex}}{L_d - L_{d1}}\right) x \qquad \text{for } x \geq L_d - L_{d1} \tag{2-46}$$

$$d(x) = d_{ex} \qquad \text{for } x \leq L_d - L_{d1} \tag{2-47}$$

In equation 2-46 and 2-47, d_{en} represents the diameter of the entrance of the die and d_{ex} represents the die diameter at the exit. L_d and L_{d1} are the die dimensions as specified in the figure 2-4. The mass flow rate of the melt in the extruder was given by m_f and the bulk density and consistency index of the melt was given by ρ and K respectively. The change in fluid pressure at each time step then was given by equation 2-48 (Alavi at al., 2003).

$$\Delta P_f = \left(\frac{dP_f}{dx}\right) V_x \Delta t \tag{2-48}$$

In the current model, these equations for studying pressure gradient of the melt inside the die were also incorporated. The computation of fluid pressure in each time step inside the die helped in understanding the melt pressure inside the die before the extrudate came out of the die.

It was also useful in computing the time for nucleation which occurs when the vapor pressure becomes greater than the melt pressure inside the die. As the extrudate exits the die, the fluid pressure becomes atmospheric pressure and its value becomes 101.325 KPa.

Since mass flow rate (m_f) was equal to product of density, area and velocity at a certain point, the velocity of the extrudate (assumed cylindrical) coming out of the die was given by equation 2-49 (Alavi et al., 2003).

$$V_x = \frac{m_f}{\rho}\frac{4}{\pi[d(x)]^2} \tag{2-49}$$

Where area of the die was calculated by $\pi d^2/4$

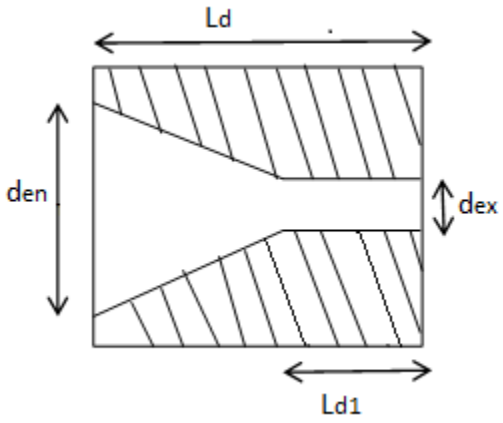

Figure 2-4 Schematic diagram of the die used in the extruder

2.6.1 Bulk diffusion of moisture

For mass transfer at the macroscopic level in the current study, the extrudate was discretized into finite number of concentric cylindrical shells (N_b). The moisture content and change in moisture content for these cylindrical shells was represented by letter C whereas for microscopic model, the moisture was represented by X_w. This was done to distinguish between the dynamics of mass transfer taking place at two different levels of bubble and the extrudate. The outermost layer of the extrudate is exposed to the atmosphere. The numerical form of the

moisture diffusion in different layers was taken from Geankoplis, (1993) and is given as equation 2-50. The mass transfer discretization step size (Δx_1) for the shells changes with change in expansion ratio during expansion and shrinkage. The effective diffusivity of the moisture content (D_{eff}) is calculated by considering porosity of the extrudate into account (equation 2-55).

$$\Delta C_j = \frac{1}{M_c}\left(\frac{2j+1}{2j}C_{j+1} - 2C_j + \frac{2j-1}{2j}C_{j-1}\right) \tag{2-50}$$

where

$$M_c = \frac{(\Delta x_1)^2}{D_{eff}\Delta t} \tag{2-51}$$

$$\Delta C_o = \frac{4}{M_c}(C_1 - C_o) \tag{2-52}$$

ΔC_o in equation 2-52 represents the change in moisture content of the innermost cylindrical shell of the extrudate. At the outer most layer of the extrudate, the moisture diffusion takes place from the inner layers as well as convection takes place at the outermost layer. Hence, the moisture content of the outermost layer at any point of time is given by equation 2-53.

$$C_{N_b} = \frac{N_b N_c}{\frac{2N_b-1}{2} + N_b N_c}C_a + \frac{(2N_b-1)/2}{\frac{2N_b-1}{2} + N_b N_c}C_{N_b-1} \tag{2-53}$$

where

$$N_c = \frac{k_{xc}\Delta x_1}{D_{eff}} \tag{2-54}$$

$$D_{eff} = \frac{1-\epsilon}{\zeta_r} \times D \tag{2-55}$$

ϵ and ζ_r in equation 2-55 represent the porosity and tortuosity of the extrudate respectively and D is the diffusivity given by equation 2-23. C_a is the ambient moisture content and in the code, it was assumed to be 0 to test for the maximum possible mass transfer condition. k_{xc} is the mass transfer coefficient of water in the starch matrix and its value was assumed to be 10^{-5}m/s in the code.

2.6.2 Heat transfer

The heat transfer which leads to lowering of temperature of extrudate was modeled similar to the bulk diffusion of moisture. In the actual process, the product cools down after it exits the die as a result of conductive and convective heat transfer along with the reduction in temperature due to evaporation as well as radiation. In this model, the heat loss due to evaporation and radiation was not taken into account. The heat transfer in the outermost layer was considered as a result of conduction in the inner layers with the adjacent layers and convection with the atmosphere at the outermost layer. . The numerical form of such type of heat transfer was taken from Geankoplis, (1993) and is given as equation 2-56.

$$\Delta T_j = \frac{1}{M_T}\left(\frac{2j+1}{2j}T_{j+1} - 2T_j + \frac{2j-1}{2j}T_{j-1}\right) \tag{2-56}$$

where

$$M_T = \frac{(\Delta x_2)^2}{\alpha_t \Delta t} \tag{2-57}$$

In equation 2-57, α_t is the thermal diffusivity in the starch matrix and Δx_2 is the discretization step for heat transfer. The change in temperature in the innermost layer is given by equation 2-58.

$$\Delta T_1 = \frac{4}{M_T}(T_2 - T_1) \tag{2-58}$$

The temperature in outermost layer which is a result of thermal conduction with the adjacent layer as well as convective transfer with the atmosphere is given as equation 2-59.

$$T_{N_b+1} = \frac{N_b N_T}{\frac{2N_b-1}{2} + N_b N_T} T_a + \frac{(2N_b-1)/2}{\frac{2N_b-1}{2} + N_b N_T} T_{N_b} \tag{2-59}$$

where

$$N_T = \frac{h\Delta x_2}{k_{eff}} \tag{2-60}$$

$$k_{eff} = k_{solid}[1 + \frac{3\epsilon(1 - \frac{k_{solid}}{k_{gas}})}{(1-\epsilon) + (2+\epsilon)\frac{k_{solid}}{k_{gas}}}] \quad (2\text{-}61)$$

h in equation 2-60 is the convective heat transfer coefficient and its value was taken as 10 W/m^2K in the current model and k_{eff} is the effective thermal conductivity of the extrudate. Its equation is given by 2-61 and it accounts for the porosity of the extrudate as well as the thermal conductivity in the solid and gas phase (Alavi et al., 2003)

2.6.3 Expansion ratio

There are several indices for defining expansion ratio of the extruded product. Most common are longitudinal expansion index (LEI) and sectional expansion index (SEI) which are used to describe axial and radial expansion respectively (Horvat & Schuchmann, 2012). LEI is given by the ratio of velocities of extrudate (equation 2-62) and the melt inside the die whereas SEI is given as the ratio of sectional area of the extrudate and the die (equation 2-63).

$$LEI = \frac{v_{extrudate}}{v_{melt}} \quad (2\text{-}62)$$

$$SEI = (\frac{d_{extrudate}}{d_{die}})^2 \quad (2\text{-}63)$$

In the current study, the expansion ratio of the extrudate was calculated from the equation 2-64. This equation was taken from Schwartzberg et al. (1995) and this expression in their study was used for calculation of expansion ratio for the popcorn upon puffing. The first term in the equation accounts for expansion due to closed cells, the second term accounts for the expansion due to open cells since Δf_o represents the change in number of open cells in a given time instant j. The constant 0.297 is the contribution of the kernel portion that does not get puffed. It should be noted that these constants were derived empirically for the popcorn. They might be different for the corn meal which was used during extrusion process which possibly contributed to the

shift of simulated values from the experimental values; however, different constant values will not change the trend of simulated values for expansion ratio. It should be noted that the expansion ratio calculated by equation 2-64 is a volumetric expansion ratio. However the experimental values for expansion ratio in chapter 3 are expressed as cross sectional expansion ratio which is typically obtained by dividing the cross sectional areas of the extrudate by cross sectional area of the die. To compare the simulated and experimental expansion ratio, the expansion ratio predicted by equation 2-64 was converted to cross sectional basis by finding the third root of the ER in equation 2-64 and then squaring it.

$$ER = 0.703[1 - f_o]_k(\frac{L_k}{L_o})^3 + 0.703\sum_{j=1}^{k}(\Delta f_o)_j(\frac{L_j}{L_o})^3 + 0.297 \quad (2\text{-}64)$$

2.7 Algorithm development of the integrated stochastic model

The algorithm for the integrated mechanistic and stochastic model for expansion and shrinkage phenomenon during extrusion process was developed in parts. As mentioned earlier in this chapter, the microscopic model was taken from the popcorn puffing model of Schwartzberg et al. (1995). The popcorn model did not account for the shrinkage in their model since popcorn puffing takes place at a really low moisture content of the range of 0.07-0.28 dry basis (db). During the puffing, there is a possibility that the melt cools down fast and the glass transition temperature is reached much earlier, even before the shrinkage can take place. Hence, they modeled only the expansion of an individual spherical bubble in the popcorn using heat and mass transfer equations.

Using this model for the popcorn system as the base, Alavi et al. (2003) modeled the expansion and shrinkage process taking place during supercritical fluid extrusion (SCFX) using CO_2 as the nucleating agent. They integrated the bubble growth model with the macroscopic

scale of expansion taking place in a cylindrical extrudate. They also modeled for the shrinkage phenomenon as well as further expansion taking place in the dryer.

In the current study, SCFX model was used as a base for development of mechanistic model for expansion and shrinkage process during extrusion for starch-based melts. The values of certain parameters such as cell density, initial bubble radius etc. were changed to account for the high temperature steam expansion because SCFX expansion takes place at relatively lower temperatures of less than 100ºC. In the SCFX model, the microscopic and macroscopic levels of the mechanistic model were integrated using temperature and moisture values. The temperature was considered same for the extrudate as well as for the bubble. Also, the loss in moisture taking place in the extrudate was also reduced proportionally depending on the current value of moisture content in the each microscopic layer. In the current model, same approach was utilized in integrating macroscopic and microscopic levels of the model. However, in the current steam based extrusion model, the average moisture loss in the extrudate layers was divided equally into the number of microscopic shells and it was later subtracted from each microscopic shell in addition to the moisture loss taking place in these spherical shells due to diffusion and vapor formation. This was done because the model assumes a microscopic system embedded in a macroscopic system. However, the dynamics of microscopic system embedded in different shells of the macroscopic system would be different. Hence, a proportionate reduction would not account for this factor. Thereby, subtraction of average moisture loss was carried out from the microscopic shells instead of the proportionate reduction.

Later a stochastic interface was developed to input the values of a selected parameter as a distribution in the mechanistic model and to display the output of the parameters involved and product characteristics as a distribution.

The typical simulation time for a mechanistic model was about 30-45 minutes depending on the computational ability of the computer. Due to time constraints, 15 mechanistic simulations were run at a time in the stochastic model to generate a distribution. The code terminated and provided the results when the temperature of the extrudate reached in the range of glass transition temperature, T_g + 30ºC (Fan et al., 1994). Also due to the computational constraints, the code stopped if the number of time steps was greater than 10^7. The algorithm for the stochastic model is given in figure 2-5 and the algorithm for the mechanistic model is given in figure 2-6.

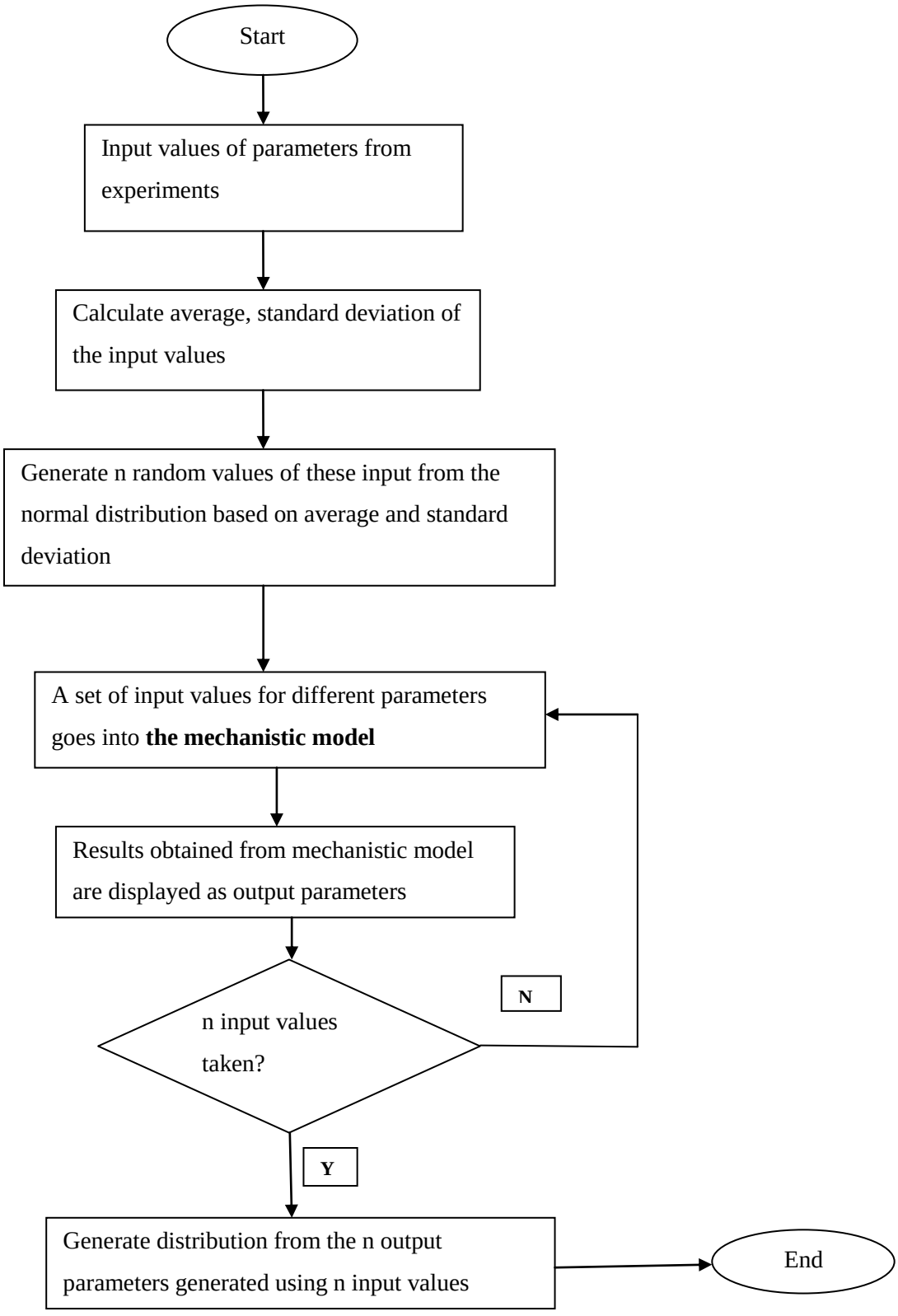

Figure 2-5: Algorithm for the stochastic model

Figure 2-6: Algorithm for the mechanistic model

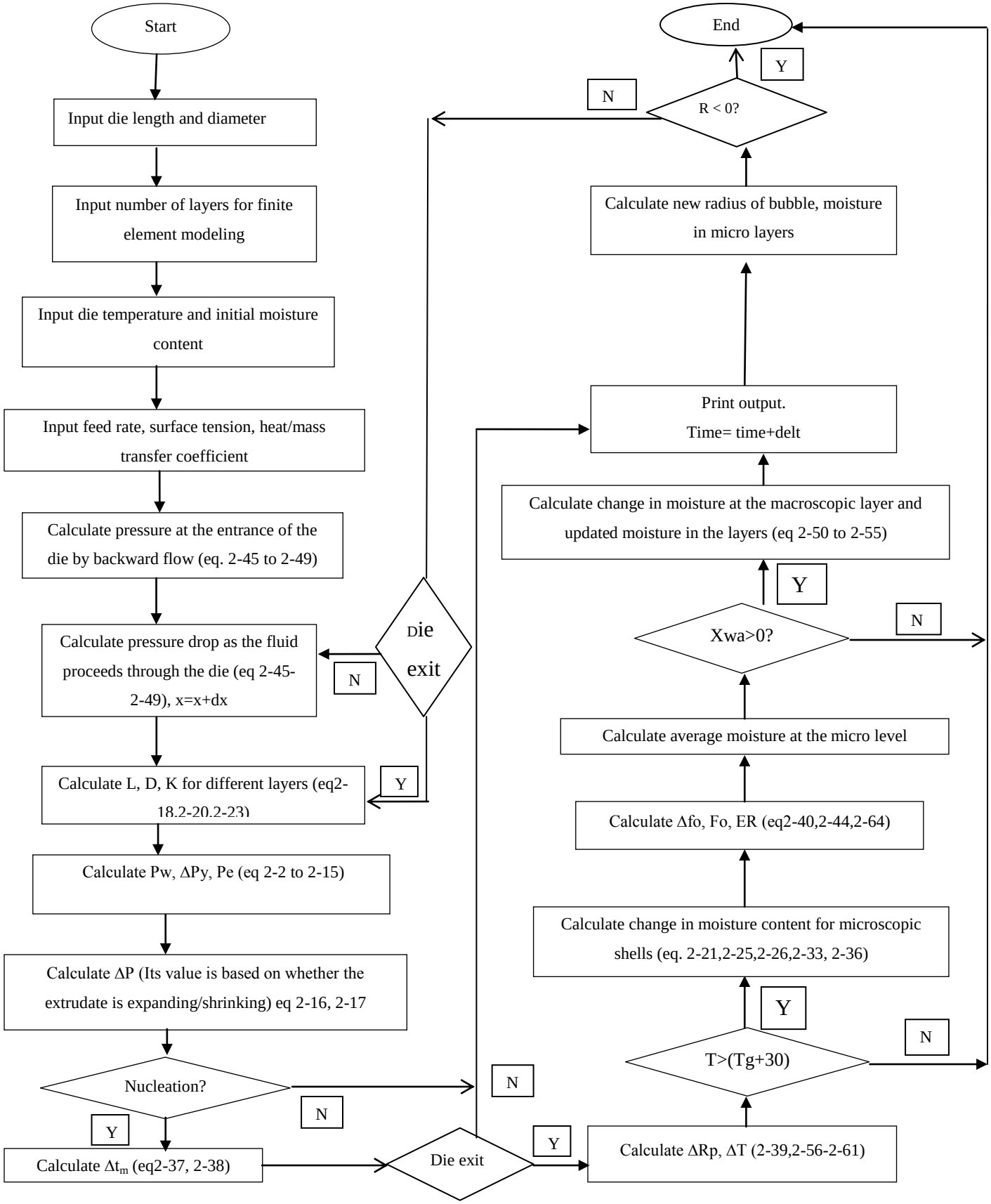

Table 2-1 List of symbols and their meaning

$\dot{R}$	Rate of change of bubble radius
$\ddot{R}$	Second derivative of bubble radius with respect to time
Δf_o	Change in f_o in time Δt
ΔM	Mass of dry matter per layer of the bubble
ΔP	Pressure difference driving expansion
ΔP_y	Yield stress
ΔQ	Change in Q in time step Δt
ΔR	Change in bubble radius in time step Δt
ΔT	Change in temperature
Δt	Minimum time step that can cause instability
Δt_m	Maximum stable time step
Δx_1	Discretization step size for mass transfer at macroscopic level
Δx_2	Discretization step size for heat transfer at macroscopic level
ΔZ	Change in Z in time step Δt
A_i	Interfacial area between layers i and i+1 in shell (m)
a_w	Water activity for given moisture content at bubble surface
B	Coefficient in the equation of a_w
C	Coefficient in the equation of a_w
C_a	Ambient moisture content
ΔC_{p1}	Change in specific heat of water at T_{g1}
ΔC_{p2}	Change in specific heat of starch at T_{g2}
C_j	Concentration of water in the j_{th} shell of the macroscopic shells (kg/kg dry matter)
C_p	Heat capacity of the material
d_{en}	Diameter of the entrance of the die
d_{ex}	Die diameter at the exit
D	Diffusivity of water in cell wall (m^2/s)
D_{eff}	Effective bulk diffusivity of water in porous extrudate (m^2/s)
D_i	Diffusivity of water in each layer of the starch matrix (m^2/s)
E	Elastic modulus of the material surrounding the bubble (Pa)
E_b	Coefficient in the equation of E
E_r	Constant in the equation of E_b
ER	Expansion Ratio
F	Term in the equation of a_w
F_o	Fraction of pore volume that is open
G	Constant in the equation of ζ
h	Convective heat transfer coefficient
I	Inertia term in equation for calculation of pressure difference at the cell wall
K	Consistency index in power law
k_{eff}	Effective thermal conductivity of the extrudate
K_f	Coefficient in equation of k
K_c	K at the inner surface of the pore
Ks	K at the outermost surface of the pore
k_{solid}	Thermal conductivity of the solid phase
k_{gas}	Thermal conductivity of the gas phase
k_{xc}	Mass transfer coefficient of water in starch matrix
L	Domain radius of the bubble

L_d	Die dimension specified in figure 2-4
L_{d1}	Die dimension specified in figure 2-4
M	Mass of dry solids in domain
M_c	Term given by equation 2-51
M_1	Mass fraction of moisture in extrudate
M_2	Mass fraction of solid starch in extrudate
M_T	Term given by equation 2-57
m_f	Flow rate of the melt
n	Flow behavior
N	Number of layers used in the microscopic model
Nb	Number of layers used in the macroscopic model
N_c	Term given by equation 2-54
N_T	Term given by equation 2-60
P_e	Elastic stress in pore wall
P_f	Pressure of the fluid inside the extruder
P_w	Pressure exerted by vapor in pore (Pa)
P_{wsat}	Saturation vapor pressure at temperature T (Pa)
Q	Mass of water vapor in pore
R	Bubble radius at any instant of time
r_i	Radial distance between center of domain and center of i^{th} layer in shell (m)
R_o	Initial value of R
S_f	Cell wall failure stress
S_w	Average tensile stress in wall of cell
T	Temperature
T_a	Ambient temperature
T_g	Glass-transition temperature
T_{g1}	Glass transition temperature of water
T_{g2}	Glass transition temperature of solid starch
T_o	Temperature at start of puffing
T_j	Temperature in the jth shell of the macroscopic shells
V_x	Velocity of the cylindrical element
W	Width of the bubble
X_{wa}	Average moisture content of the shells of the bubble
X_{wc}	Moisture content at the core of the bubble
X_{wi}	Average value of X in the i^{th} layer of shell
ΔX_{wi}	Average value of X in the i^{th} layer of bubble (microscopic model)
λ	Latent heat changes caused by evaporation of water from shell.
υ	Specific volume of the vapor in the pore of the bubble
ρ_s	Density of the material in the matrix (Kg/m3)
ρ_i	Density of dry matter in i^{th}shell of the individual bubble
τ_o	Flow yield stress (Pa)
τ_r	Coefficient in the equation of τ_o
Ψ	Spread factor in open cell fraction distribution
L	Radius of the domain
Ps	Pressure at outer surface of domain, i.e., at interfaces between domains (Pa)
ϰ	Term in equation of ΔX_{wc} given by equation 2-34

θ	Term given by equation 2-34
ε	Porosity of the extrudate
α	Coefficient in equation of ΔQ
α_t	Thermal diffusivity in the starch matrix
ζ	Coefficient in equation of ΔQ
ζ_r	Tortuosity of the extrudate
σ	Surface tension at pore-shell interface
ξ	Term in equation 2-16 calculated using equation 2-17
β_f	Coefficient in the equation of E

References

Agbisit, R., Alavi, S., Cheng, E., Herald, T & Trater, A. (2007). Relationships between microstructure and mechanical properties of cellular cornstarch extrudates. Journal of Texture Studies, 38, 199-219.

Alavi, S.H., Rizvi, S.S.H., & Harriott, P. (2003). Process dynamics of starch-based microcellular foams produced by supercritical fluid extrusion. I: Model development. Food Research International, 36, 309-319.

Cheng, E.M., Alavi, S., Pearson, T., & Agbisit, R. (2007). Mechanical-acoustic and sensory evaluations of cornstarch-whey protein isolate extrudates. Journal of Texture Studies, 38, 473-498.

Cheng, H. & Friis, A. (2010). Modeling extrudates expansion in a twin screw food extrusion cooking process through dimensional analysis methodology. Food and Bioproducts Processing, 88, 188-194.

Chinnaswamy, R. & Hanna, M.A. (1988). Optimum extrusion-cooking conditions for maximum expansion of corn starch. Journal of Food Science, 53(3), 834-836

Chin-Hsien Li (1999). Modelling extrusion cooking. Institution of Chemical Engineers, 77C, 0960-3085.

Dolan, K.D., & Mishra, D.K. (2013). Parameter estimation in food science. Annual Review in Food Science and Technology, 4, 401-422.

Fan, J., Mitchell, J.R., & Blanshard, J.M.V. (1994). A computer simulation of the dynamics of bubble growth and shrinkage during extrudate expansion. Journal of Food Engineering, 23, 337-356.

Fan, X., Meng, Z., Zhou, J., Xu, W., Xiang, H., & Yang, G. (2012). Investigation of bubble growth in extrusion expansion of cornstarch with CFD method. International Journal of Food Engineering, 8, 2(13).

Feyissa, A.H., Gernaey, K.V., & Nissen, J.A. (2012). Uncertainty and sensitivity analysis: Mathematical model of coupled heat and mass transfer for a contact baking process. Journal of Food Engineering, 109, 281-290.

Geankoplis, C.J. (1993). Transport processes and unit operations. (3rd ed.). Geankoplis, Englewood Cliffs, NJ: Prentice Hall.

Genovese, D.B., and Rao, M.A. (2006). Vane yield stress of starch dispersions. Journal of Food Science, 68(7), 2295-2301.

Horvat, M. and Schuchmann, H.P. (2012). Investigation of growth and shrinkage mechanisms in vapor-induced expansion of extrusion-cooked corn grits. Food Bioprocess Technology, 10.1007/s11947-012-0977-4

Karkle, E.L., Alavi, S., & Dogan, H. (2012). Cellular architecture and its relationship with mechanical properties in expanded extrudates containing apple pomace. Food Research International, 46, 10-12.

Lach, L. (2006). Modelling vapour expansion of extruded cereals. Ph.D. thesis. Ecole Polytechnique Federale de Lausanne, Lausanne.

Lai, L.S., & Kokini, J.L. (1991). Physicochemical changes and rheological properties of starch during extrusion (A review).Biotechnology progress, 7, 251-266.

Moraru, C.I. & Kokini, J.L. (2003). Nucleation and expansion during extrusion and microwave heating of cereal foods. Comprehensive Reviews in Food Science and Food Safety, Vol 2.

Parkert,R., Ollett, A.L., Lai-Fook, R.A., & Smith, A.C. (1989). The rheology of food ‘melts’ and its application in extrusion processing. In rheology and food biological and pharmaceutical materials, ed. R.E. Carter. Elsevier, London.

Schwartzberg, H.G., Wu, J.P.C., Nussinovitch, A., & Mugerwa, J. (1995). Modelling deformation and flow during vapor-induced puffing. Journal of Food Engineering, 25, 329-372.

Sin, G., Gernaey, K.V., & Lantz, A.E. (2009). Good modeling practice for PAT applications: propagation of input uncertainty and sensitivity analysis. American Institute of Chemical Engineers, 10.1021, 166.

Vergnes, B., & Berzin, F. (2006). Modeling of reactive systems in twin screw extrusion: challenges and applications. Comptes Rendus Chimie, 9, 1409-1418.

Wang, L., Ganjyal, G., Jones, D.D., Weller, C.L., & Hanna, M.A. (2005). Modeling of bubble growth dynamics and nonisothermal expansion in starch-based foams during extrusion. Advances in Polymer Technology, 24(1), 29-45.

Chapter 3 - Stochastic modeling of expansion and shrinkage phenomena during extrusion for starch-based melts: II Modeling results and validation

3.1 Introduction

Extrusion cooking has become extremely popular for production of snacks, ready-to-eat food and other food categories. Several changes take place inside an extruder such as starch gelatinization, protein denaturation, breakdown of anti-nutritional factors etc. due to extreme processing conditions present inside the extruder (Lai and Kokini, 1991). One of the remarkable phenomena taking place during extrusion cooking is expansion of the extrudate and a fundamental understanding of this expansion process at both the microscopic and macroscopic level can help in better operation, product quality, and process control.

Wang et al.(2005) modeled the bubble growth dynamics during extrusion for starch-based foams at both microscopic and macroscopic levels. Fan et al.(2012) used computational fluid dynamics method for modeling the bubble growth dynamics during expansion of corn starch. Alavi et al.(2003) also modeled the process dynamics that take place during super-critical fluid extrusion using carbon-di-oxide. In their model, carbon-di-oxide played the major role in expansion as the extrudate came out of the die. The role of water as a blowing agent was not considered in their model during extrusion; however, moisture content in the extrudates resulted in further expansion during oven drying.

In the first part of this study, initially a mechanistic mathematical model was developed at microscopic (individual spherical bubble) and macroscopic (cylindrical extrudate) scale using equations from literature for material properties, heat, mass and momentum transfer. The

mechanistic model developed was later integrated with stochastic interface to capture the variability in product characteristics as a result of variability in input parameters. Feyissa et al (2012) performed a sensitivity analysis using the heat and mass transfer model of a contact baking process to rank the relative impact of different input parameters on the output. They used Monte Carlo simulation method to understand the propagation of uncertainty in input parameters (such as heat and mass transfer coefficients, evaporation rate parameters, thermo-physical properties etc.) to the uncertainty in output. For sensitivity analysis, they developed a linear regression model for each output parameter and the linear least squares method was used for finding corresponding regression coefficients. For example, for output parameters such as product temperature, they found that evaporation rate constant was most important factor affecting it. Based on study by Feyissa et al. (2012), stochastic interface developed in the current study also used Monte Carlo simulation method for predicting uncertainty in the output as a result of uncertainty in the input. The code was written in Microsoft Visual Basic with Excel as interface for taking the input values and representing the output.

The major objectives of this part of the study was to (1) understand the dynamics of different parameters involved during expansion and shrinkage process such as bubble radius, domain radius, width, pressure difference acting on the bubble wall etc. with the help of mechanistic model (2) characterize the variability in input using DAQ and later understand the variability in output as a result of variability in the input using the stochastic model (3) perform a sensitivity analysis to investigate the impact level of different input factors on product variability.

3.2 Materials and Methods

3.2.1 Input parameters in the mechanistic and stochastic model

The input parameters in the mechanistic model include in-barrel moisture content, die temperature, number of discretization shells in macroscopic and microscopic levels, material constant (k_f), feed rate etc. Typically in a deterministic model, a point estimate of these parameters is fed into the model which results in one value for output. However, in the stochastic model, a distribution of different input parameters was fed into the mechanistic model, one set of values at a time, which resulted in a distribution of output parameters. This distribution of input parameters was obtained by generation of random numbers from a normal distribution. This normal distribution was created using the average and standard deviation values of the experimental data obtained for a parameter using DAQ. The input parameters were assumed to have a normal distribution because normal or Gaussian distribution is the most commonly assumed distribution to characterize the variability in the data in many scientific disciplines (Limpert et al., 2001).

In the current study, distributions of 3 selected input parameters: die temperature, in-barrel moisture content, and material constant (k_f) were generated and fed into the mechanistic model which resulted in output for product characteristics as a distribution. The in-barrel moisture content was calculated based on the moisture in the feed and the extruder water that was input during extrusion. In-barrel moisture content was calculated using equation 3-1 and using data recorded by DAQ such as extruder water in the equation. k_f (equation 2-18) affects the viscosity of the melt which in turn plays an important role in bubble growth and shrinkage.

$$\text{In} - \text{barrel moisture content} = \frac{\text{mc}(\dot{m}_f) + \dot{m}_{sp} + \dot{m}_{wp} + \dot{m}_{se} + \dot{m}_{we}}{\dot{m}_f + \dot{m}_{sp} + \dot{m}_{wp} + \dot{m}_{se} + \dot{m}_{we}} \quad (3\text{-}1)$$

Where,

mc: moisture content in the feed

$\dot{m}_f$ is the feed rate

$\dot{m}_{sp}$ is the rate of steam flow inside the pre-conditioner

$\dot{m}_{wp}$ is the rate of water flow inside the pre-conditioner

$\dot{m}_{se}$ is the rate of steam flow inside the extruder

$\dot{m}_{we}$ is the rate of water flow inside the extruder

The simulation process for the mechanistic and stochastic model ended after the simulated temperature of the extrudate reached the glass transition temperature (equation 3-2)

$$T_g = \frac{M_1 \Delta C_{p1} T_{g1} + M_2 \Delta C_{p2} T_{g2}}{M_1 \Delta C_{p1} + M_2 \Delta C_{p2}} \quad (3\text{-}2)$$

Where

M_1 : mass fractions of moisture, M_2 : mass fraction of solid starch.

ΔC_{p1}: change in specific heat of water at T_{g1}, ΔC_{p2}: change in specific heat of starch at T_{g2}

T_{g1}: Glass transition temperature of water, T_{g2}: glass transition temperature of solid starch

3.2.2 Extrusion (pilot scale)

Degermed yellow corn meal (CCM 260, Bunge, Atchison, KS) was used for production of corn-based expanded products using Wenger TX 52 twin screw extruder. The density of the material used was 41 lbs./ft^3 or 656.76 Kg/m^3. The L/D ratio for screws was 19.5:1. A 4x2 factorial design was used with varying levels of in-barrel moisture contents (0.19, 0.23, 0.28 and 0.33 (db)), each at two screw speeds (250 rpm and 350 rpm). All the extrusion runs with 8 different processing conditions were carried out on the same day and the product from each run was collected for about 10 minutes after 10 minutes of stabilization time (after the processing conditions were set for a particular run). Different screw speeds as well as in-barrel moisture contents resulted in different die temperatures which was also the input in the model. The feed

rate for the extrusion run was set at 70 kg/h. The moisture content in the feed was measured as 0.11 dry basis (db). The schematic diagram of screw profile is provided in figure 3-1. A low shear screw profile was used for corn meal. Camire et al. (1991) found that torque requirement for corn meal was 6-12% lower for samples containing only corn meal than the samples containing 25% cottonseed flour.

L and R in figure 3-1 represent the left and right screws which were identical except that the first two elements were double flight in left screw and single flight in right screw. Such kind of set up promotes smooth flow of the material from the feeder to the screws. The decision for keeping the left screw elements as double flight and right screw as single flight depends on the rotation of the screws. As the material progresses in the screw from the feed end to the die, the pitch of the elements is reduced to compress the material. Hence, the elements are changed from full pitch to ¾ pitch as the material moves towards the die.

A tapered die with opening of 4.2 mm was used. The land length of the die was 4.7mm. The dimensions and shape of the die are given in figure 3-2. The die dimensions have an impact on expansion of the extrudate. Bouzaza et al. (1996) found that the lower die diameter resulted in higher expansion anisotropy in the extrudates whereas it was not majorly affected by the land length of the die. The product was dried using a 2 pass dryer and 1 pass cooler (Wenger 4800 series). The residence time of the product in the dryer was 5 minutes on each belt i.e. 15 minutes in total at 212 F. Samples were collected both out of extruder as well as out of dryer. Product characteristics such as cross sectional radii, length and weight of each piece were measured using a caliper and a weighing balance. This product data was later compared with the simulated values obtained from mechanistic and stochastic model.

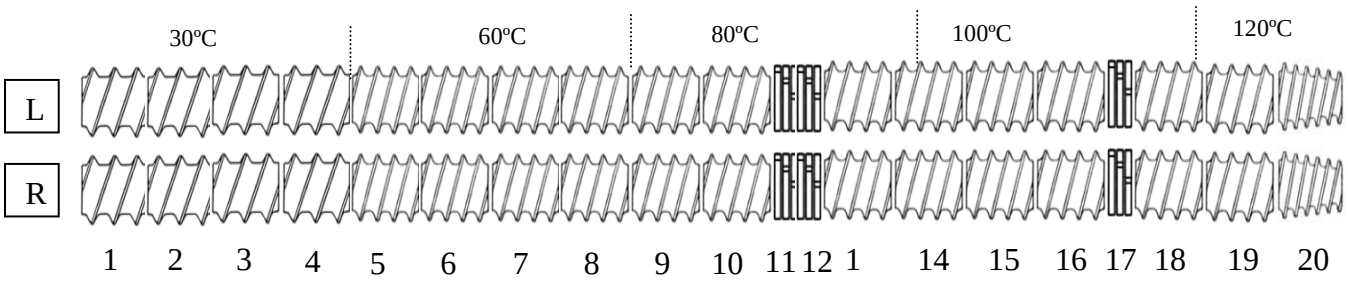

Element no.

1*= SE-FP-9U-DF-F, 2*= SE-FP-9U-DF-F, 3= SE-FP-9U-DF-F, 4= SE-FP-9U-DF-F, 5= SE-3/4P-9U-DF-F, 6= SE-3/4P-9U-DF-F, 7= SE-3/4P-9U-DF-F, 8= SE-3/4P-9U-DF-F, 9= SE-3/4P-9U-DF-F, 10= SE-3/4P-9U-DF-F, 11=KB-F, 12= KB-B, 13= SE-3/4P-6U-DF-F, 14= SE-3/4P-9U-DF-F, 15= SE-3/4P-9U-DF-F, 16= SE-3/4P-9U-DF-F, 17=KB-F, 18= SE-3/4P-9U-DF-F, 19= SE-3/4P-9U-DF-F, 20=cone

SE: Screw element, FP: Full pitch, 3/4P: ¾ Pitch, U: Units, DF: Double Flight, KB: Kneading block, F: Forward, B: Backward

* First 2 elements are single flight in right screw and double flight in left screw.

Figure 3-1: Low shear screw profile used for making expanded products using corn meal

The processing conditions for extrusion run were set at a particular value; however, these values kept fluctuating which was recorded by data acquisition system (DAQ). DAQ records the values of input parameters every second which helps in understanding the variability associated with these parameters. Die temperature was measured by inserting a resistance temperature detector (RTD) inside the spacer just before the die. This value for die temperature measured was then recorded by DAQ.

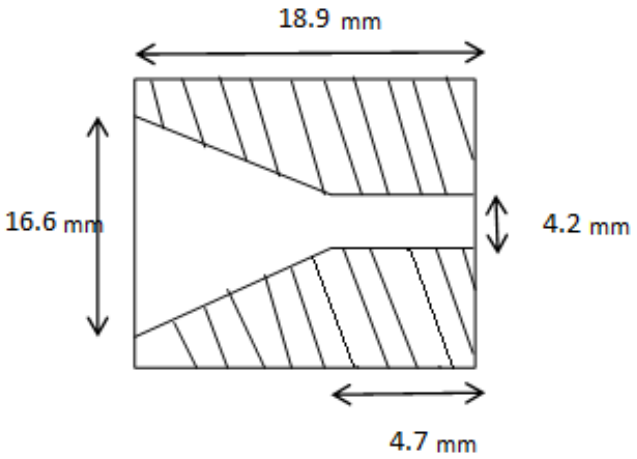

Figure 3-2: Die dimensions of the tapered die used during extrusion runs

3.3 Results and Discussions

3.3.1. Experimental results

The variability in two of the input parameters, die temperature and extruder water, as recorded by DAQ during extrusion processing is given in figure 3-3 along with the average value and the value recorded from control panel. The intersection point of control panel data and actual DAQ data reflects the instant at which the value was recorded. Hence, the difference in average DAQ value and the control panel value emphasizes on the presence of variability in input parameters during extrusion. The variability in input parameters (as recorded by DAQ) gets translated into variability in output (product characteristics). The DAQ data was plotted using ~400 data points for each processing condition (figure 3-3).

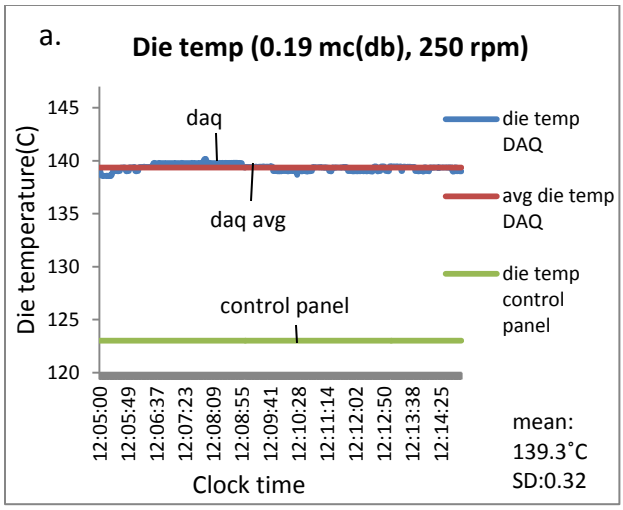
a.
Die temp (0.19 mc(db), 250 rpm)
Die temperature(C)
145
140
135
130
125
120
daq
daq avg
control panel
die temp DAQ
avg die temp DAQ
die temp control panel
12:05:00
12:05:49
12:06:37
12:07:23
12:08:09
12:08:55
12:09:41
12:10:28
12:11:14
12:12:02
12:12:50
12:13:38
12:14:25
Clock time
mean: 139.3˚C
SD:0.32

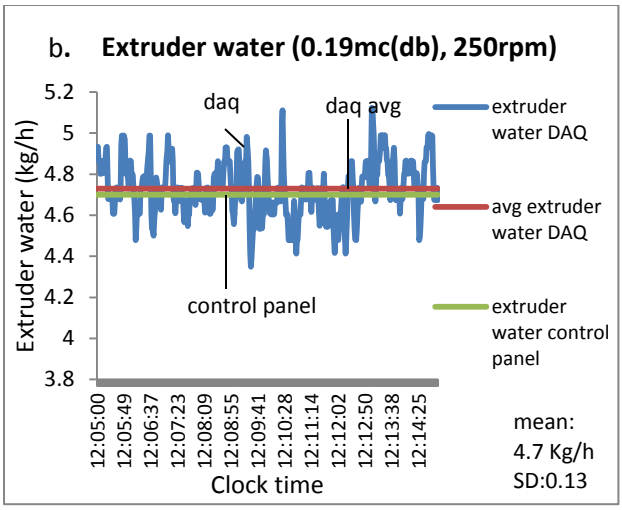
b.
Extruder water (0.19mc(db), 250rpm)
Extruder water (kg/h)
5.2
5
4.8
4.6
4.4
4.2
4
3.8
daq
daq avg
control panel
extruder water DAQ
avg extruder water DAQ
extruder water control panel
12:05:00
12:05:49
12:06:37
12:07:23
12:08:09
12:08:55
12:09:41
12:10:28
12:11:14
12:12:02
12:12:50
12:13:38
12:14:25
Clock time
mean: 4.7 Kg/h
SD:0.13

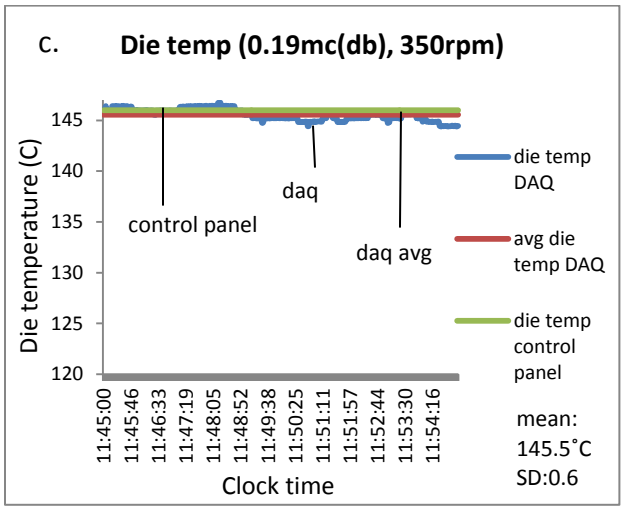
c.
Die temp (0.19mc(db), 350rpm)
Die temperature (C)
145
140
135
130
125
120
control panel
daq
daq avg
die temp DAQ
avg die temp DAQ
die temp control panel
11:45:00
11:45:46
11:46:33
11:47:19
11:48:05
11:48:52
11:49:38
11:50:25
11:51:11
11:51:57
11:52:44
11:53:30
11:54:16
Clock time
mean: 145.5˚C
SD:0.6

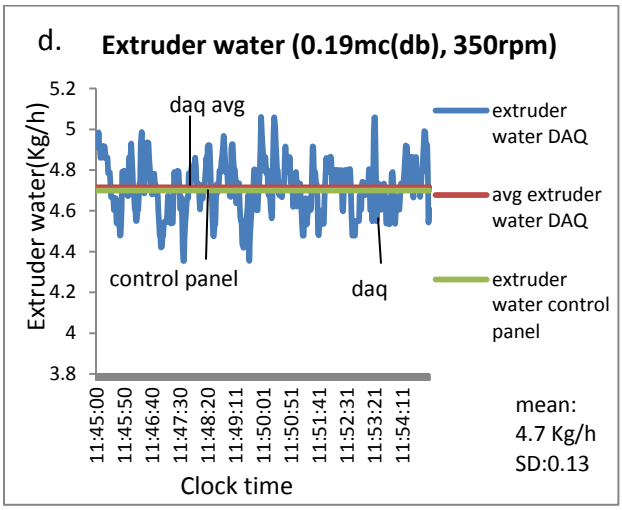
d.
Extruder water (0.19mc(db), 350rpm)
Extruder water(Kg/h)
5.2
5
4.8
4.6
4.4
4.2
4
3.8
daq avg
control panel
daq
extruder water DAQ
avg extruder water DAQ
extruder water control panel
11:45:00
11:45:50
11:46:40
11:47:30
11:48:20
11:49:11
11:50:01
11:50:51
11:51:41
11:52:31
11:53:21
11:54:11
Clock time
mean: 4.7 Kg/h
SD:0.13

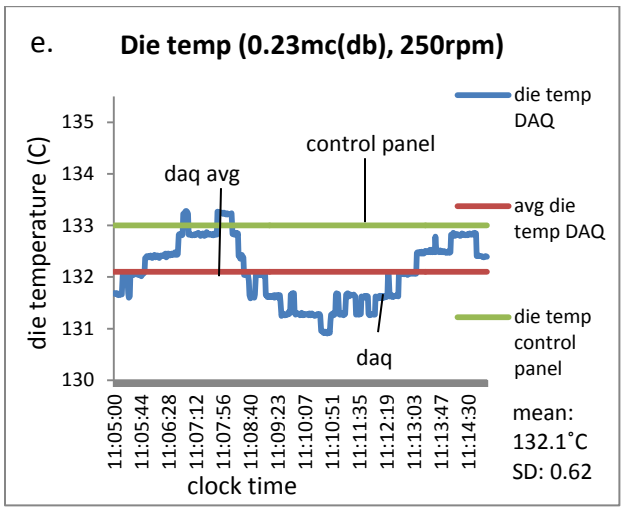
e.
Die temp (0.23mc(db), 250rpm)
die temperature (C)
135
134
133
132
131
130
daq avg
control panel
daq
die temp DAQ
avg die temp DAQ
die temp control panel
11:05:00
11:05:44
11:06:28
11:07:12
11:07:56
11:08:40
11:09:23
11:10:07
11:10:51
11:11:35
11:12:19
11:13:03
11:13:47
11:14:30
clock time
mean: 132.1˚C
SD: 0.62

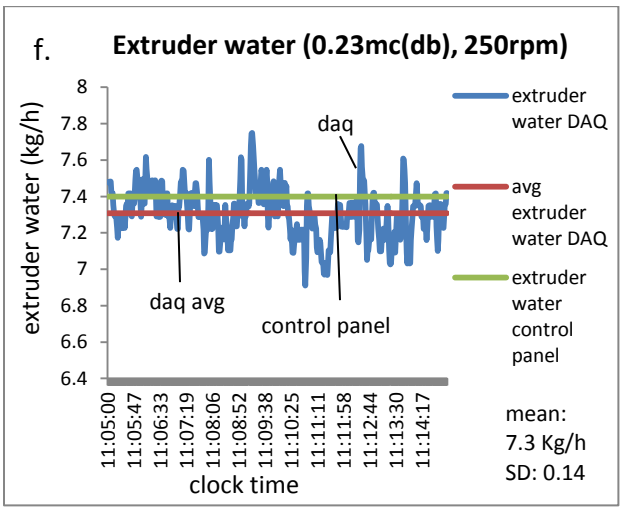
f.
Extruder water (0.23mc(db), 250rpm)
extruder water (kg/h)
8
7.8
7.6
7.4
7.2
7
6.8
6.6
6.4
daq
daq avg
control panel
extruder water DAQ
avg extruder water DAQ
extruder water control panel
11:05:00
11:05:47
11:06:33
11:07:19
11:08:06
11:08:52
11:09:38
11:10:25
11:11:11
11:11:58
11:12:44
11:13:30
11:14:17
clock time
mean: 7.3 Kg/h
SD: 0.14

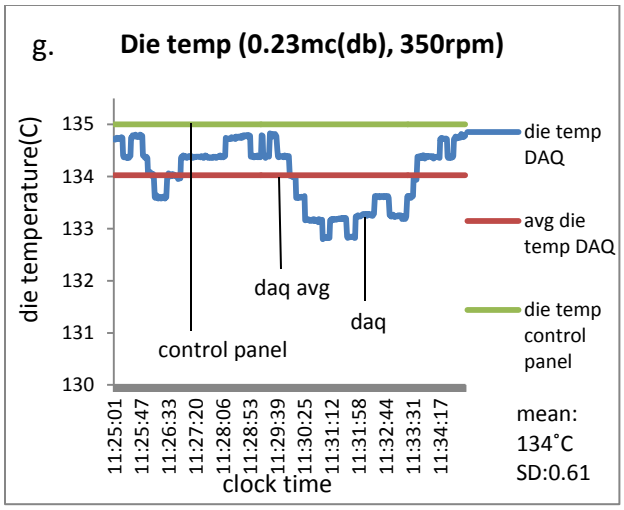
g.
Die temp (0.23mc(db), 350rpm)
die temperature(C)
135
134
133
132
131
130
daq avg
daq
control panel
die temp DAQ
avg die temp DAQ
die temp control panel
mean: 134˚C SD:0.61
11:25:01
11:25:47
11:26:33
11:27:20
11:28:06
11:28:53
11:29:39
11:30:25
11:31:12
11:31:58
11:32:44
11:33:31
11:34:17
clock time

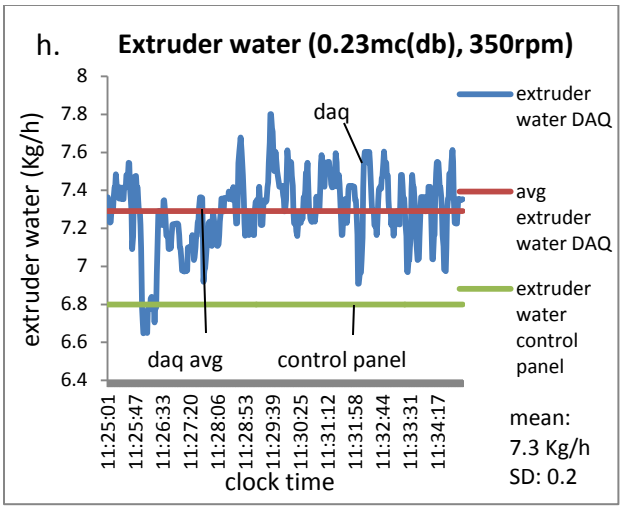
h.
Extruder water (0.23mc(db), 350rpm)
extruder water (Kg/h)
8
7.8
7.6
7.4
7.2
7
6.8
6.6
6.4
daq
daq avg
control panel
extruder water DAQ
avg extruder water DAQ
extruder water control panel
mean: 7.3 Kg/h SD: 0.2
11:25:01
11:25:47
11:26:33
11:27:20
11:28:06
11:28:53
11:29:39
11:30:25
11:31:12
11:31:58
11:32:44
11:33:31
11:34:17
clock time

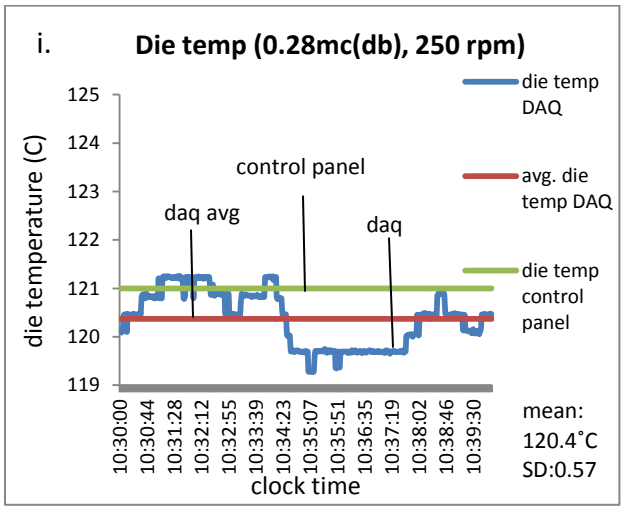
i.
Die temp (0.28mc(db), 250 rpm)
die temperature (C)
125
124
123
122
121
120
119
control panel
daq avg
daq
die temp DAQ
avg. die temp DAQ
die temp control panel
mean: 120.4˚C SD:0.57
10:30:00
10:30:44
10:31:28
10:32:12
10:32:55
10:33:39
10:34:23
10:35:07
10:35:51
10:36:35
10:37:19
10:38:02
10:38:46
10:39:30
clock time

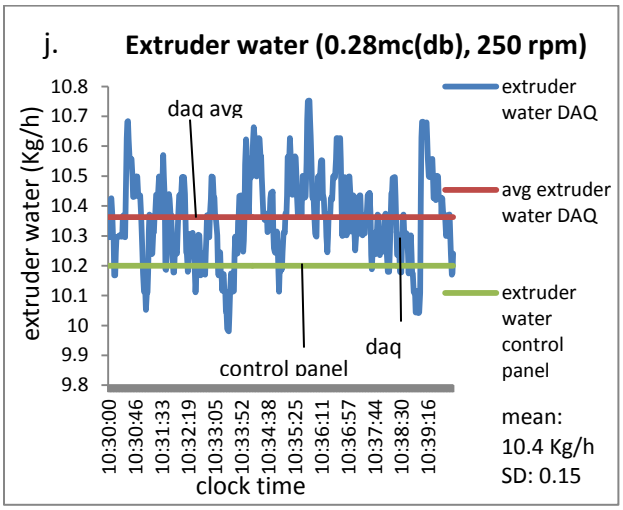
j.
Extruder water (0.28mc(db), 250 rpm)
extruder water (Kg/h)
10.8
10.7
10.6
10.5
10.4
10.3
10.2
10.1
10
9.9
9.8
daq avg
control panel
daq
extruder water DAQ
avg extruder water DAQ
extruder water control panel
mean: 10.4 Kg/h SD: 0.15
10:30:00
10:30:46
10:31:33
10:32:19
10:33:05
10:33:52
10:34:38
10:35:25
10:36:11
10:36:57
10:37:44
10:38:30
10:39:16
clock time

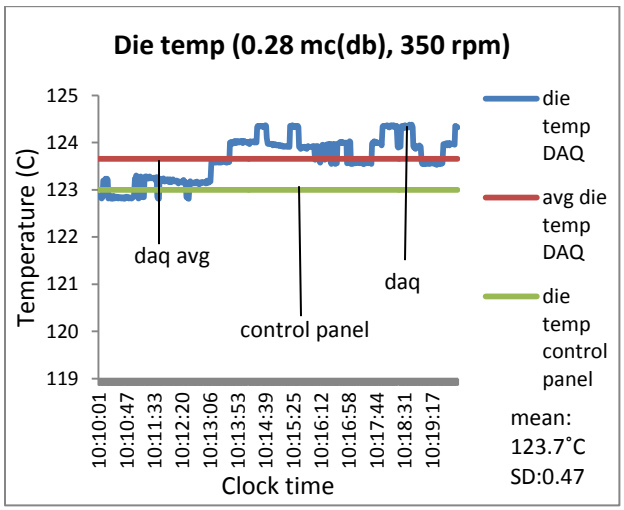
Die temp (0.28 mc(db), 350 rpm)
Temperature (C)
125
124
123
122
121
120
119
daq avg
daq
control panel
die temp DAQ
avg die temp DAQ
die temp control panel
mean: 123.7˚C SD:0.47
10:10:01
10:10:47
10:11:33
10:12:20
10:13:06
10:13:53
10:14:39
10:15:25
10:16:12
10:16:58
10:17:44
10:18:31
10:19:17
Clock time

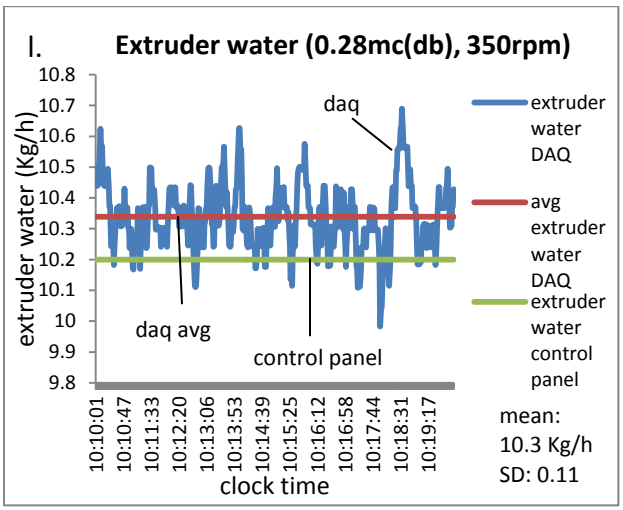
l.
Extruder water (0.28mc(db), 350rpm)
extruder water (Kg/h)
10.8
10.7
10.6
10.5
10.4
10.3
10.2
10.1
10
9.9
9.8
daq
daq avg
control panel
extruder water DAQ
avg extruder water DAQ
extruder water control panel
mean: 10.3 Kg/h SD: 0.11
10:10:01
10:10:47
10:11:33
10:12:20
10:13:06
10:13:53
10:14:39
10:15:25
10:16:12
10:16:58
10:17:44
10:18:31
10:19:17
clock time

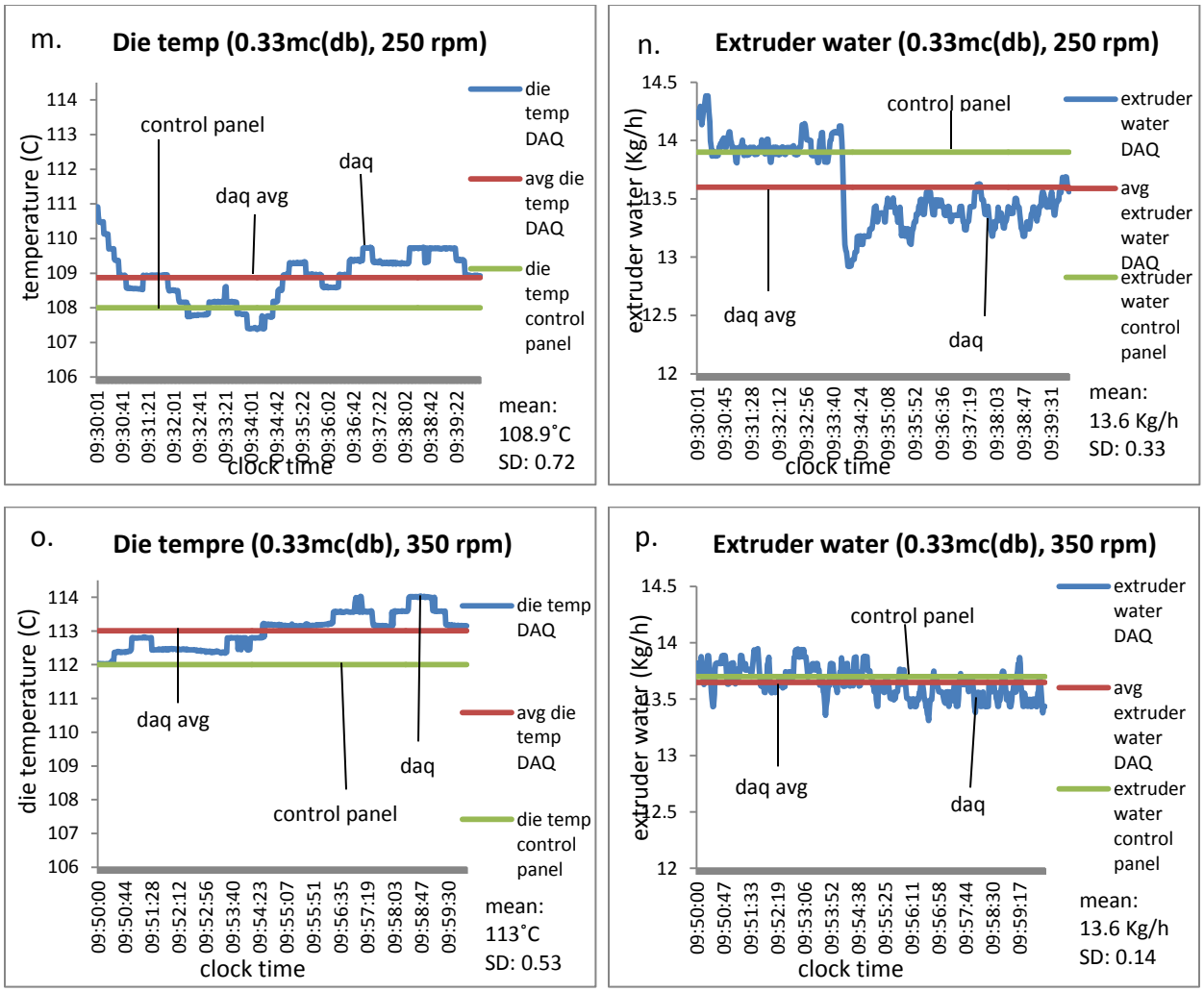

Figure 3-3: a.-p. represent variability data for input parameters (die temperature and extruder water) obtained from DAQ for different extrusion conditions ranging from 0.19-0.33 mc (db) at 250 and 350 rpm screw speed

Table 3-1 summarizes the mean value, standard deviation (SD) and coefficient of variation (CV) observed in the input parameters for 8 different extrusion runs. The mean, SD and CV for input parameters are calculated from DAQ data for each processing condition. The CV for moisture content ranged from 0.62%-1.6%. It should be noted that CV for die temperature would vary depending on the scale (˚C, K or ˚F) used for mean value. Hence to remove this bias from the scale used, base normalization procedure was used for the CV for die temperature by subtracting

the room temperature from the average value of temperature. This normalized CV for die temperature ranged from 0.29%-0.91%. The CV for die temperature was lower as compared to CV for in-barrel moisture content. This variability for CV in input parameter such as 0.29% in die temperature and 0.62% in moisture content does not seem very significant; however, the translation of variability in input to variability in output was much larger as can be seen from the results in table 3-2. The mean, SD and CV for expansion ratio as reported in table 3-2 were calculated by measuring 30 randomly selected and representative pieces of extrudates from each processing condition. Since the product continuously coming out of the die was collected in multiple bags, to maintain maximum randomness in selection, random pieces were selected from different bags for the same processing condition. Diameter of the extrudates was taken as the mean of major and minor diameters of the same cross section of the extrudate.

Table 3-1 Experimental variability data for in-barrel moisture content and die temperature for different extrusion runs

Run	In-barrel moisture content (db)			Die temperature (K)		
m.c.(db),RPM	mean	SD	CV(%)	mean	SD	CV(%)
0.19, 250	0.1887	0.0021	1.12	412.3490	0.3243	0.29
0.19, 350	0.1885	0.0021	1.13	418.5462	0.5971	0.52
0.23, 250	0.2297	0.0022	0.95	405.0985	0.6169	0.6
0.23, 350	0.2295	0.0031	1.37	407.0256	0.6132	0.59
0.28, 250	0.2783	0.0023	0.84	393.3737	0.5755	0.64
0.28, 350	0.2779	0.0017	0.62	396.6596	0.4656	0.49
0.33, 250	0.3298	0.0053	1.60	381.8687	0.7187	0.91
0.33, 350	0.3305	0.0022	0.67	386.0022	0.5318	0.64

Figure 3-4 Products obtained from 8 different processing conditions

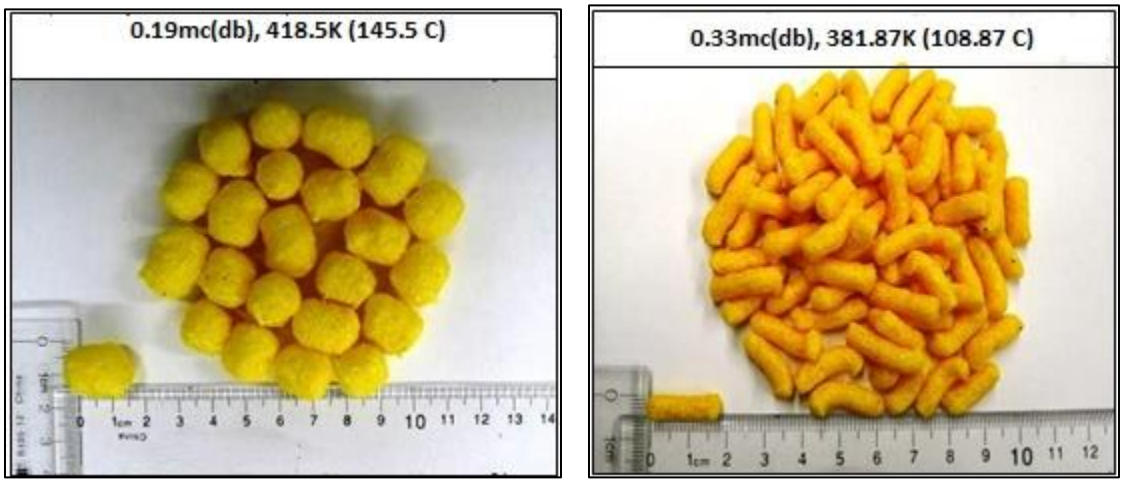

Figure 3-5 Scale comparison of the expansion for product with highest sectional expansion and lowest sectional expansion.

It can be observed from the product pictures obtained from different extrusion runs (figure 3-4) that there was non-uniformity in products. This variability in the product characteristics was captured using the stochastic model. Figure 3-5 gives the scale comparison of products with highest sectional expansion and lowest sectional expansion. The knife speed for all processing

conditions was kept same. It should be noted that the product at higher moisture content had lower sectional expansion but it was longer than the piece extruded at lower moisture content. This could be due to the higher flow rate at higher moisture (lower viscosity) which could have resulted in greater longitudinal expansion.

The variability in the experimentally obtained product is given in table 3-2. The CV for extrudates out of the extruder ranged from 5.85-8.94% and that for extrudates out of the dryer ranged from 5.2-9.4%. It can be seen from table 3-2, how the variability in input parameters affect the variability in output i.e. expansion ratio of the extrudates. For example, a high CV of 8.94% was observed in the extrudate out of extruder for 0.33mc (db) and 250 rpm. The CV for moisture content and die temperature for this condition was 1.6% and 0.91% respectively.

Hence, it can be seen that a cumulative effect of not very significant variability in different input parameters (in-barrel moisture content, die temperature, feed rate etc.) can lead to high variability in output which can become a major concern for the industries. It is interesting to note that the mean values of expansion ratio obtained out of the dryer were higher than the values of expansion ratio out of the extruder. It is common to experience change in volume during drying. The product could either shrink due to further decrease in moisture content or could further expand due to more pore or gas formation (Rahman, M.S., 2001). Alavi et al. (2003) modeled the expansion of extrudates in the dryer. In their study, the extrudates produced by supercritical fluid extrusion using carbon-di-oxide were high in moisture content and had more closed pore fraction (open cell fraction ranging between 0.15 and 0.36) which facilitated in further expansion upon drying. The final bubble radius and open cell fraction in their study increased with increase in temperature of the oven during drying.

Table 3-2 Experimental variability data for expansion ratio of the extrudates for different extrusion run conditions

Run	Out of extruder			Out of dryer		
m.c.(db),RPM	mean	SD	CV(%)	mean	SD	CV(%)
0.19, 250	9.46	0.55	5.85	10.48	0.55	5.22
0.19, 350	10.89	0.76	6.94	11.79	0.85	7.24
0.23, 250	4.46	0.29	6.51	4.91	0.31	6.42
0.23, 350	4.99	0.33	6.51	5.92	0.32	5.36
0.28, 250	2.88	0.19	6.74	3.27	0.24	7.22
0.28, 350	3.60	0.27	7.47	3.95	0.25	6.36
0.33, 250	2.34	0.21	8.94	2.31	0.22	9.4
0.33, 350	3.05	0.19	6.31	3.03	0.17	5.66

The distribution of expansion ratio was studied to understand the variability of the output using histograms (figure 3-6). It was observed that the distribution for expansion ratio obtained from different extrusion runs did not necessarily follow a normal distribution. The distributions could be either skewed to the right, bi-modal etc. It should be noted that since these distributions/histogram were generated using 30 randomly selected pieces, the distribution for a particular processing condition may be different if another set of pieces was selected. Looking at the histograms is a way of understanding how the variability in the products looks like. No conclusions were derived for the type of distribution assumed by expansion ratio at different processing conditions. However, a shift in the values of expansion ratio could be easily observed from the histograms for different processing conditions.

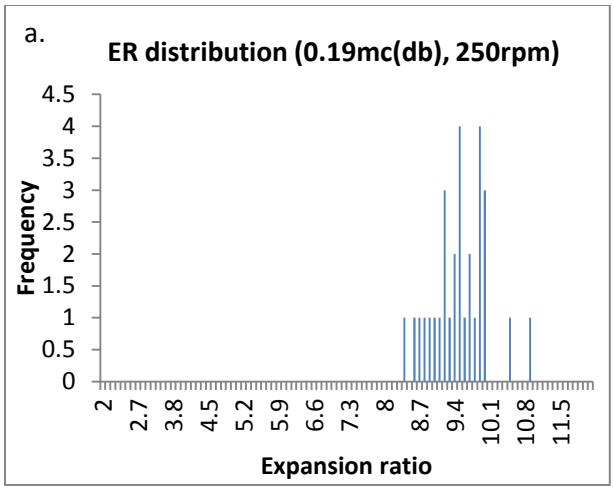
a.
ER distribution (0.19mc(db), 250rpm)
Frequency
Expansion ratio

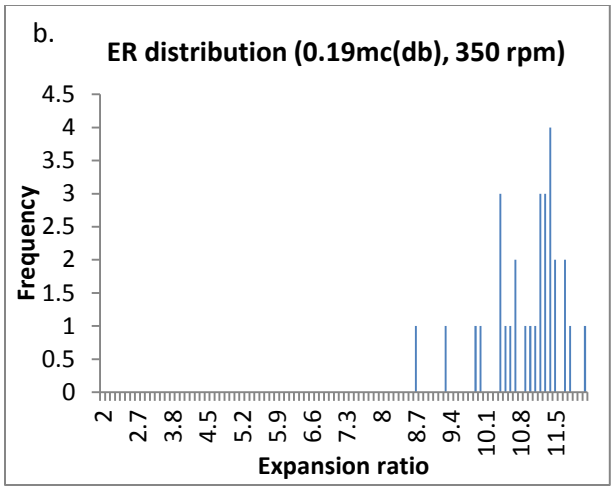
b.
ER distribution (0.19mc(db), 350 rpm)
Frequency
Expansion ratio

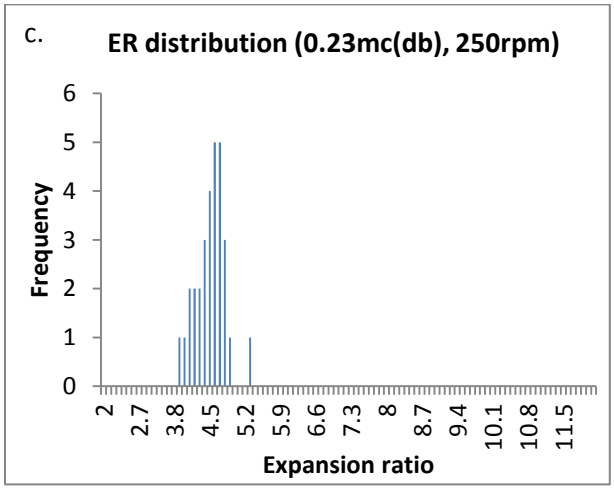
c.
ER distribution (0.23mc(db), 250rpm)
Frequency
Expansion ratio

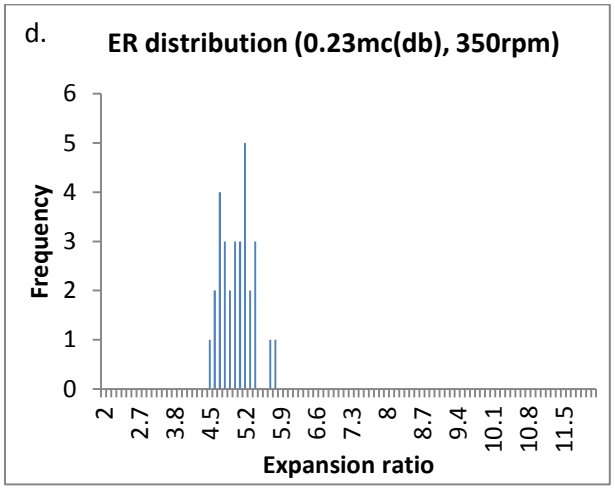
d.
ER distribution (0.23mc(db), 350rpm)
Frequency
Expansion ratio

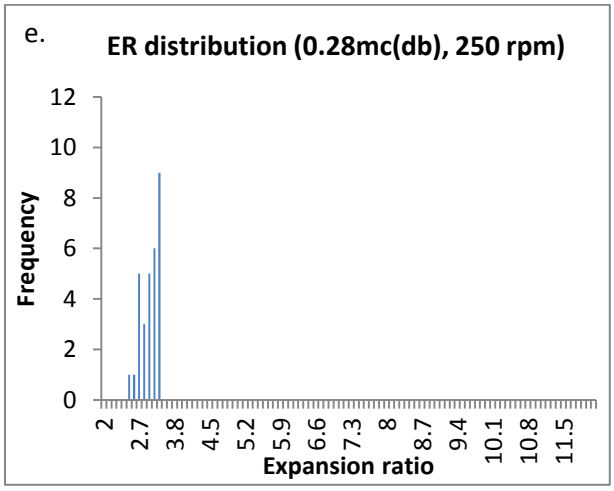
e.
ER distribution (0.28mc(db), 250 rpm)
Frequency
Expansion ratio

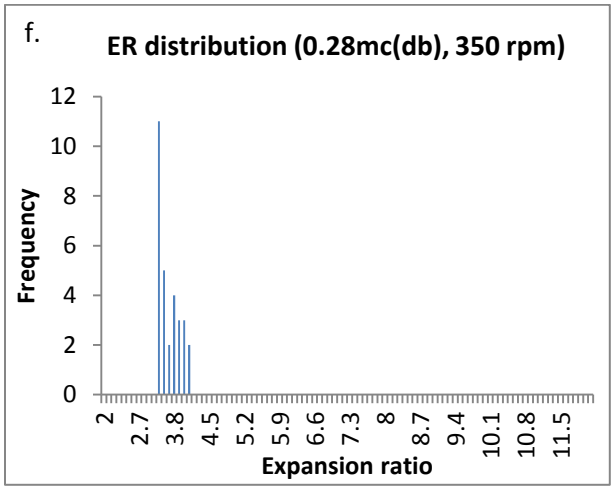
f.
ER distribution (0.28mc(db), 350 rpm)
Frequency
Expansion ratio

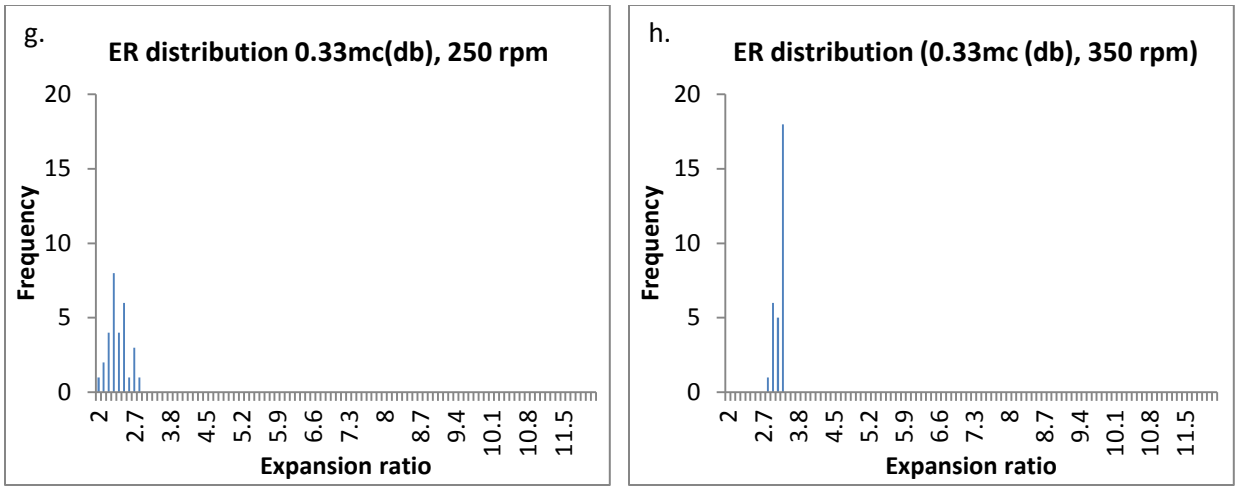

Figure 3-6: a.-h. represent distributions of expansion ratio values (out of extruder) obtained experimentally from different extrusion processing conditions

3.3.2 Deterministic model results

3.3.2.1 Dynamics for different parameters from the deterministic model

As the melt flows out of the extruder, it undergoes expansion followed by collapse also known as shrinkage (Fan et al., 1994). The expansion and shrinkage are interesting phenomena observed in the extrudates due to the resultant pressure (difference of vapor pressure, atmospheric pressure and other viscoelastic forces) acting on the wall of an individual cell, either in the outward (during expansion) or inward direction (during shrinkage) on the wall of an individual cell. This is clearer from the figure 2-2. Initially, the vapor pressure inside the bubble is high due to high temperature and moisture in the bubble. The vapor pressure can overcome the opposing stresses such as elastic stress, yield stress, tensile stress and atmospheric pressure.

Eventually the moisture and temperature decreases which results in a lower vapor pressure. The opposing stresses are higher and due to this, the resultant pressure acts in the inward direction. At this point of time, the yield stress acts towards prevention of collapse and acts in the outward direction. Thus when the resultant pressure is in inward direction, it leads to shrinkage. The temperature reduces further and the extrudate solidifies when its temperature

goes down below its glass transition temperature range, ~Tg+30 (Fan et al., 1994) after which no further shrinkage takes place. Study of the dynamics of different parameters involved in the bubble expansion and shrinkage phenomena provide better understanding of the process.

Figure 3-7 provides the detailed dynamics of resultant pressure (or the pressure difference) acting on the bubble wall and the resulting bubble growth. The negative values of the resultant pressure are used to represent the pressure acting in the inward direction on the cell wall during the shrinkage phase. Till the time, pressure difference has a positive value, the radius of the bubble increases. As the pressure difference becomes zero, there is no change observed in the bubble radius. Later, the bubble radius decreases as the pressure difference becomes less than zero (i.e. acts in the inward direction). Eventually the rate of decrease in bubble radius becomes very low and the radius stabilizes. The expansion and shrinkage stops once glass transition temperature is reached. It is interesting to note that for higher moisture content 0.33mc(db), the simulation process went on for a long time (~150 s) as compared to lower moisture content 0.23 mc(db) (~20s). This could be a result of lower value of glass transition temperature at higher moisture content. Since, the code does not stop until glass transition temperature is reached; the process was simulated for a long time. For the processing condition of 0.33 mc(db) and 386K, the pressure difference value as shown in figure 3-7(c) showed a cyclical trend over time i.e., the value for pressure difference was negative in the shrinkage period; it dropped down to zero and became negative again, which is thermodynamically infeasible. Further research was conducted on the underlying code and the simulated results for finding the reason for cycling of pressure difference. For the processing condition of 0.33 mc(db) and 386K, it was found that after shrinkage started (at around 1.2883 seconds), the value of temperature started increasing after 1.3044 seconds. Vapor pressure (Pw), one of the components in the pressure difference equation,

is the product of saturation vapor pressure and water activity which are dependent on temperature and moisture content of the inner most microscopic shell (Xwc). An increase in temperature or moisture results in increase in vapor pressure and vice versa (see appendix B, table 1 for sample calculations of vapor pressure as a function of temperature and moisture content). It was found that till the time Xwc was decreasing (while temperature was increasing after shrinkage), it compensated for the increase in temperature and it did not lead to rise in the value of Pw. But at around 1.3066 seconds, the value of Xwc became the minimum set value in the code for moistures in microscopic shells (0.004). Now, since Xwc reached its minimum value but the temperature was increasing, it resulted in increase in the value of Pw. Later when temperature started decreasing again, during that time there was an increase in moisture content of innermost microscopic shell which again increased the vapor pressure. During this time, the other components of pressure such as elastic stress, yield stress, and surface tension increased but at a slower pace as compared to the vapor pressure. As a result, the value of negative pressure (pressure in the inward direction during shrinkage period) reduced and reached zero. Eventually, further reduction in the temperature reduced the Pw and there was an increase in the value of other pressure components in the opposite direction as well. Hence the net value of the pressure difference (ΔP) became negative again, thereby showing a cyclical trend. Upon investigating the processing condition of 0.23mc (db) and 405.09K, same trend was observed. The fluctuation/increase in temperature was observed at 3.0015 seconds but during this time the moisture content in the innermost layer of microscopic shells (Xwc) decreased rapidly and reached its minimum set value in the code (0.004). As a result, there was a slight increase observed in Pw at 3.0092 seconds which resulted in decrease in negative pressure (pressure in the inward direction during the shrinkage phase), however, in this case, the increase in Pw was

not very high and the pressure difference remained negative i.e. in the inward direction. Hence, the cyclical trend was not observed in this case. Hence, this thermodynamic infeasibility in pressure difference value was an outcome of instability observed in temperature and moisture content dynamics. Hence, this can be prevented by stabilizing the dynamics of macroscopic temperature and microscopic moisture content.

From figure 3-7, it can be observed that the simulated bubble radius increased suddenly in a very short period of time as the melt flowed out of the die. This could be due to sudden release of pressure as the melt exits the die. Within few seconds of exiting the die, shrinkage takes place reducing the bubble radius, for example, shrinkage took place in around 2 seconds for 0.23mc (db). A greater collapse was observed at higher moisture content. This could be due to lower viscosity at higher moisture content which provides lesser resistance to the collapse. The final values of bubble diameter predicted by the mechanistic model ranged from 0.04mm for the processing condition of 0.33 mc (db) and 250 rpm to 0.49mm for the processing condition of 0.19 mc(db) and 250 rpm. The bubble diameter for the processing condition 0.19 mc (db) and 350 rpm could not be simulated because of the limitation of the model, not being able to simulate temperatures higher than 410K. The actual die temperature for the processing condition 0.19 mc(db) and 250 rpm was 412 K but it was simulated at 410 K. Karkle et al. (2012) used X-ray microtomography to study the cellular architecture of the extrudates formed by blends of corn flour and apple pomace. For 0% apple pomace in the formulation, their average cell diameter ranged from 0.75-1.05 mm depending on the moisture content. The average cell diameter decreased with increase in moisture content which was the same trend as predicted by the mechanistic model simulations. Trater et al. (2005) studied the microstructure of extrudates formed by brittle corn starch with different percentages of whey protein concentrate (WPC) in

the formulation. For 0.35 mc (db), and 5% WPC, the average cell diameter was measured as 1.7mm. Cheng et al. (2007) also measured the average cell size for extrudates of corn starch and whey protein isolates (WPI). For 0% WPI, their cell size varied from 1.57-2.94 mm depending on the in-barrel moisture content during extrusion. Agbisit et al (2007) found the average cell diameter ranging from 2.07-6.32mm depending on the in-barrel moisture content (0.29-0.41 (db)) during extrusion.

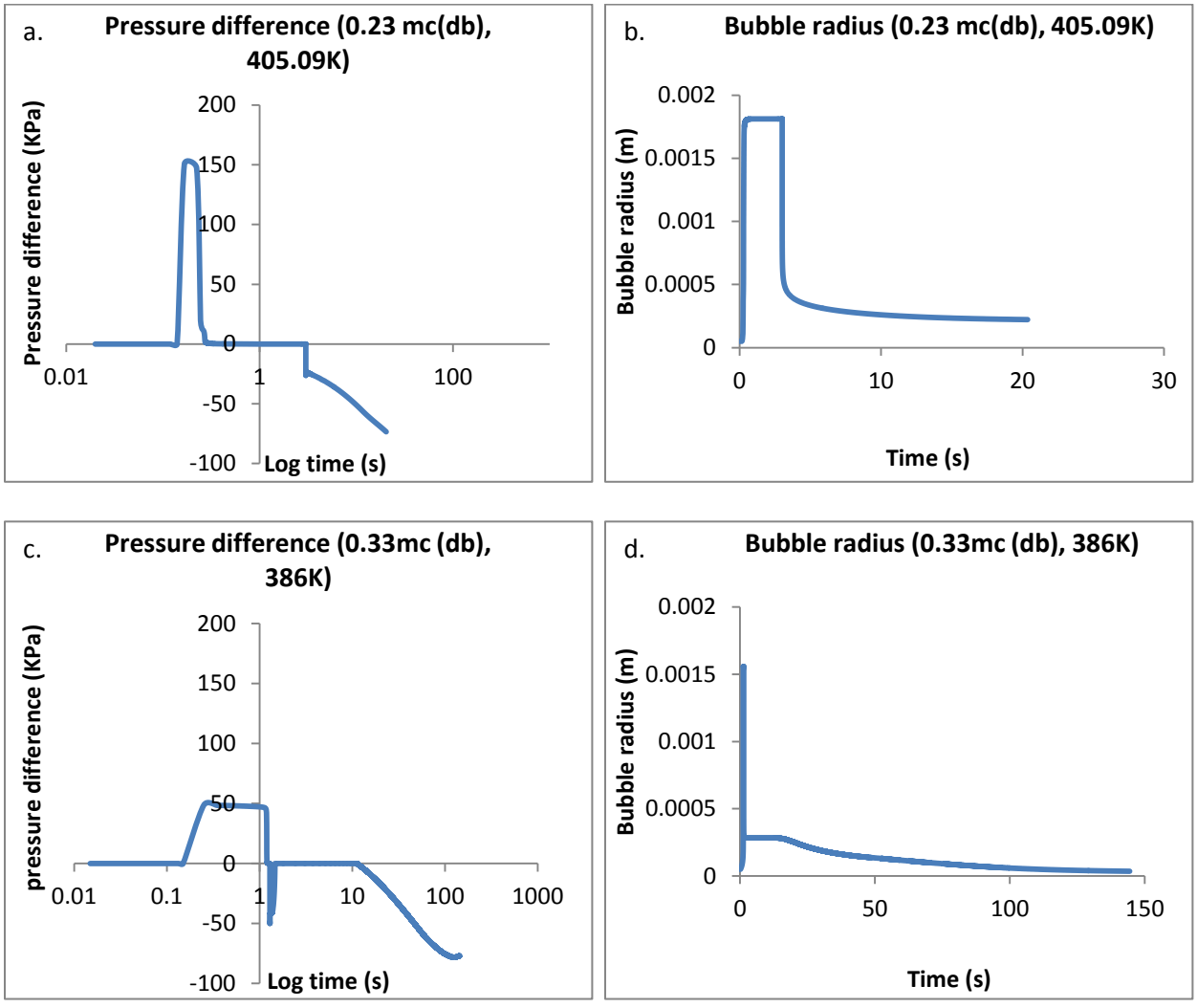

Figure 3-7 Dynamics for bubble radius growth and shrinkage for 0.23mc(db) and 0.33mc(db)

The predicted cell size was smaller than the average cell size measured in different studies on cellular architectural analysis. This could be due to the fact that during extrusion, the cells coalesce during expansion when the wall thickness reduces drastically, thereby increasing the final cell size. However, the microscopic level of the mechanistic model simulates the growth and shrinkage dynamics of an individual bubble and the resultant cell size of the single bubble was thereby smaller than the experimental values obtained from literature.

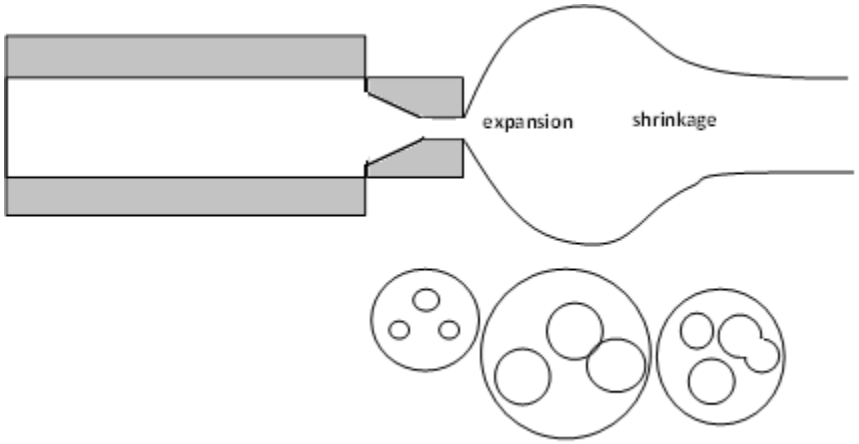

Figure 3-8 Schematic diagram of expansion, shrinkage and stabilization as observed at the macroscopic level

Figure 3-8 is a schematic of how expansion and shrinkage looks like for the extrudate (at the macroscopic level) coming out of the die. The domain radius (figure 3-9 a. and b.) follows the same trend as bubble radius. However, the domain radius does not decrease as rapidly as the bubble radius. The wall thickness of the bubble decreases during expansion. Towards the end of expansion, the width of the bubble becomes close to zero (few micrometers). Wang et al. (2005) observed the same trend in their simulation and suggested that at this point of extremely small thickness, the cell might rupture depending on factors such as domain temperature, moisture etc. The eventual increase in cell wall thickness (figure 3-9 c. and d.) could be explained as a result

of shrinkage. The bubble radius and domain radius decrease during shrinkage, but the domain radius decreases less rapidly as compared to bubble radius, hence, the cell wall thickness increases again. Similar trend for cell wall thickness was observed by Fan et al., 2012. It should be noted that for the processing condition of 0.33 mc(db) and 386K, the cell wall thickness increased up to 200 µm after collapse which is not realistic. It could probably be occurring due to instability in the model at this processing condition which was also observed as cycling in pressure difference, temperature fluctuation and microscopic moisture instability at this processing condition.

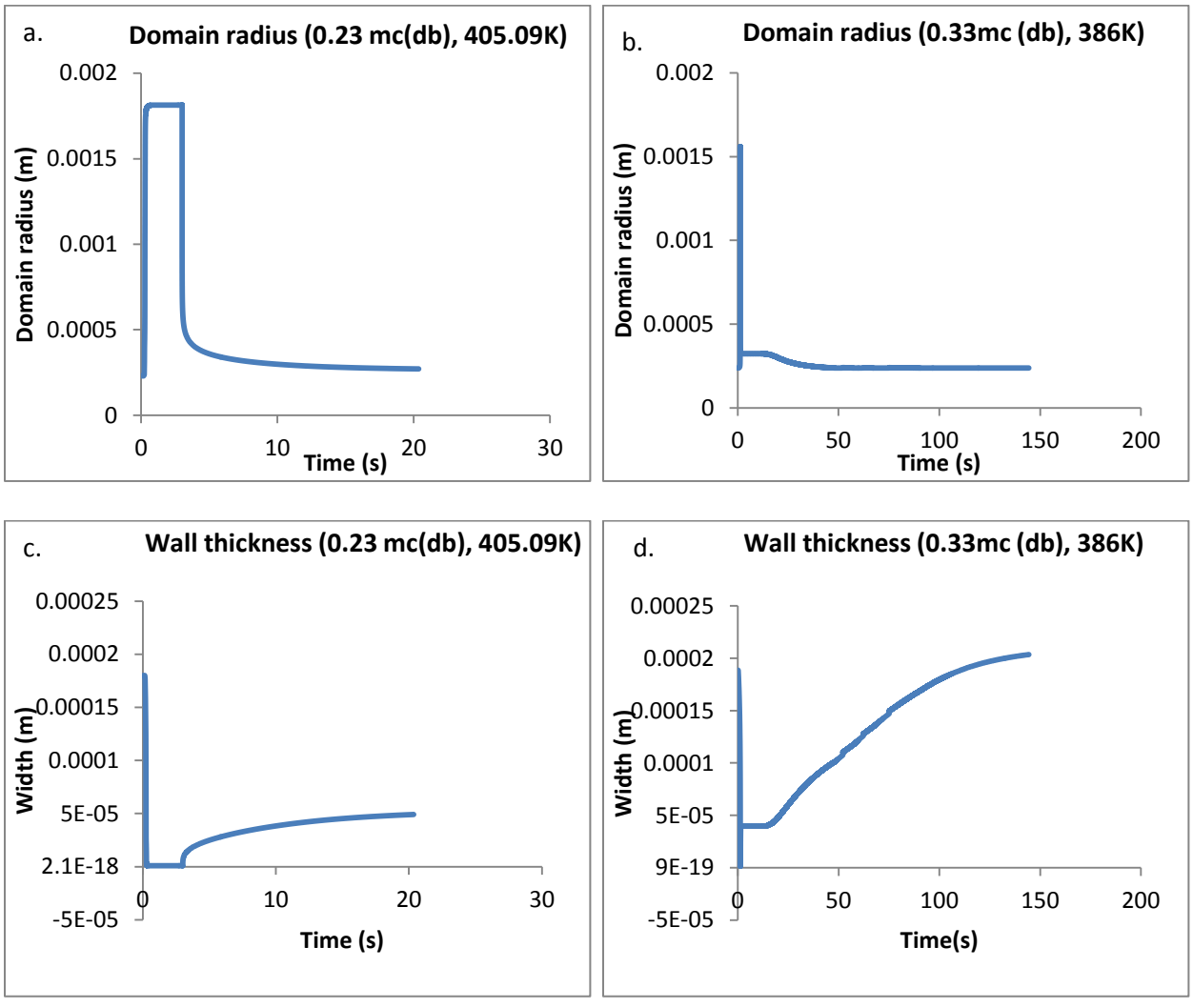

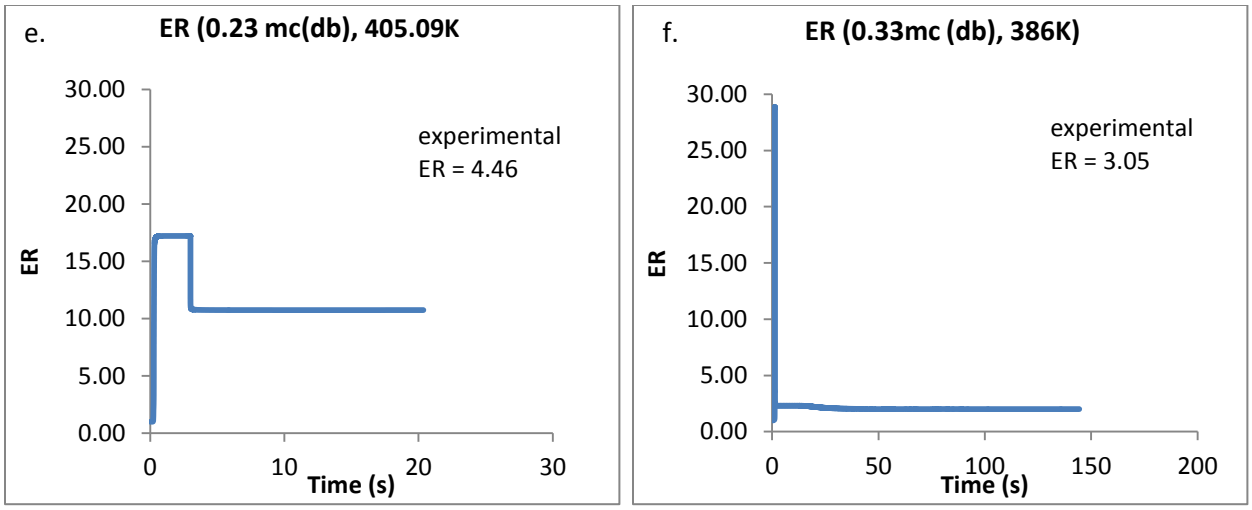

Figure 3-9 Dynamics of domain radius, width and expansion ratio of the bubble for 0.23 mc(db) and 0.33mc(db).

The expansion ratio (figure 3-9 e. and f.) also followed the same trend as bubble radius where it increased until expansion and then decreased during shrinkage period. The final expansion ratio decreased with increase in moisture content from 0.23 (db)-0.33 (db). However, it is interesting to note that the maximum expansion ratio was higher at higher moisture content. This is due to lower viscosity at higher moisture content which provides the ease of higher expansion but at the same time it leads to higher collapse. The simulated values of final expansion ratio ranged from 1.16-12.86 depending on the processing conditions (table 3-3). Chinnaswamy and Hanna (1988) studied the expansion ratio of normal corn starch at different processing conditions. In their study, the expansion ratio ranged from 7.5-14.2 as the moisture content ranged from 0.06-0.3 (db). The expansion ratio increased with increase in moisture content up to 0.14(db) and decreased sharply with further increase in moisture content. The expansion ratio measured by Karkle et al. (2012) ranged from 5.9-10.5 depending on the moisture content (0.21-0.33 (db). In their study, the expansion ratio decreased with increase in moisture content which was the same trend obtained by the mechanistic model. Hence, the

expansion ratio predicted by the mechanistic model was similar to the range of expansion ratio measured experimentally in different studies.

Figure 3-10 represents the dynamics of bulk temperature with time as a result of heat transfer with in cylindrical layers. The simulated temperature reduced gradually but there was a small fluctuation observed in the simulated value for bulk temperature at 0.23 mc(db) as well as 0.33 mc(db) which is thermodynamically infeasible.. Upon investigation it was found that fluctuation in the temperature was an outcome of fluctuation in the outermost layer because the temperature in the inner layers decreased gradually. Temperature in the outermost layer was a function of Δx_2 $\left(\Delta x_2 = \frac{d_{ex} \times ER^{\frac{1}{3}}}{2 \times (N_b - 1)}\right)$ and $T_{Nb.}$ So during the shrinkage period, ER reduced and as a result Δx_2 also reduced. Also when ER reduced, ϵ reduced, since it was defined as (ϵ = 1-1/ER) in the code. This resulted in increase in $k_{eff.}$ An increase in k_{eff} and decrease in Δx_2 led to decrease in the term N_T defined by ($N_T = h^* \Delta x_2 / k_{eff}$). A decrease in N_T led to increase in the value of T_{Nb+1} (outer most layer of the macroscopic shells) which possibly resulted in the observed fluctuation in temperature. As the temperature in the adjacent layer (T_{Nb}) went down, the effect of N_T was compensated and the temperature of the outermost macroscopic shell decreased again. Sample calculations were done (shown in Appendix B, table 2) to see the impact of decreasing values of T_{Nb} and N_T upon $T_{Nb+1.}$ It was found that when T_{Nb} was constant in the sample calculations and N_T decreased, the value of T_{Nb+1} increased but when the value of T_{Nb} was also reduced, it compensated for the effect of N_T and the resulting value of T_{Nb+1} also decreased. It is important to note that the stability criterion for the macroscopic heat transfer is set by the term M_T ($M_T = \Delta x_2^2 / (\alpha_t \times \Delta t)$). In this term, the Δt used is calculated based on the mass transfer in spherical system of microscopic shells. It is possible that this Δt is not suitable for stability of different equation systems at all times. In heat transfer at macroscopic scale, since

Δt is small, it satisfies the stability condition of $M_T \geq 4$ (Geankoplis, 1993). However, it is not checked whether α_t is suitable enough and later T_{Nb+1} is computed using α_t. Hence, apart from checking the suitability of Δt for different equation systems, the stability condition for boundary should also be checked which is given as follows (Marek and Götz, 1995)

$$F_o \leq \frac{1}{2(2+Bi)}$$

where F_o is the Fourier number ($F_o = \frac{\alpha_t \times \Delta t}{\Delta x_2^2}$) and Bi is the Biot number ($Bi = \frac{h \times \Delta x_2}{k_{eff}}$).

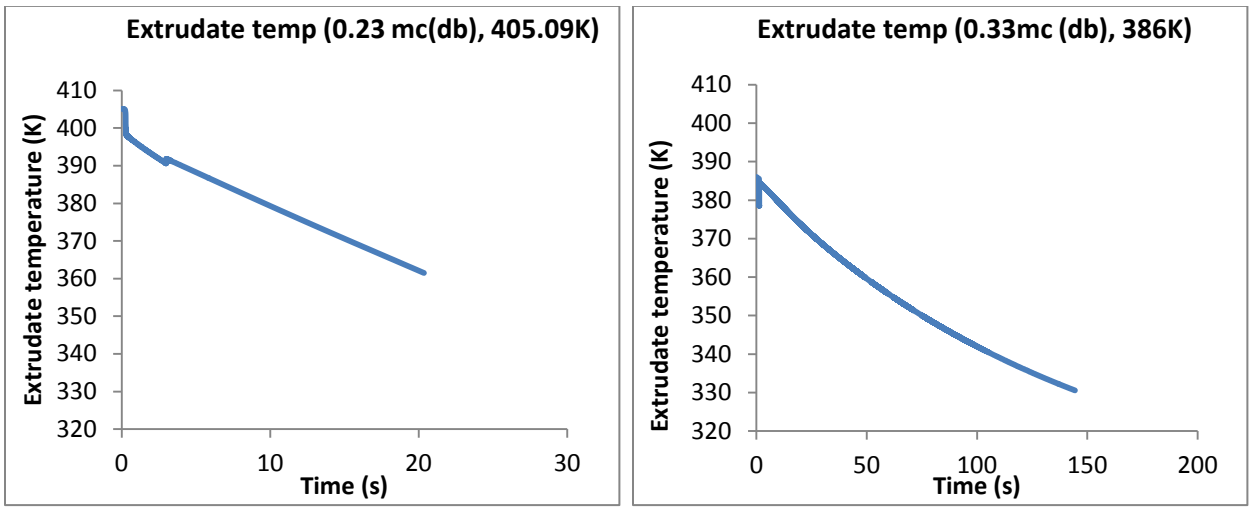

Figure 3-10 Dynamics of temperature of the extrudate with time for 0.23 mc(db) and 0.33mc(db)

The simulation process stops when temperature of the bulk (extrudate) reaches glass transition temperature range (T_g+30). When moisture content was 0.23 mc(db), the process stopped when temperature reached 363K (90˚C) i.e. at a glass transition temperature of about 60˚C. At 0.33 mc (db), the process stopped at ~331K (58˚C) i.e. at a glass transition temperature of about 28˚C. These values of glass transition temperatures are in comparable range of the glass transition temperature values available in literature. Zeleznak and Hoseney (1987) performed a

study on glass transition temperature for wheat starch. They found that at a moisture content of 0.23(db), the glass transition temperature for wheat starch was ~45˚C and for 0.28mc (db) was ~ 25˚C.

Figure 3-11 represent the change in bulk moisture (extrudate) with time. There was an initial steep reduction in the simulated bulk moisture which could be due to sudden loss of moisture from the outermost layer as the material flows out of the die. Later on the moisture did not decrease drastically or stabilized as can be seen from the straightened out line in figure 3-11. It is interesting to note that the extrudate moisture did not change significantly even when the temperature was higher than 100˚C. This was due to the parameter values computed in the mechanistic model where diffusivity of the moisture within the cylindrical shells of the extrudate was not very high but the mass transfer coefficient for the outermost layer was high enough. As a result, the moisture from only the outermost layer decreased significantly but the moisture from the inner layers did not reduce significantly. Hence, the average value of moisture in all the cylidrical shells of the extrudate did not decrease significantly as represented in figure 3-11.

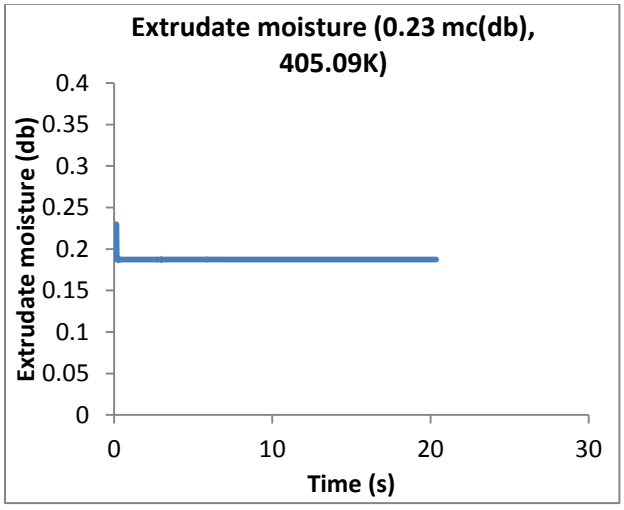

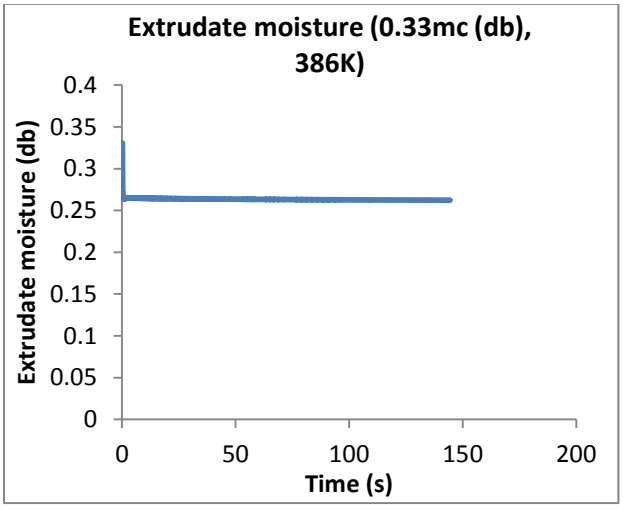

Figure 3-11 Dynamics of average extrudate moisture with time for 0.23 mc(db) and 0.33 mc(db)

As the bubbles expand, some of the cells burst open and lose their ability to expand further. Such cells are accounted for by open cell fraction. In figure 3-12, it can be seen that for 0.23mc (db), more expansion resulted in greater number of open cells. However, value of open cell fraction as 1 is unrealistic because physically it means that all the cells are open which does not happen in real life. Nevertheless, the simulated results provided a comparison for open cell fraction at lower and higher moisture content. At 0.33 mc (db), lesser expansion took place and greater number of bubbles was intact. Thus the open cell fraction at this condition was much lower (~0.4). Karkle et al. (2012) measured the void fraction as 0.59 for extrudates from corn flour (0% apple pomace) when moisture content was 0.33mc (db) which is close to the simulated value. They also obtained the similar trend where the void fraction decreased (0.76-0.59) as the moisture content was increased (0.21-0.33 (db))

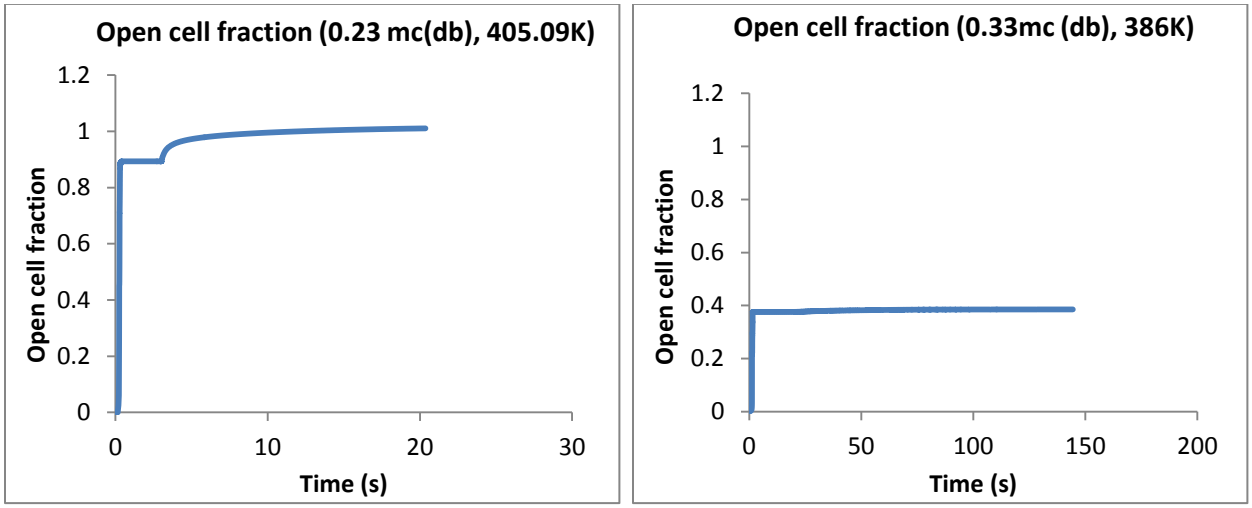

Figure 3-12 Open cell fraction for processing conditions: 0.23 mc(db), 405.09K and 0.33mc(db), 386K with time

Trater et al. (2005) measured the void fraction as ratio of the void volume of the extrudate sample to the total volume of the sample. In their study, the void fraction ranged from

0.629-0.842 depending on the formulation (percentage of whey protein concentrate and moisture content).

In figure 3-13, Xwc represents the moisture content in the inner most shell of the bubble, Xwi(N) represents the moisture content in the outermost shell of the bubble and Xwa represents the average moisture content of all the shells of the bubble. The moisture from the bubble shells migrates to the inner most shell of the bubble and is formed into vapor. As a result more moisture migrates from the matrix into the bubble. At higher moisture (0.33 mc (db)), the glass transition temperature was lower and as a result the simulation process stopped after a long time. In the simulated results, thermodynamic instability was encountered in the moisture content of microscopic shells (as can be seen from moisture content dynamics of outermost microscopic shell in figure 3-13) which led to fluctuations in average microscopic shells moisture as well. The zoomed out results for the different layers help in better understanding of the dynamics in the microscopic shells. It can be seen that for both processing conditions, an increase in moisture in the inner most layer (X_{wc}) can be observed. Microscopic moisture fluctuations were analyzed and it was found that the moisture content increased in the innermost layer before the spike in the moisture of the outer layer was observed. The dynamics for moisture content in different layers before the spike was observed in outer layer are given in figure A-6. It was observed that the moisture content in the innermost layer was constantly increasing before the fluctuations started, however the moisture was stable in the other layers. Hence, this increase in moisture in the innermost layer eventually led to increase in moisture in the intermediate layers since moisture was transferred to the intermediate layer from both the outer layers as well as the inner layers. Later on, this increase in moisture was propagated to the outer layers observed as thermodynamically infeasible spike in Xwi(N) where moisture became higher than the initial

value. To remove this instability, apart from defining Δt suitably, the definition of Δr should also be investigated since it contains a point of discontinuity.

A slight increase in the moisture in the innermost layer of microscopic shells was also observed in the popcorn puffing model by Schwartzberg et al. (1995). They explained this increase in X_{wc} as a balancing effect of increase in radius and decrease in pressure difference towards the end of expansion. According to them, at large values of bubble radius (X_{wa}-X_{wc}) was proportional to multiple of ΔP and R. So when ΔP decreased near the end of expansion, it compensated for the increase in R and as a result (X_{wa}-X_{wc}) decreased which was observed as a fluctuation in X_{wc}.

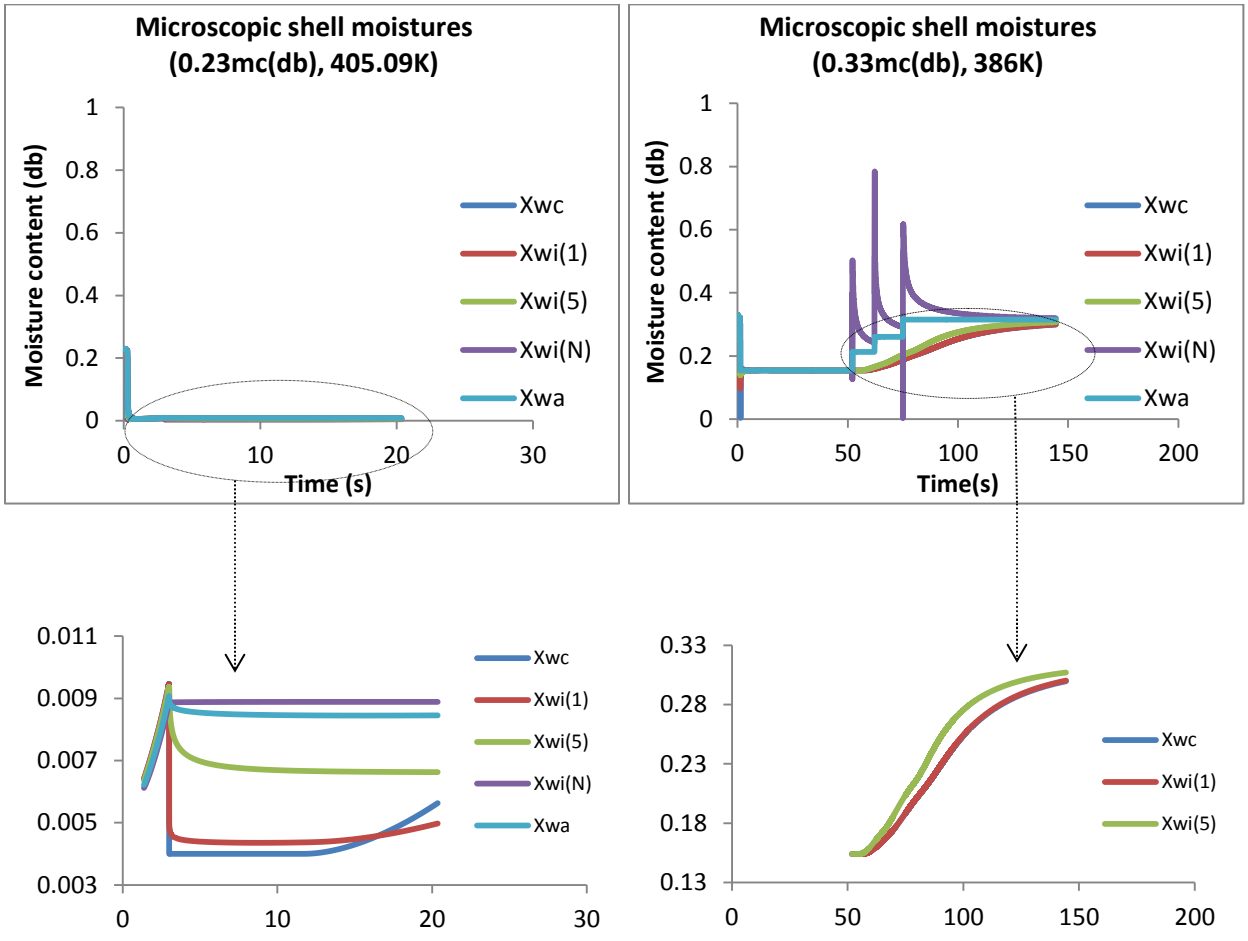

Figure 3-13 Microscopic shell moistures for different layers for 0.23mc(db) and 0.33mc(db).

3.3.2.2 Expansion ratio of extrudates (experimental and simulated)

The expansion ratio of the extrudates was simulated by mechanistic model using experimental values of die temperature and in-barrel moisture content for each processing condition. The model showed computational instability at temperature above 410K. Hence, it was not possible to simulate the processing condition of 0.19 mc(db) and 350 rpm which had a die temperature of 418K. Initially, the computational instability was encountered for temperature above 400K. To remove this, the number of shells in the microscopic layer was increased from 25 to 50 which increased the simulation time by a factor of 4. It took about 45 minutes to an hour to run one mechanistic simulation depending on the computational ability of the computer when 50 microscopic spherical shells were used. Further reduction in time step or discretization step for achieving stability in finite element method led to impractical computation time requirements. For example, upon increasing the number of microscopic shells by 100, the computation time for mechanistic model became almost 24 hours and it led to stability up to 412 K, not further. Hence, considering time constraints, further reduction in discretization was not carried out to remove instability in computation for temperatures above 410K. It was interesting to note that upon increasing the number of spherical shells from 25 to 50, the dynamics for different parameters shifted a little because changing number of shells led to change in mass per layer (ΔM) which in turn affected equations for calculation of domain radius and change in moisture for microscopic shells. However, the shape and trend for the dynamics of parameters did not change significantly. Similar result was obtained by Lach, L. (2006) who observed significant difference in the results when the number of microscopic shells was increased from 10 to 25. However, they did not observe significant difference upon further increasing the number of spherical shells at the microscopic level. They explained this trend as a result of

insufficient discretization of the bubble interface for computation purposes when the number of microscopic shells was 10.

The simulated and experimental values of expansion ratio for different processing conditions are listed in table 3-3. It can be seen from the results that the simulated value was less than the experimental value for low and high moisture content of 0.19 mc(db) and 0.33mc(db). For other two moisture contents (0.23(db) and 0.28(db)), the simulated value was higher than the experimental value. Hence, it is difficult to comment on the bias of the model. More clarity on comparison of simulated and experimental values could be obtained from observing the trend of these values for different processing conditions (figure 3-14).

The trend of expansion ratio for experimental values in figure 3-14 shows that as the moisture content was increased beyond 0.19mc(db), the expansion ratio reduced. This could be due to the decrease in viscosity with increasing moisture content. Lower viscosity in turn results in low shear in the extruder as well as greater collapse during shrinkage phase which leads to lower final expansion. For a particular value of in-barrel moisture content, the expansion ratio increased with increase in screw speed from 250 rpm to 350 rpm. This is a result of higher amount of shear experienced in the extruder with increase in screw speed. From the experimental results, it can be observed that 0.19 mc (db) is the optimum value of moisture content for obtaining highest expansion ratio.

Table 3-3 Comparison for simulated values of expansion ratio with average values of expansion ratio obtained experimentally for different extrusion processing conditions

In-barrel moisture content (db)	Temperature (K)	Simulated value	Average experimental value
0.1887	412.3	6.53 (used 410K)	9.46
0.1885	418.5	-	10.89

0.2297	405.1	10.74	4.46
0.2295	407	12.86	4.99
0.2783	393.4	6.65	2.88
0.2779	396.7	10.59	3.60
0.3298	381.9	1.16	2.34
0.3305	386	2.00	3.05

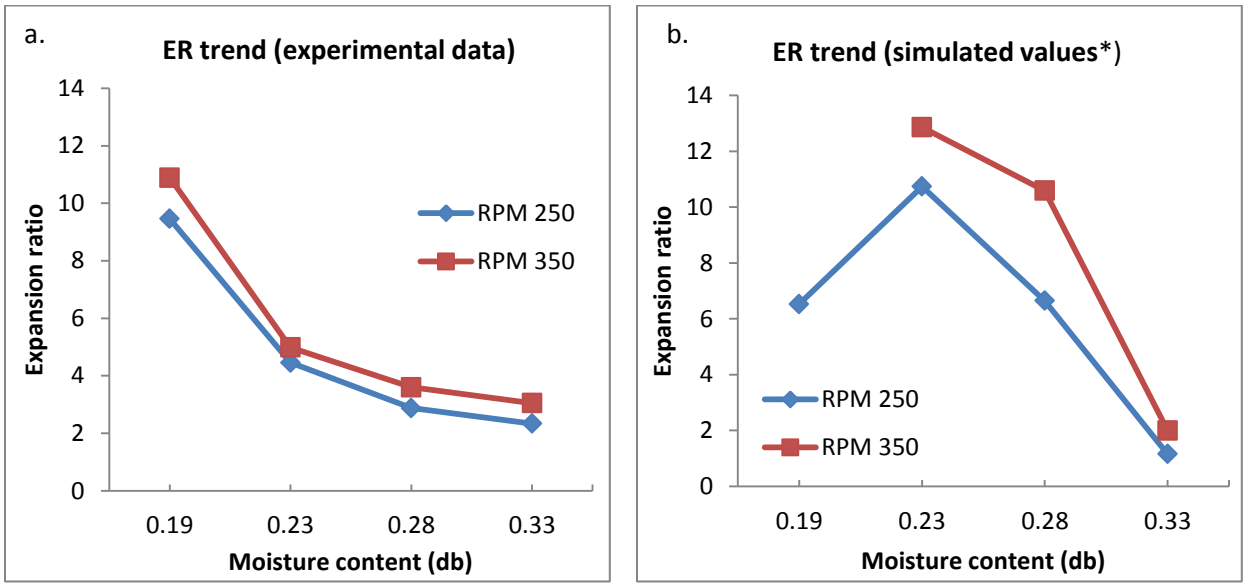

Figure 3-14 Expansion ratio trends with increasing moisture content for experimental and simulated values.

*the model gets unstable at values of temperature higher than 410K. Hence, expansion ratio for 0.19 mc(db) at 350 rpm (418.5K) could not be simulated. Also 410K was used instead of 412.3K for 0.19mc(db) at 250 rpm.

The trend for simulated values of expansion ratio is shown in figure 3-14(b). The expansion ratio increased initially with increase in moisture content from 0.19-0.23(db). With further increase in moisture content, the expansion ratio decreased. A similar trend was observed by Chinnaswamy and Hanna (1988) who investigated the optimum process conditions for obtaining maximum expansion. They observed an expansion ratio of 9 at low moistures of 0.08 (db) and the maximum expansion ratio of ~15 at about 0.16 (db) which reduced on further increase in moisture content. One of the reasons for lower final expansion ratio at higher

moisture content is greater amount of collapse due to lower viscosity at higher moisture content. Della Valle et al. (1997) reported a decrease in volumetric expansion index with increase in moisture content due to greater collapse at higher moisture content. Moraru and Kokini (2003) explained that the extrudate melt with lower viscosity is prone to collapse of the cellular matrix at higher vapor pressure. Collapse was also simulated by Fan et al. (2012) and Wang et al. (2005).

It should be noted that the simulated expansion ratio for higher screw speed was higher at a specific moisture content which again matches with the experimental trend for expansion ratio. There was a shift in simulated expansion ratio values from the experimental results. This difference in values could be a result of material properties that are input into the mechanistic model. The equations for material properties such as diffusivity, consistency index etc. were taken from literature which was measured for a comparable material but not exactly the same material that was extruded (corn meal). For example, the equation of consistency index derived by Parker et al. (1989) for maize starch was used in the model. Similarly, the correlation of diffusivity with respect to temperature and moisture, used in the model, was measured by Van der Lijn (1976) for maltose system. The literature comparisons for expansion ratio and cell size diameters are provided in table 3-4.

Table 3-4 Literature comparisons

Author	Year	Material used	Moisture content	temperature	Expansion ratio	Cell size (diameter mm)
Chinnaswamy, R. and Hanna, M.A.	1988	Normal corn starch	0.06-0.3 (db)	140˚C (413K)	7.5-14.2	
Karkle et al.	2012	Corn flour[*1]	0.21(db)	-	10.5	~1.05

			0.25(db)		8.0	~0.9
			0.33(db)		5.9	~0.75
Cheng et al.	2007	Corn	0.29 (db)	140˚C (413K)		2.94
		starch[*2]	0.37(db)			1.57
Trater et al.	2005	Corn starch	0.35 (db)	-		1.7
		with WPC	with 5%			
			WPC			
Agbisit et al.	2007	cornstarch	0.29-	140˚C (413K)		2.07-6.32
			0.41(db)			
Babin et al.	2007	Maize*[3]	0.25(db)	163±3˚C		3.02
		with	0.25(db)	187±2˚C		0.35,1.03
		different	0.32(db)	187±2˚C		0.86
		amylose%				

*1 corn flour with apple pomace was used at different concentration. For comparison, 0% pomace compositions are mentioned here

*2 corn starch was used in combination with whey protein isolate. For comparison, 0% WPI composition is mentioned here

*3 maize with high amylose content was used. For comparison, results for maize with 23% amylose is mentioned here

3.3.2.3 Sensitivity analysis using mechanistic model

The mechanistic model was used for performing a sensitivity analysis for 3 selected input parameters: in-barrel moisture content, die temperature and material constant (k_f) in consistency index equation. It was carried out by varying value of one parameter and keeping the value of rest of the input parameters constant.

For example, the three selected parameters for the processing condition 0.33 mc(db), 350 rpm (die temperature 386K), were increased and decreased by 15% and the resulting expansion ratio was observed in each case. For the processing condition of 0.23 mc(db), 250 rpm (die temperature 405. 09K), only 5% increase and decrease in the input parameters was considered and the simulation results are presented in figure 3-15. This was done because even 5% increase

in the temperature (normalized) was equal to 410K and a further increase in temperature was not possible to simulate considering model constraints as mentioned above.

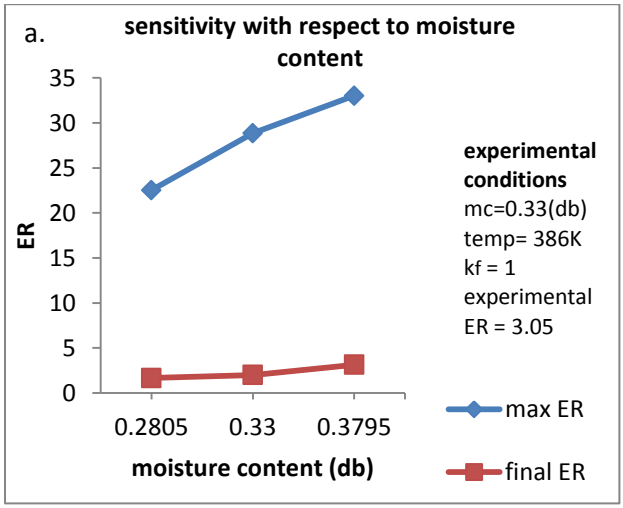

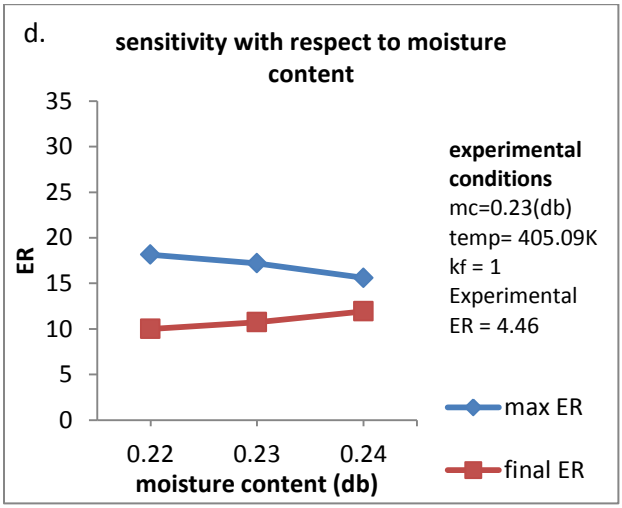

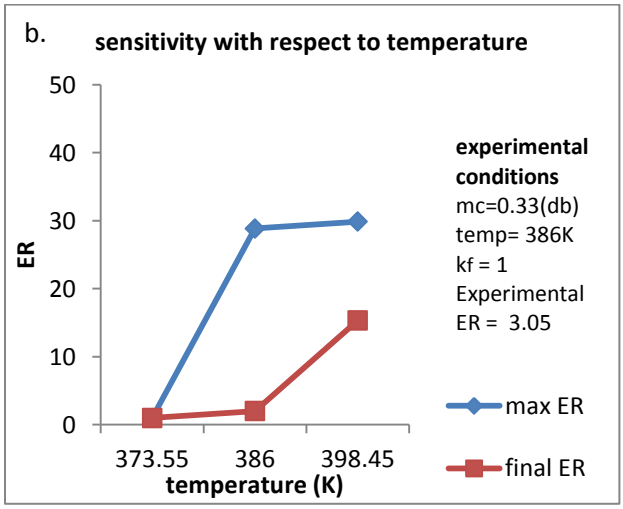

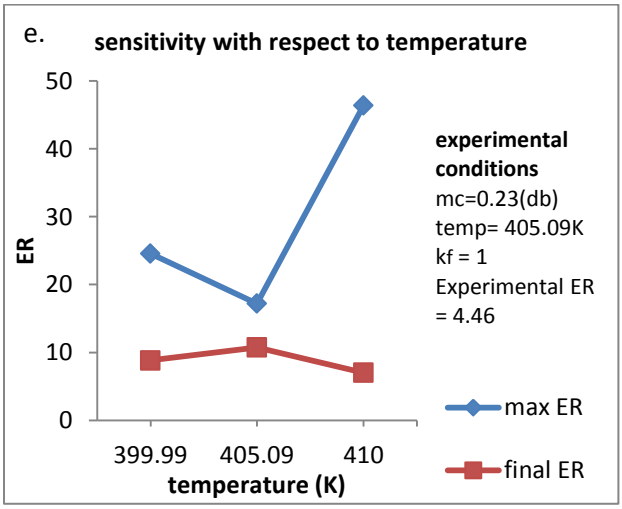

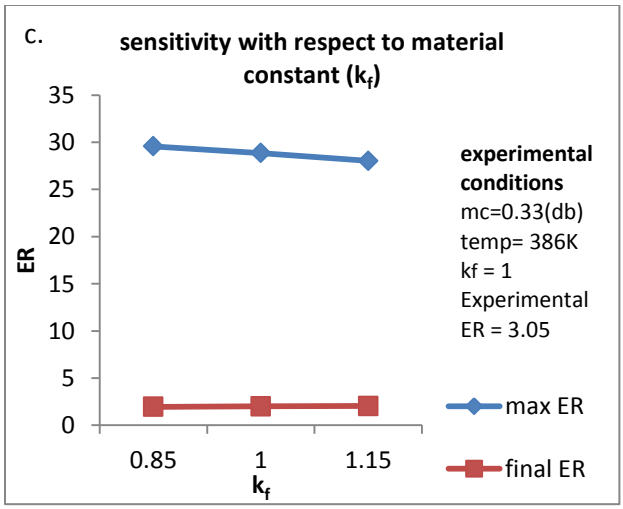

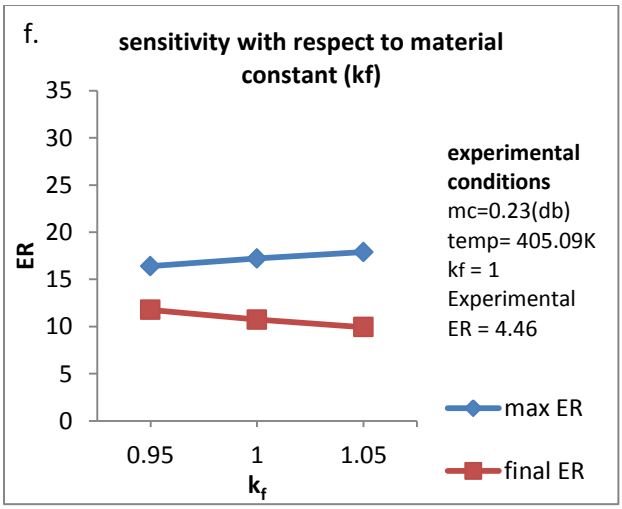

Figure 3-15 Sensitivity analysis results from the mechanistic model for 2 different processing conditions (0.33mc(db), 386K) and (0.23mc(db), 405.09K)

For the experimental conditions, 0.33 mc(db) and die temperature 386K, increase in moisture content reduced the viscosity which led to higher maximum expansion ratio but it can be observed that the collapse was also higher at higher moisture content. With increase in temperature, the expansion ratio increased and there was a huge difference between expansion ratio at 373.55K and 386K. This indicated that expansion ratio was very sensitive to temperature. Upon increase in material constant value (k_f), no significant difference was observed in final expansion ratio; however, it is worthy to note that the collapse was lower as the consistency index was increased.

For the processing condition, 0.23 mc(db) and die temperature 405.09K, with increase in moisture content, the final expansion ratio increased. The final expansion ratio increased upon increasing the temperature from 399.99 to 405.09K but decreased with further increase in temperature. With increase in consistency index, the final expansion ratio reduced. For this processing condition, the results for maximum expansion ratio were inconsistent.

3.3.2.4 Comparison of porosities of experimental and simulated values

It was observed that the sectional expansion ratio at higher moisture content was lower than sectional expansion at lower moisture content. However, it was observed that the product with smaller sectional expansion was longer in size even though the knife speed was same at all processing conditions. Hence, to compare the actual expansion for different processing conditions, porosity(ϵ) for experimental and simulated values was calculated using equation 3-2 and the results are summarized in table 3-5. It can be observed that experimental and predicted

porosity values were similar. This provides a better comparison for expansion of extrudates at different processing conditions.

$$\epsilon = 1 - \frac{1}{VEI} \tag{3-2}$$

where VEI represents the volumetric expansion ratio.

Table 3-5 Simulated and experimental porosity of extrudates at different processing conditions

Moisture content	Temperature	Simulated porosity	Experimental porosity
0.1887	412.3	0.94	0.97
0.1885	418.5	-	0.97
0.2297	405.1	0.97	0.89
0.2295	407	0.98	0.91
0.2783	393.4	0.94	0.80
0.2779	396.7	0.97	0.85
0.3298	381.9	0.20	0.72
0.3305	386	0.65	0.81

3.3.3 Stochastic modeling results

Stochastic model helped in capturing the variability in output parameters (product characteristics such as expansion ratio) as a result of variability in input parameters. To understand the existing variability in the extruded products, a commercial product, Cheetos puffs, was tested by measuring diameter of 30 randomly selected pieces. A coefficient of variation of 2.7% was observed in the diameter for this commercial product. Hence, it is important to understand and address this variability with the help of a stochastic model for better process and quality control.

The stochastic interface developed for the mechanistic model in the current study could input a distribution of each parameter (generated by n values) into the mechanistic model and resulted in the n values of output which were used for generating the distribution for output. In the current study, due to time constraints, 15 values each for 3 selected parameters (in-barrel moisture content, die temperature and material constant (k_f) in consistency index equation) were input into the mechanistic model and 15 values of expansion ratio were obtained for different processing conditions which were used to analyze the variability in the output. Each stochastic simulation comprising of 15 mechanistic simulations took 8-9 hours to run depending on the computational ability of the computer.

Stochastic simulation were carried out for 3 different processing conditions (0.33 mc(db) and 386K, 0.28mc(db) and 393.37K, and 0.23mc(db) and 405.10K). It was not possible to perform a stochastic simulation for 0.19mc(db) since the average value of temperature at that moisture content was above 410K. During stochastic simulation, the random values generated for input parameters were higher or lower than the average value by one or two standard deviation values. Since the code showed instability at temperature values higher than 410K, the stochastic simulation for lowest moisture content was not performed.

Using these stochastic simulations, sensitivity analysis was carried out for three selected input parameters at different processing conditions. The sensitivity analysis was carried out by varying CV of one parameter, keeping the CV of other two parameters constant and observing its effect on the CV of expansion ratio.

Table 3-6 Sensitivity analysis of expansion ratio with respect to moisture content (0.23mc(db) and 405.10K)

Moisture content (db)			Temperature (K)			Material constant (k_f)			ER (simulated)		
Mean	SD	CV(%)	Mean	SD	CV(%)	Mean	SD	CV(%)	Mean	SD	CV(%)

0.23	**0.0022**	**0.95**	**405.10**	**0.6125**	**0.60**	**1**	**0.02**	**2**	**10.81**	**1.05**	**9.7**
0.23	0.0020	0.85	405.10	0.6125	0.60	1	0.02	2	11.10	1.37	12.30
0.23	0.0024	1.05	405.10	0.6125	0.60	1	0.02	2	10.57	0.95	9.00
0.23	0.0057	2.5	405.10	0.6125	0.60	1	0.02	2	10.60	1.42	13.39
Experimental values for expansion ratio of extrudates (30 pieces)									4.46	0.29	6.51

Table 3-7 Sensitivity analysis of expansion ratio with respect to die temperature (0.23mc(db) and 405.10K)

Moisture content (db)			Temperature (K)			Material constant (k_f)			ER (simulated)		
Mean	**SD**	**CV(%)**	**Mean**	**SD**	**CV(%)**	**Mean**	**SD**	**CV(%)**	**Mean**	**SD**	**CV(%)**
0.23	**0.0022**	**0.95**	**405.10**	**0.6125**	**0.60**	**1**	**0.02**	**2**	**10.81**	**1.05**	**9.7**
0.23	0.0022	0.95	405.10	0.5105	0.50	1	0.02	2	10.86	1.07	9.89
0.23	0.0022	0.95	405.10	0.7147	0.70	1	0.02	2	11.15	1.11	9.92
0.23	0.0022	0.95	405.10	2.55	2.5	1	0.02	2	10.26	1.89	18.45
Experimental values for expansion ratio of extrudates (30 pieces)									4.46	0.29	6.51

Table 3-8 Sensitivity analysis of expansion ratio with respect to material constant (k_f) (0.23mc(db) and 405.10K)

Moisture content (db)			Temperature (K)			Material constant (k_f)			ER (simulated)		
Mean	**SD**	**CV(%)**	**Mean**	**SD**	**CV(%)**	**Mean**	**SD**	**CV(%)**	**Mean**	**SD**	**CV(%)**
0.23	**0.0022**	**0.95**	**405.10**	**0.6125**	**0.60**	**1**	**0.02**	**2**	**10.81**	**1.05**	**9.7**
0.23	0.0022	0.95	405.10	0.6125	0.60	1	0.01	1	10.99	1.09	9.91
0.23	0.0022	0.95	405.10	0.6125	0.60	1	0.03	3	10.64	1.06	9.99
0.23	0.0022	0.95	405.10	0.6125	0.60	1.00	0.025	2.5	10.95	1.03	9.44
Experimental values for expansion ratio of extrudates (30 pieces)									4.46	0.29	6.51

Table 3-6, 3-7 and 3-8 represent the sensitivity analysis with respect to moisture content, die temperature and material constant (k_f) respectively for the processing condition of 0.23 mc(db) and 405.10K. The experimental value of CV for moisture content (0.95%) and for die temperature (0.6%) was used initially. A CV of 2% was assumed for material constant (k_f). Using these three values of CV, a CV of 9.7% was obtained for expansion ratio from the

stochastic simulations. Later CV was varied for one parameter at a time, keeping CV for other two parameters as constant.

It is interesting to note in table 3-6 that when CV for moisture content was increased by 0.1%, CV for expansion ratio decreased and when the CV for moisture content was decreased by 0.1%, CV for expansion ratio increased. This trend is counter-intuitive but it is due to the complex non-linear partial differential equations present in the mechanistic model which could lead to such trends. Also, since the difference in CV was very less and the values of the parameters were generated randomly, it is highly likely, that CV could increase or decrease for another set of simulation. Similar trend was observed for other parameters as well. Hence for a better clarity of the change in CV of expansion ratio upon changing the CV of input parameters, a higher value of CV (2.5%) was used for each parameter. A much higher CV for the processing condition of 0.23 mc(db) and 405.10K would lead to instability since for this condition, with higher CV, a higher value of temperature could be generated (more than 410K) and due to the limitation of the model, simulation could not be carried out at temperature above 410K.

A 2.5% CV in moisture content resulted in 13.39% CV in expansion ratio whereas a 2.5% CV in die temperature resulted in 18.45% CV in expansion ratio. For 2.5% CV in material constant (k_f), 9.44% CV in expansion ratio was observed. Hence, the variability in temperature had the greatest impact on the variability in expansion ratio at 0.23 mc(db) and 405.10K.

Table 3-9 Sensitivity analysis of expansion ratio with respect to moisture content (0.28mc(db) and 393.37K)

Moisture content (db)			Temperature (K)			Material constant (k_f)			ER (simulated)		
Mean	SD	CV(%)	Mean	SD	CV(%)	Mean	SD	CV(%)	Mean	SD	CV(%)
0.28	**0.0023**	**0.84**	**393.37**	**0.5786**	**0.64**	**1**	**0.02**	**2**	**6.89**	**0.65**	**9.37**
0.28	0.0021	0.74	393.37	0.5786	0.64	1	0.02	2	6.98	0.88	12.55
0.28	0.0026	0.94	393.37	0.5786	0.64	1	0.02	2	6.50	0.58	8.99

0.28	0.0139	5.00	393.37	0.5786	0.64	1	0.02	2	6.77	1.19	17.53
	Experimental values for expansion ratio of extrudates (30 pieces)								2.88	0.19	6.74

Table 3-10 Sensitivity analysis of expansion ratio with respect to die temperature (0.28mc(db) and 393.37K)

Moisture content (db)			Temperature (K)			Material constant (k_f)			ER (simulated)		
Mean	**SD**	**CV(%)**	**Mean**	**SD**	**CV(%)**	**Mean**	**SD**	**CV(%)**	**Mean**	**SD**	**CV(%)**
0.28	**0.0023**	**0.84**	**393.37**	**0.5786**	**0.64**	**1**	**0.02**	**2**	**6.89**	**0.65**	**9.37**
0.28	0.0023	0.84	393.37	0.4882	0.54	1	0.02	2	6.39	0.48	7.52
0.28	0.0023	0.84	393.37	0.6690	0.74	1	0.02	2	6.75	0.65	9.61
0.28	0.0023	0.84	393.4	4.5187	5.00	1	0.02	2	6.15	3	49.67
	Experimental values for expansion ratio of extrudates (30 pieces)								2.88	0.19	6.74

Table 3-11 Sensitivity analysis of expansion ratio with respect to material constant (k_f) (0.28mc(db) and 393.37K)

Moisture content (db)			Temperature (K)			Material constant (k_f)			ER (simulated)		
Mean	**SD**	**CV(%)**	**Mean**	**SD**	**CV(%)**	**Mean**	**SD**	**CV(%)**	**Mean**	**SD**	**CV(%)**
0.28	**0.0023**	**0.84**	**393.37**	**0.5786**	**0.64**	**1**	**0.02**	**2**	**6.89**	**0.65**	**9.37**
0.28	0.0023	0.84	393.37	0.5786	0.64	1	0.01	1	7.13	0.77	10.78
0.28	0.0023	0.84	393.37	0.5786	0.64	1	0.03	3	6.53	0.53	8.17
0.28	0.0023	0.84	393.37	0.5786	0.64	1	0.05	5	6.72	0.62	9.21
	Experimental values for expansion ratio of extrudates (30 pieces)								2.88	0.19	6.74

Tables 3-9, 3-10 and 3-11 provide the results for sensitivity analysis for the processing condition 0.28 mc(db) and 393.37K. The first row in each table represents the variability in input parameters obtained experimentally and the variability in simulated values of expansion ratio obtained using these experimental values of variability in input. Similar inconsistent trends were observed upon smaller variation in CV values as for the earlier processing condition. Hence, a higher value of CV (5%) was used for obtaining better clarity. A CV of 5% in moisture content resulted in a CV of 17.53% in expansion ratio, keeping the CV of other two parameters constant.

A CV of 5% in die temperature resulted in CV of 49.67% in simulated values of expansion ratio and a CV of 5% in material constant (k_f) resulted in a CV of 9.21% in expansion ratio. Hence, the variability in temperature had the major impact on variability in expansion ratio as compared to other two factors.

Similarly, tables 3-12, 3-13 and 3-14 represent the results from the sensitivity analysis carried out for 0.33 mc(db) and 386K. It can be seen that 5% variability in moisture, temperature and material constant (k_f) resulted in 25.58%, 78.99% and 17.9% CV in simulated values of expansion ratio. Hence, clearly for all three processing conditions, temperature was the strongest factor in deciding the variability in the output, which is expansion ratio in this case. Owusu-Ansah et al. (1983) developed a regression model to find the dependence of transformation (gelatinization, melting etc.) of corn starch upon different input factors during extrusion cooking. They found out that after the moisture and temperature interaction term, temperature was the second most important factor which affected these changes. Moisture content and screw speed were other important factors for transformation during twin screw extrusion of corn starch. These results are consistent with the results from the sensitivity analysis in this study.

Table 3-12 Sensitivity analysis of expansion ratio with respect to moisture content (0.33 mc (db) and 386K)

Moisture content (db)			Temperature (K)			Material constant (k_f)			ER (simulated)		
Mean	**SD**	**CV(%)**	**Mean**	**SD**	**CV(%)**	**Mean**	**SD**	**CV(%)**	**Mean**	**SD**	**CV(%)**
0.33	**0.0022**	**0.67**	**386**	**0.5312**	**0.64**	**1**	**0.02**	**2**	**2.09**	**0.37**	**17.83**
0.33	0.0021	0.66	386	0.5312	0.64	1	0.02	2	2.13	0.61	28.64
0.33	0.0023	0.68	386	0.5312	0.64	1	0.02	2	2.10	0.39	18.65
0.33	0.02	5.00	386.00	0.53	0.64	1.00	0.02	2.00	2.24	0.57	25.58
Experimental values for expansion ratio of extrudates (30 pieces)									3.06	0.19	6.31

Table 3-13 Sensitivity analysis of expansion ratio with respect to die temperature (0.33 mc (db) and 386K)

Moisture content (db)			Temperature (K)			Material constant (k_f)			ER (simulated)		
Mean	SD	CV(%)	Mean	SD	CV(%)	Mean	SD	CV(%)	Mean	SD	CV(%)
0.33	**0.0022**	**0.67**	**386**	**0.5312**	**0.64**	**1**	**0.02**	**2**	**2.09**	**0.37**	**17.83**
0.33	0.0022	0.67	386	0.5229	0.63	1	0.02	2	2.15	0.51	23.90
0.33	0.0022	0.67	386	0.5395	0.65	1	0.02	2	2.02	0.31	15.43
0.33	0.0022	0.67	386	4.15	5	1	0.02	2	3.24	2.56	78.99
Experimental values for expansion ratio of extrudates (30 pieces)									3.06	0.19	6.31

Table 3-14 Sensitivity analysis of expansion ratio with respect to material constant (k_f) (0.33 mc (db) and 386K)

Moisture content (db)			Temperature (K)			Material constant (k_f)			ER (simulated)		
Mean	SD	CV(%)	Mean	SD	CV(%)	Mean	SD	CV(%)	Mean	SD	CV(%)
0.33	**0.0022**	**0.67**	**386**	**0.5312**	**0.64**	**1**	**0.02**	**2**	**2.09**	**0.37**	**17.83**
0.33	0.0022	0.67	386	0.5312	0.64	1	0.01	1	2.04	0.43	21.15
0.33	0.0022	0.67	386	0.5312	0.64	1	0.03	3	2.08	0.41	19.87
0.33	0.0022	0.67	386	0.5312	0.64	1	0.05	5	1.86	0.33	17.91
Experimental values for expansion ratio of extrudates (30 pieces)									3.06	0.19	6.31

3.5 Conclusions

The mechanistic and stochastic model results were compared with the experimental and literature values. The simulated values for expansion ratio deviated from the experimental values, possibly due to the difference in material properties that were input in the model and the material properties of the corn meal which was used for validation. However, the trend of expansion ratio for both simulated and experimental values at different processing conditions was similar. The stochastic model was useful in conducting a sensitivity analysis to rank the input parameters depending on their impact on the variability in the product characteristics such as expansion ratio. In this study, die temperature was found as the most prominent factor impacting the variability in expansion ratio. In-barrel moisture content also affected the

variability in expansion ratio considerably; however, material constant in consistency index equation did not have a considerable effect on the variability of expansion ratio.

References

Alavi, S.H., Rizvi, S.S.H. and Harriott, P. (2003). Process dynamics of starch-based microcellular foams produced by supercritical fluid extrusion. I: model development. Food Research International, 36, 309-319

Agbisit, R., Alavi, S., Cheng, E., Herald, T & Trater, A. (2007). Relationships between microstructure and mechanical properties of cellular cornstarch extrudates. Journal of Texture Studies, 38, 199-219.

Babin, P., Della Valle, G., Dendievel, R., Lourdin, D. & Salvo, L. (2007). X-ray tomography study of the cellular structure of extruded starches and its relations with expansion phenomenon and foam mechanical properties. Carbohydrate Polymers, 68, 329-340.

Bouzaza, D., Arhaliass, A., & Bouvier, J.M. (1996). Die design and dough expansion in low-moisture extrusion cooking process. Journal of Food Engineering, 29(2), 139-152.

Camire, M.E., King, C.C., & Bittner, D.R. (1991). Characteristics of extruded mixtures of cornmeal and glandless cottonseed flour. Cereal Chemistry, 68(4), 419-424.

Cheng, E.M., Alavi, S., Pearson, T., & Agbisit, R. (2007). Mechanical-acoustic and sensory evaluations of cornstarch-whey protein isolate extrudates. Journal of Texture Studies, 38, 473-498.

Chinnaswamy, R. and Hanna, M.A. (1988). Optimum extrusion-cooking conditions for maximum expansion of corn starch. Journal of Food Science, 53(3), 834-836

Della Valle, G., Vergnes, B., Colonna, P. & Patria, A. (1997). Relations between rheological properties of molten starches and their expansion behavior in extrusion. Journal of Food Engineering, 31, 277-296.

Fan, J., Mitchell, J.R., & Blanshard, J.M.V. (1994). A computer simulation of the dynamics of bubble growth and shrinkage during extrudate expansion. Journal of Food Engineering, 23, 337-356.

Fan, X., Meng, Z., Zhou, J., Xu, W., Xiang, H., & Yang, G. (2012). Investigation of bubble growth in extrusion expansion of cornstarch with CFD method. International Journal of Food Engineering, 8(2), article 13.

Feyissa, A.H., Gernaey, K.V., & Nissen, J.A. (2012). Uncertainty and sensitivity analysis: Mathematical model of coupled heat and mass transfer for a contact baking process. Journal of Food Engineering, 109, 281-290.

Karkle, E.L., Alavi, S., & Dogan, H. (2012). Cellular architecture and its relationship with mechanical properties in expanded extrudates containing apple pomace. Food Research International, 46, 10-12.

Lai, L.S., & Kokini, J.L. (1991). Physicochemical changes and rheological properties of starch during extrusion (A review).Biotechnology Progress, 7, 251-266.

Limpert, E., Stahel, W.A., & Abbt, M. (2001). Log-normal distributions across the sciences: keys and clues. American Institute of Biological Sciences, 51(5), 341-352.

Marek, R. & Götz, W. (1995). Numerische lösung von partiellen differentialgleichungen mit finiten differenzen. Moreno-Verlag.

Moraru, C.I. & Kokini, J.L. (2003). Nucleation and expansion during extrusion and microwave heating of cereal foods. Comprehensive Reviews in Food Science and Food Safety, 2, 147-165.

Owusu-Ansah, J., van de Voort, F.P., & Stanley, D.W (1983). Physico-chemical changes in cornstarch as a function of extrusion variables. Cereal Chemistry, 60(4), 319-324.

Parkert,R., Ollett, A.L., Lai-Fook, R.A., & Smith, A.C. (1989). The rheology of food ‘melts’ and its application in extrusion processing. In rheology and food biological and pharmaceutical materials,ed. R.E. Carter. Elsevier, London.

Rahman, M.S. (2001). Toward prediction of porosity in foods during drying: A brief review. Drying Technology, 19(1), 1-13.

Schwartzberg, H.G., Wu, J.P.C., Nussinovitch, A., & Mugerwa, J. (1995). Modelling deformation and flow during vapor-induced puffing. Journal of Food Engineering, 25, 329-372.

Trater, A.M., Alavi, S., & Rizvi, S.S.H. (2005). Use of non-invasive X-ray microtomography for characterizing microstructure of extruded biopolymer foams. Food Research International, 38, 709-719.

Van der Lijn, J. (1976). Simulation of heat and mass transfer in spray drying. PhD thesis, Agricultural university of Wageningen, The Netherlands, pp 77-80.

Wang, L., Ganjyal, G.M., Jones, D.D., Weller, C.L.,& Hanna, M.A. (2005). Modeling of bubble growth dynamics and nonisothermal expansion in starch-based foams during extrusion. Advances in Polymer Technology, 24(1), 29-45.

Zeleznak, K.J. and Hoseney, R.C. (1987). The glass transition in starch. Cereal Chemistry, 64(2), 121-124.

Chapter 4 - Conclusions and Future Work

A mathematical model was developed to understand the expansion and shrinkage phenomena taking place during extrusion processing and to capture the variability in output or product characteristics as a result of variability in input parameters using a stochastic interface.

4.1 Background of the study

The mechanistic model was developed at the microscopic (individual bubble) as well as macroscopic level (extrudate). This deterministic part of the model formed backbone of overall stochastic modeling approach and to develop this model, expansion phenomenon from the popcorn puffing model (Schwartzberg et al., 1995) and shrinkage phenomenon from supercritical fluid extrusion model (Alavi et al., 2003) were adapted. The uniqueness of this approach was to model shrinkage phenomenon for steam-based extrusion which takes place at higher temperatures as compared to supercritical fluid extrusion where the expansion model was kept same as vapor induced puffing in a popcorn system.

The code developed in Visual Basic for supercritical fluid extrusion was provided and the current model was based on this code. A fraction of code written for supercritical fluid extrusion was altered in order to model the steam based extrusion and some new coding was added for the development of stochastic interface.

4.2 Thermal infeasibilities in the simulated results and major modeling flaws

The mechanistic model is useful in understanding the dynamics of different parameters involved in the process of expansion and shrinkage. However, the current model does not capture expansion or collapse phenomenon as the simulated dynamics of certain parameters obtained

from mechanistic model are thermodynamically infeasible. This invalidates the results from stochastic model which was based on mechanistic model. For instance, at processing condition of 0.33 mc(db) and 386K, cycling in pressure difference and accompanying change in bubble radius obtained from simulation(figure A-1, appendix A) are thermodynamically not feasible and reflect fundamental defect in the current modeling approach. Some other results that reflect this flaw in modeling approach include discontinuity in macroscopic temperature (figure A-3, appendix A) and fluctuations in moisture content of microscopic shells (figure A-4, appendix A). For the same processing condition, anomalous behavior was observed for simulated dynamics of cell wall thickness (figure A-2, appendix A). These instabilities are related to fundamental flaws in the modeling approach involving computation of macroscopic temperature, microscopic moisture and possibly coupling of heat and mass transfer at microscopic and macroscopic levels.

4.3 Discussion on addressing flaws in the current modeling approach

The mechanistic model which formed the basis of overall stochastic modeling approach resulted in several parameter dynamics that are thermodynamically infeasible. Hence, to obtain a better understanding of possible reasons and approaches to address these fundamental flaws in the current model, incorrect parameter dynamics as well as entire coupled microscopic and macroscopic modeling approach were further examined.

Upon investigating the structure of entire model, it was observed that time step (Δt) is a major contributor in stability while computing non-linear partial differential equations by numerical techniques. In the current model, Δt is computed based on mass transfer taking place in spherical shells of the microscopic model. It uses the Von-Neumann or the Fourier stability condition such that ($\alpha \Delta t_m / \Delta x^2 \leq ½$). This concept of largest value of time (Δt_m) that can provide computational stability, Δt_m was adapted from popcorn model and the actual time step used in

the current model was $\Delta t = 0.7^* \Delta t_m$. The discretization term Δx used in calculating this time step was computed based on the outermost layer of concentric spherical shells and was taken as $(L-r_N)^2$. The same time step was then used for numerically computing heat and mass transfer equations at macroscopic level in the model. It is possible that due to multiple partial differential equations involved in the model, it forms a system of stiff equations (Kass, M., 1997, Fasshauer, G., 2007) such that the stability condition which satisfies one set of equations might not be sufficient for the other set of equations. This can lead to fluctuations or instabilities in parameter dynamics predicted by the model. Since, in current model, all systems of equations are interdependent which can possibly lead to a complex feedback error, a better approach would be to consider a fixed minimum time step for achieving stability rather than using an adaptive method for calculating Δt. This is because the adaptive approach for calculation of Δt does not consider all sets of equations and the minimum requirement of Δt could vary with time for different systems of equations. However, while deciding upon the time step, it should be noted that very small values of Δt can degrade the accuracy of results where the error can be very large (report by Buttsworth, D.R., University of Oxford). These thermal infeasibilities in parameter dynamics and possible solutions are discussed in following sections.

4.3.1 Fluctuations in the macroscopic temperature

Temperature in current process is expected to decrease gradually as product comes out of the die, however, a fluctuation was observed in average temperature value which is thermodynamically infeasible. This fluctuation in temperature occurred after the shrinkage phase started. Hence, to find out the starting point and location of this fluctuation, temperature dynamics for different macroscopic cylindrical shells was observed. It was found that the temperature reduced gradually in all other macroscopic cylindrical shells except the temperature

in outermost shell which fluctuated (figure A-5, appendix A). This eventually resulted in the fluctuation in average value of temperature. In simulated results from deterministic model, it was observed that for the processing condition of 0.33 mc(db) and 386 K, shrinkage phenomenon started at around 1.27 seconds and an increase in outermost layer started at around 1.288 seconds. Since temperature in other layers was decreasing gradually, the temperature increase in outermost layer T_{Nb+1} was observed as increase in average temperature at around 1.29 seconds. Upon observing the numerical form of temperature equation used for computing heat transfer in outermost layer, it was found to be a function of Biot number (N_T) and the adjacent layer (T_{Nb}). It should be noted that for equations system of heat transfer in macroscopic model, stability was decided by the term M_T ($M_T = \Delta x_2^2/(\alpha_t \times \Delta t)$). M_T which has same expression as that of the Fourier number should be greater than equal to 4 for stability (Geankoplis, 1993) and this stability condition can be achieved by setting up appropriate discretization (Δx_2) and Δt. M_T could be made larger by either increasing Δx_2 or decreasing Δt. If Δt is very small then this condition is satisfied, however, suitability of Δx_2 gets overlooked in the process.

In current model, Δt was computed based on the system of spherical microscopic shells and the same value was then transferred to cylindrical macroscopic shells. Since, Δt was very small, it satisfied the condition of $M_T \geq 4$; however, no adjustment was made to Δx_2. While computing T_{Nb+1}, this Δx_2 played an important role and if not suitable enough, it could lead to fluctuations as observed in the current model. Sample calculations were done to observe the impact of Δx_2 and T_{Nb} on the value of temperature in outermost layer. After the shrinkage started, expansion ratio (ER) reduced leading to a decrease in the value of Δx_2 ($\Delta x_2 = (d_{ex} * ER^{1/3})/(2*(N_b-1))$). Also decrease in ER resulted in an increase in value of k_{eff} (because of decrease in ϵ ($\epsilon = 1-1/ER$)). As a result, it led to a decrease in value of Biot number (N_T) which increased the value of

T_{Nb+1}. Eventually a decrease in the value of T_{Nb} compensated for the decrease in N_T (sample calculations provided in appendix B, table 2) and the final value of temperature decreased. From these sample calculations, it can be seen that when the value of N_T decreased while T_{Nb} was constant, the value of temperature increased, however, when value of T_{Nb} was also decreased, it compensated for the decrease in N_T and as a result the value of T_{Nb+1} decreased.

In order to prevent this instability leading to thermodynamically infeasible results, apart from assigning a value of Δt suitable for all systems for equations, value of Δx_2 should also be checked. A possible way to do that would be checking stability condition at the boundary layer for heat transfer (Marek & Götz, 1995) given by

$$F_o \leq \frac{1}{2(2+Bi)}$$

where F_o is the Fourier number ($F_o = \frac{\alpha_t \times \Delta t}{\Delta x_2^2}$) and Bi is the Biot number ($Bi = \frac{h \times \Delta x_2}{k_{eff}}$).

Hence, it should be checked whether this condition is satisfied by Δx_2 and Δt at all times which could possibly remove the stability error in temperature dynamics.

4.3.2 Microscopic moisture fluctuations

Microscopic moisture fluctuations were analyzed and it was found that the moisture content increased in innermost layer before the spike in moisture of outer layer was observed. The dynamics for moisture content in different layers before the spike was observed in outer layer are given in figure A-6, appendix A. It was observed that the moisture content in the innermost layer was constantly increasing before fluctuations started, however moisture was stable in other layers. Hence, this increase in moisture in innermost layer eventually led to increase in moisture in intermediate layers since moisture was transferred to the intermediate layer from both the outer layers as well as the inner layers. Later on, this increase in moisture

was propagated to outer layers and the outcome was observed as thermodynamically infeasible spike in Xwi(N) where moisture content became higher than the initial value.

4.3.2.1 Role of time step (Δt)

The mass transfer equations governing the dynamics of moisture content in spherical shells of microscopic model were investigated for both the intermediate layers as well as boundary conditions. It was found that certain stability criterions were defined in the popcorn model for achieving computational stability. Once such criterion was Δt which was defined based on discretization in the outermost layer $(L\text{-}r_N)^2$. Schwartzberg et al., 1995 mentioned that Δt_m occurred while computing ΔX_{ws}, however, since the current model was based on a different system as compared to the popcorn system; it could be useful to investigate how Δt_m varies if it is defined based on discretization in core or inner layer of spherical shells. For example, results could vary if Δt_m is defined as $\Delta t_m = \frac{(r_1 - R)^2}{2 * D_{wc}}$) instead. The actual value of Δt was taken as $0.7 * \Delta t_m$ in the model which might not be sufficient for different systems of equations at certain time points. Hence, stability of entire system could be improved by lowering the value of time step. Also, it was found that Δt increased considerably as well as fluctuated towards the end of simulation process (figure A-7, appendix A) which could also lead to instability in entire system comprising of different sets of heat and mass transfer equations. It might satisfy one system but might lead to divergence in other systems. It can be observed from figure A-7 that fluctuations in Xwi(N) and Δt were encountered around the same time. Hence, the rate of change of Δt should be a matter of investigation and a good way would be to set a suitable minimum fixed value of Δt instead of using the adaptive method to compute Δt based on a particular system since the system is greatly interdependent and has high chances of feedback instability.

4.3.2.2 Role of Δr

Another possible reason for these fluctuations could be the definition of Δr at different time points based on the dynamics of bubble and more specifically the radius of innermost shell and pore radius. In the popcorn model, this criterion was defined as

$$\Delta r = \frac{R}{3} when\ (r_1 - R > R)$$

$$\Delta r = (r_1 - R) when\ ((r_1 - R) < R)$$

This definition of Δr involves a point of discontinuity. Since Δr controls the dynamics of moisture in the core ΔX_{wc} which in turn affects moisture dynamics of rest of the layers, instabilities could arise if Δr is not suitably defined. Figure A-7 appendix A, represent the dynamics of Δr for processing condition of 0.33 mc(db) and 386K. A spike was observed in X_{wc} when the value of Δr became suddenly very low, almost approaching zero. Hence a possible solution could be to define Δr such that there are minimum fluctuations in Δr which could possibly help in achieving stability in the microscopic moisture dynamics.

4.3.2.3 Role of coupling of microscopic and macroscopic heat and mass transfer

The coupling effect of microscopic and macroscopic models was also tested to investigate if thermodynamically infeasible results could be due to the way these two levels of model are coupled. The mass transfer of microscopic and macroscopic models were decoupled by not subtracting the average moisture loss in macroscopic shells from microscopic shells and keeping mass transfer in two systems independent (figure A-8, appendix A). In this case, multiple fluctuations in outermost microscopic shell were not observed, however, instability in moisture content of outermost microscopic shell was still observed where moisture content spiked to a value greater than the initial value. This indicated that coupling of these two levels of

the model might not be a major cause of these instabilities. Figure A-8 represents the dynamics of moisture content in different layers and also dynamics of Δt and Δr in the decoupled model. It can be observed that fluctuations in Δt and Δr still occurred and instabilities in moisture content were observed around the same time when these fluctuations occurred.

4.3.3. Cycling of Pressure difference

Pressure difference is dependent on different components and vapor pressure is one of the major pressure components driving the expansion process. Vapor pressure is dependent upon temperature and moisture content of the product. Higher temperature and higher moisture content in the inner most microscopic shell results in higher vapor pressure (sample calculations provided in appendix B, table 1, for vapor pressure as a function of temperature and moisture content of the inner most microscopic shell, X_{wc}). It was found that for processing condition of 0.33mc(db) and 386K, when temperature increased after shrinkage started, the moisture content in inner most microscopic shell (X_{wc}) was still decreasing and as a result, increase in vapor pressure was not observed. However, when moisture content in innermost microscopic shell reached to a minimum and temperature was still increasing, it resulted in an increase in vapor pressure. Also, the increase in moisture content of the inner most layer when temperature value was decreasing, again led to an increase in vapor pressure. At this time, other components of pressure in the opposite direction were also increasing but at a slower pace as compared to vapor pressure. As an outcome, the pressure difference value became less negative and reached zero. Later, with further reduction in temperature (reducing the vapor pressure) and increase in the value of other pressure components in opposite direction, the resultant pressure was negative again which was observed as cycling of pressure difference. Similar observation was made for the other processing condition of 0.23 mc (db) and 405.09K. A slight increase in vapor pressure

was observed for this processing condition as well but in this case, when the temperature increased, moisture content in innermost microscopic shell decreased very rapidly and net pressure difference in inward direction did not become significantly less negative. Hence it did not reach zero and the cycling of pressure difference was not observed in this case.

Figure A-9 represents dynamics of pressure difference for the processing condition of 0.33mc (db) and 386K during the time points when cycling of pressure difference occurred. It can be seen that the temperature increased first followed by X_{wc} which resulted in an increase in vapor pressure and less negative value of ΔP. Hence, it is possible that the stability in macroscopic temperature and microscopic moisture dynamics can help in preventing this thermodynamically infeasible dynamics of pressure difference. Hence, to summarize, following steps can be taken to prevent the instability in the model which results in thermodynamically infeasible parameter dynamics:

1) Δt should be defined such that it promotes stability in different equation systems. Other definitions of Δt such as those including discretization based on the inner shells rather than outer shells can be tried. However, it would be most suitable to define a fixed value of Δt rather than using the adaptive approach which would not only reduce the varying parameters but also promote stability in the stiff equation system of the current model.
2) A check must be kept on the value of Δx_2 based on the stability condition, so that temperature fluctuations in the boundary layer can be prevented.
3) Discontinuities in Δr should be checked and it should be defined appropriately in order to promote stability in the dependent parameter dynamics.
4) In general, there are several conditional equations used in the model such as definition of flow yield stress, elastic modulus etc. which have a point of discontinuity depending on

moisture content in microscopic shells. Coefficients used in these equations and switching points should be decided on suitably to prevent discontinuities which affects the stability of the system and leads to random fluctuations in simulated results.

4.4 Other limitations of the model and future studies

The mechanistic model had a limitation of temperature and encountered instability for temperatures higher than 410K. The highest temperature at which mechanistic code could execute stably increased from 400K to 410K when number of microscopic shells in the model was increased from 25 to 50. However, increasing the number of microscopic shells greatly increased the computation time and each mechanistic simulation took about 45 minutes to 1 hour depending on computational ability of computer. Further increase in number of microscopic shells led to impractical computational time, for example, a further increase in number of microscopic shells (N = 100) led to computation time of about 24 hours and the computational stability was achieved up to 412K. Hence, within the scope of this thesis, results for different processing conditions have been given for 50 microscopic shells and up to die temperature of 410K. In future studies, methods should be explored for increasing the stability of the model at higher temperatures such as further reduction of computational time step etc.

The results from mechanistic simulations could be made more generalized to different types of extruders if more number of independent variables is input in the model and intermediate parameters are calculated using characteristic equations. For example, die temperature is an input in the current model, however, it depends on several factors such as screw speed, screw roughness, in-barrel moisture content etc. and hence, the die temperature value could differ for different extruders for the same set of processing conditions.

Hence, a more comprehensive modeling could be done to include all independent parameters which will make the application of the mechanistic model more generalized. Also, it was observed that the simulated and experimental values did not match quantitatively and the model under predicted and over predicted the expansion ratio values for certain processing conditions. However, upon plotting trends for expansion ratio, the simulated trend was found similar to the experimental trend with a shift in optimum value. This shift in values could be a result of material properties such as diffusivity, consistency index etc. which were taken from literature. Hence, it would be worthwhile to perform experimentation to derive equations for material properties for the specific material which was used for validation to test the accuracy of the model. Certain equations could be further investigated such as the equation for expansion ratio which is based on the popcorn puffing model and depends on open cell fraction. The constants and coefficients used in that expansion ratio equation were empirically derived for the popcorn system and modifications of those constants to match the material used for validation would further improve the model predictions. Another interesting area for further investigation could be an integration of microscopic and macroscopic level in the mechanistic model. It should be noted that microscopic model is developed for an individual bubble and the dynamics of heat and mass transfer could change depending on location of that individual bubble in entire macroscopic model. Hence, a more generalized approach in defining microscopic and macroscopic systems would make the model sturdier. The model could be broadened from simple starch-based melts to formulations with other components such as proteins, fats etc.

In current study, the mechanistic model was integrated with stochastic interface to understand the impact level of variability in different input parameters on variability in output parameters. Sensitivity analysis was carried out for three selected input parameters by varying

the CV of one parameter and keeping the CV of other two parameters constant. This was done for three processing conditions, taking average values of moisture and temperature from the experimental data. For further studies in this area, a broader range of CV could be tested for these three as well as other parameters during sensitivity analysis. Depending on the computational ability, greater number of mechanistic simulations could be carried out in one stochastic simulation which would provide better clarity of the process.

References

Alavi, S.H., Rizvi, S.S.H. and Harriott, P. (2003). Process dynamics of starch-based microcellular foams produced by supercritical fluid extrusion. I: model development. Food Research International, 36, 309-319

Department of Engineering Science, University of Oxford. (OUEL report number 2130/97). A finite difference routine for the solution of transient one dimensional heat conduction problems with curvature and temperature-dependent thermal properties. D.R. Buttsworth.

Fasshauer, G. (2007). Lecture on stiff equations. Personal collection of G. Fasshauer. Illinois Institute of Technology, Chicago, IL.

Geankoplis, C.J. (1993). Transport processes and unit operations. (3rd ed.). Geankoplis, Englewood Cliffs, NJ: Prentice Hall.

Kass, M. (1997). Lecture on An Introduction to Physically Based Modeling: Energy Functions and Stiffness. Personal collection of M. Kass. Carnegie Mellon University, Pittsburgh, PA.

Marek, R. & Götz, W. (1995). Numerische lösung von partiellen differentialgleichungen mit finiten differenzen. Moreno-Verlag.

Schwatzberg, H.G., Wu, J.P.C., Nussinovitch, A., & Mugerwa, J. (1995). Modelling deformation and flow during vapor-induced puffing. Journal of Food Engineering, 25, 329-372.

Appendix A - Charts representing thermodynamic instabilities in the mechanistic model

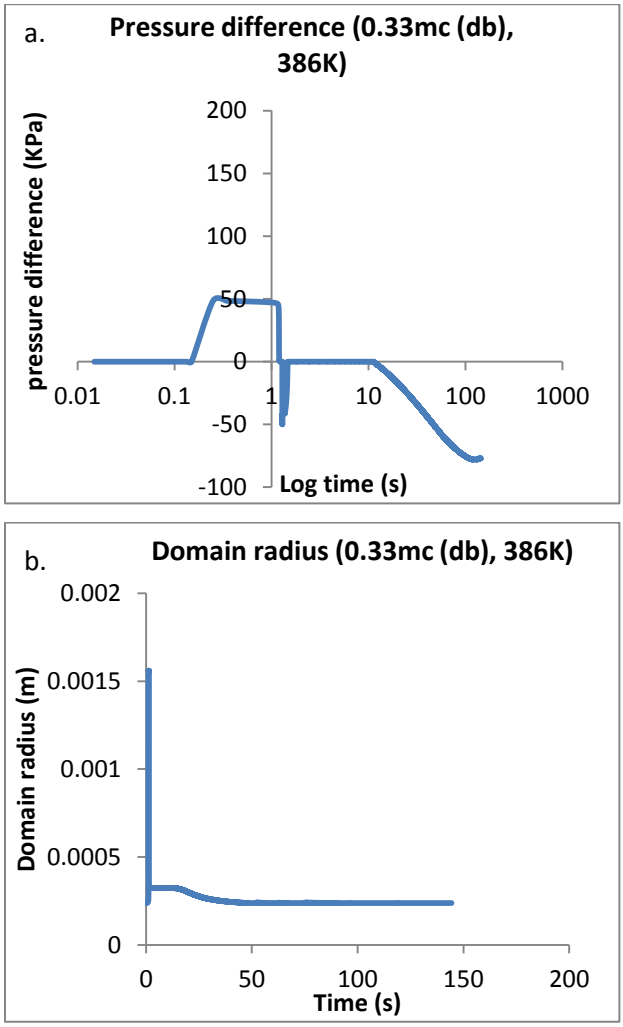

Figure A-1 Dynamics for (a.) pressure difference and (b.) resulting bubble growth radius and shrinkage for 0.33mc(db)

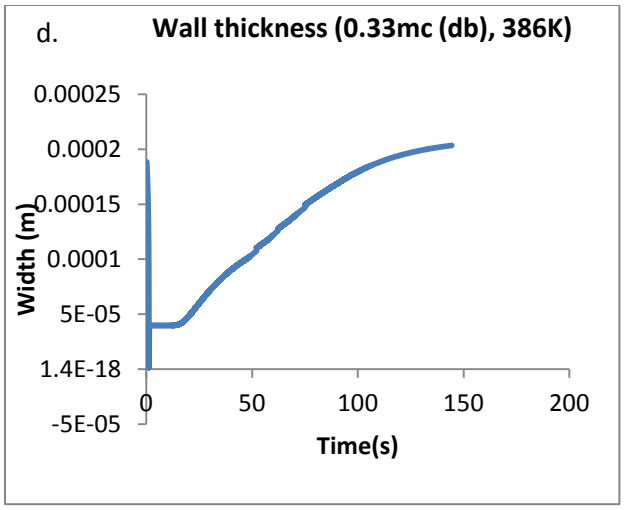

Figure A-2 Dynamics of cell wall thickness of the bubble for 0.33 mc(db)

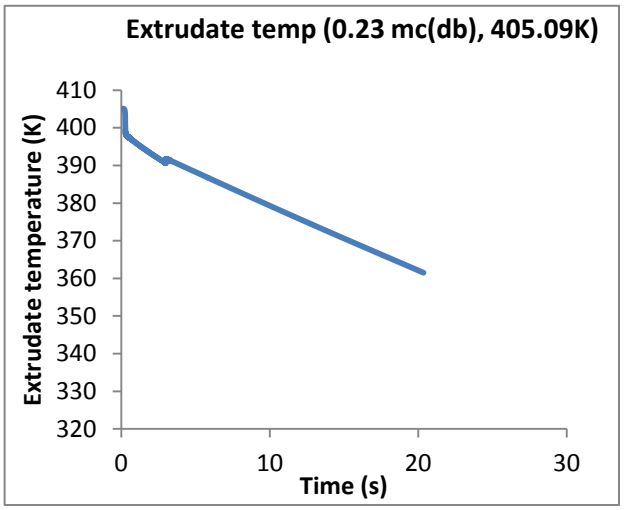

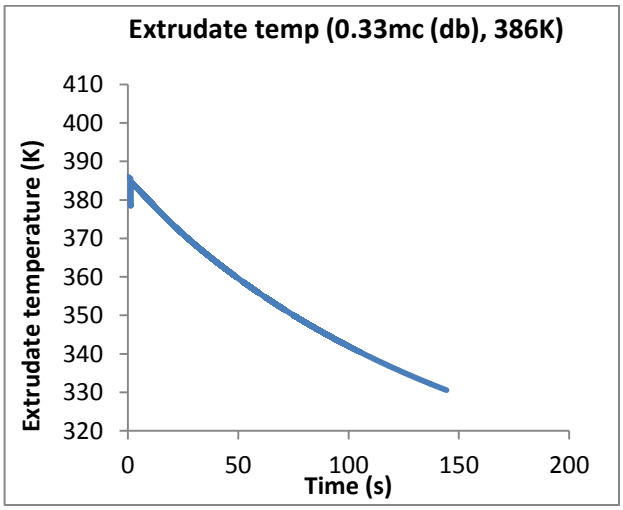

Figure A-3 Dynamics of the temperature of the extrudate with time for 0.23mc(db) and 0.33 mc(db)

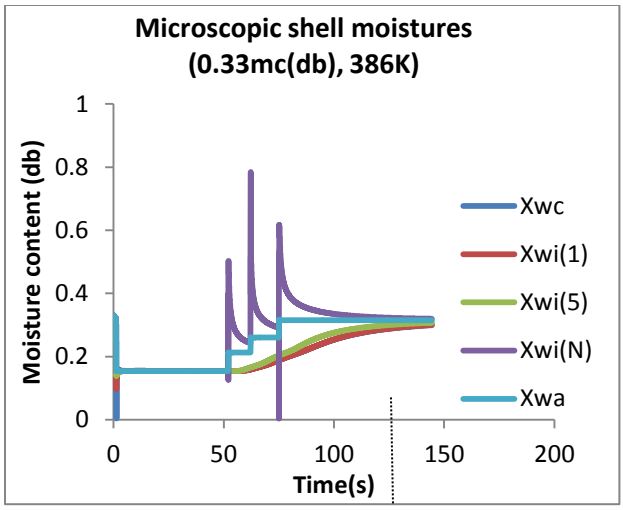

Figure A-4 Microscopic shell moistures for different layers with time for 0.33 mc(db)

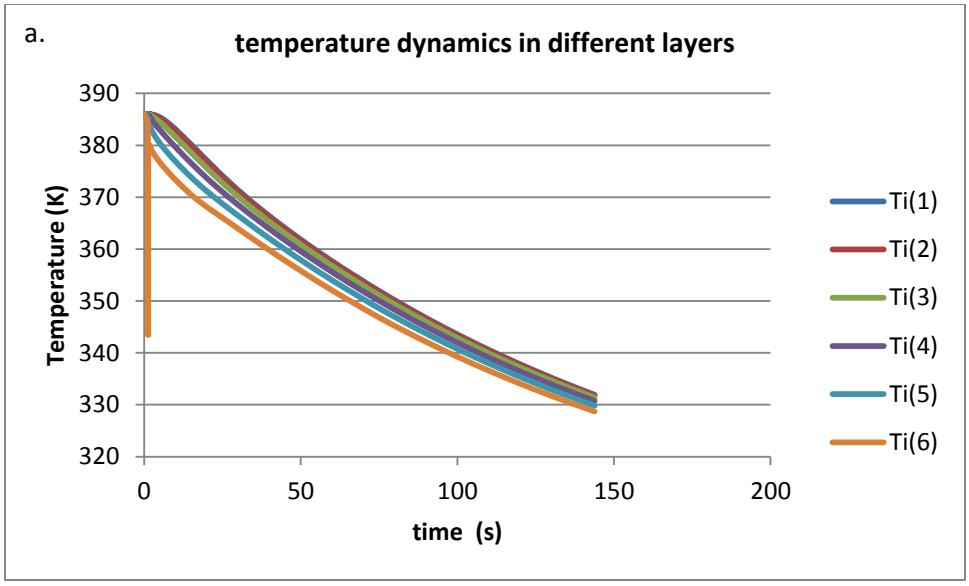

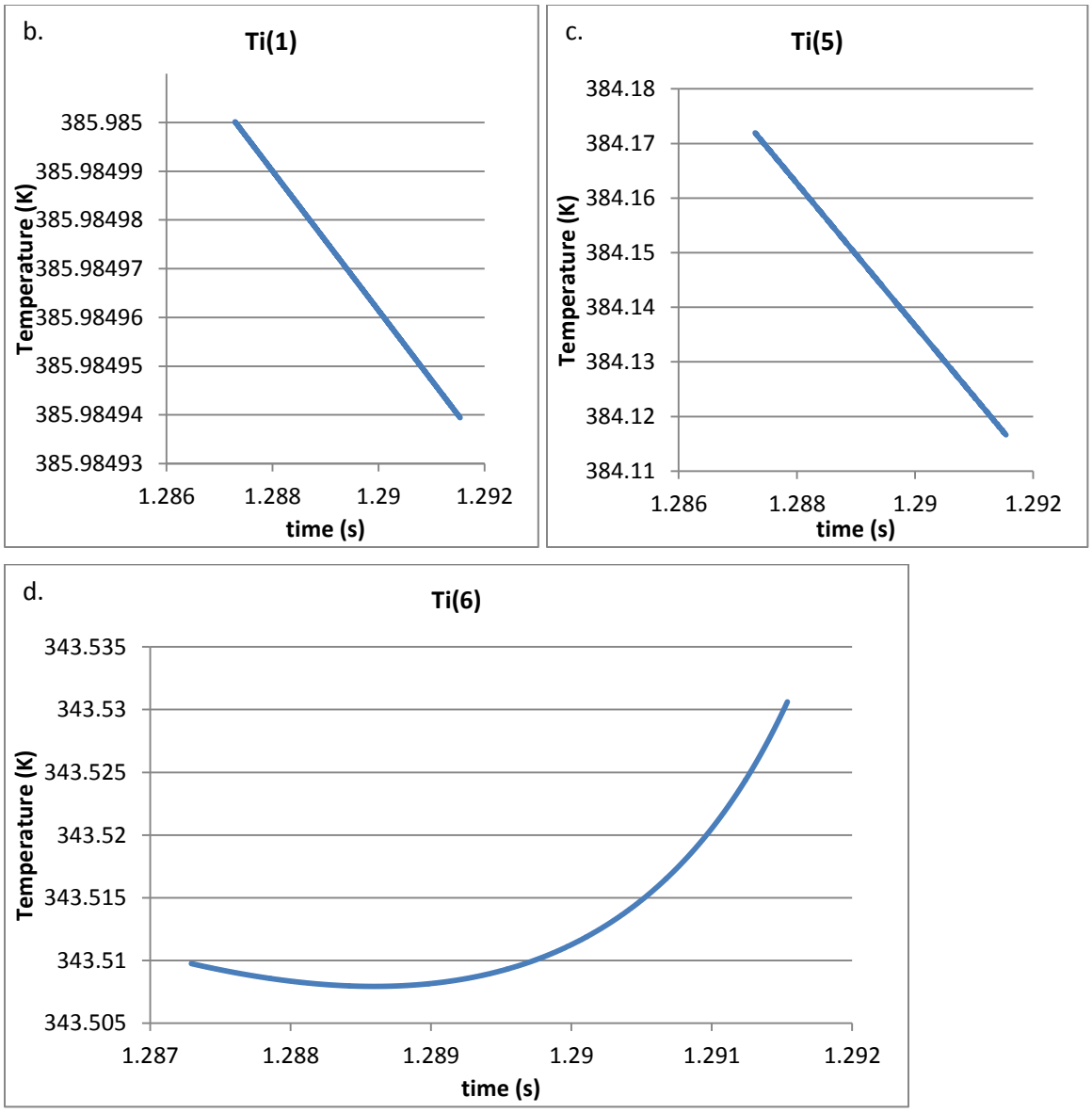

Figure A-5 (a)Temperature dynamics in different layers of macroscopic shells. (b.) temperature dynamics in the inner most layer when the fluctuation occurs. (c.) temperature dynamics in the adjacent layer to the outermost layer when the fluctuation occurs. (d) temperature dynamics in the outermost layer when the fluctuation occurs.

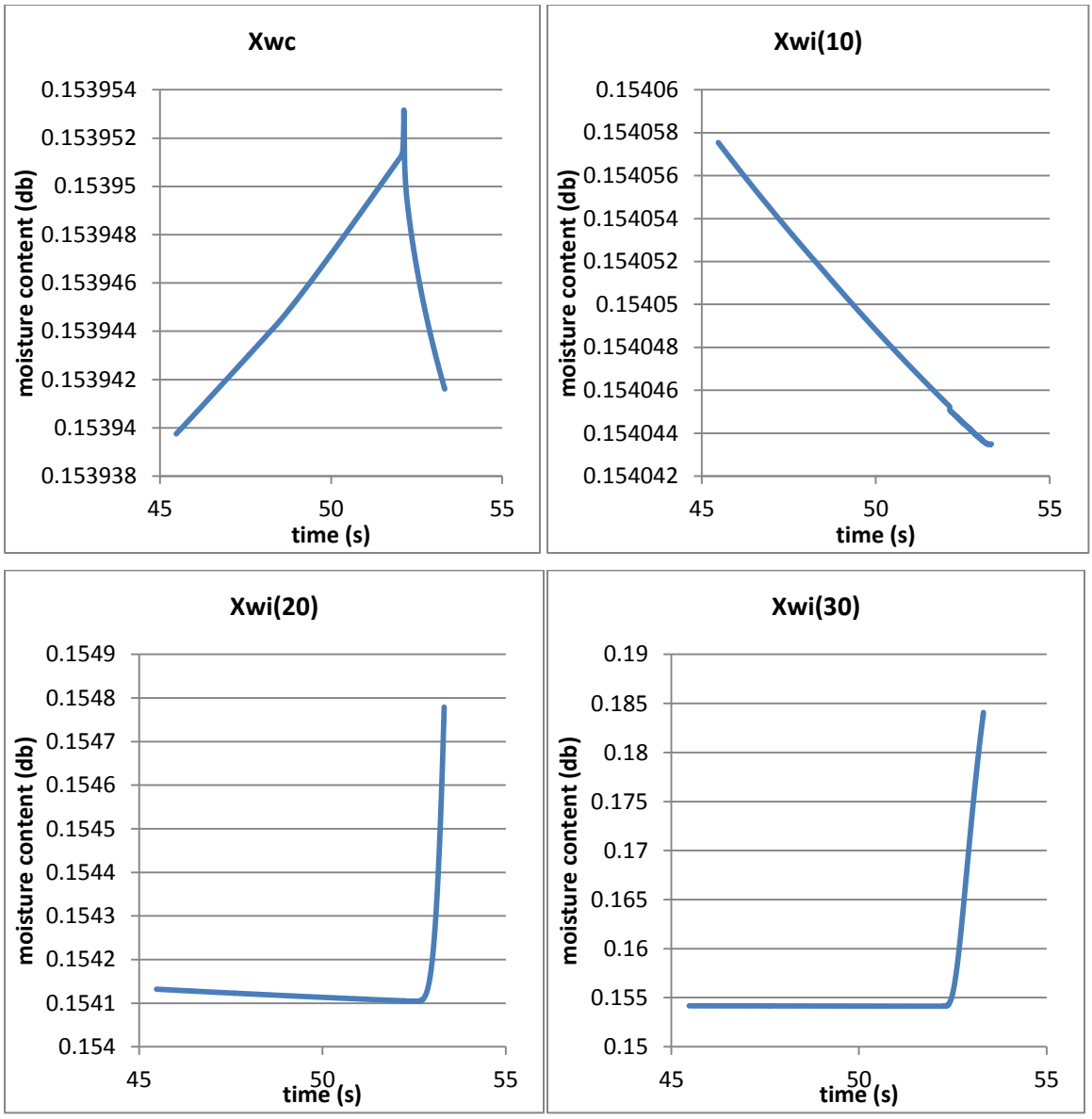
Xwc
0.153954
0.153952
0.15395
0.153948
0.153946
0.153944
0.153942
0.15394
0.153938
moisture content (db)
45
50
55
time (s)
Xwi(10)
0.15406
0.154058
0.154056
0.154054
0.154052
0.15405
0.154048
0.154046
0.154044
0.154042
moisture content (db)
45
50
55
time (s)
Xwi(20)
0.1549
0.1548
0.1547
0.1546
0.1545
0.1544
0.1543
0.1542
0.1541
0.154
moisture content (db)
45
50
55
time (s)
Xwi(30)
0.19
0.185
0.18
0.175
0.17
0.165
0.16
0.155
0.15
moisture content (db)
45
50
55
time (s)

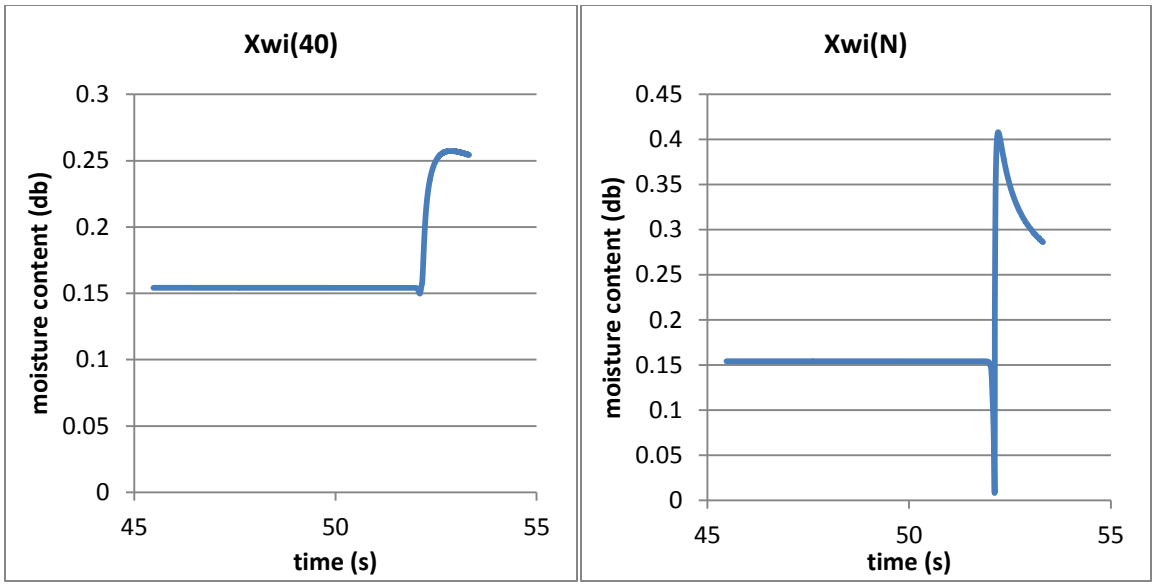

Figure A-6 Dynamics for moisture content in different microscopic shells before observing the spike in Xwi(N).

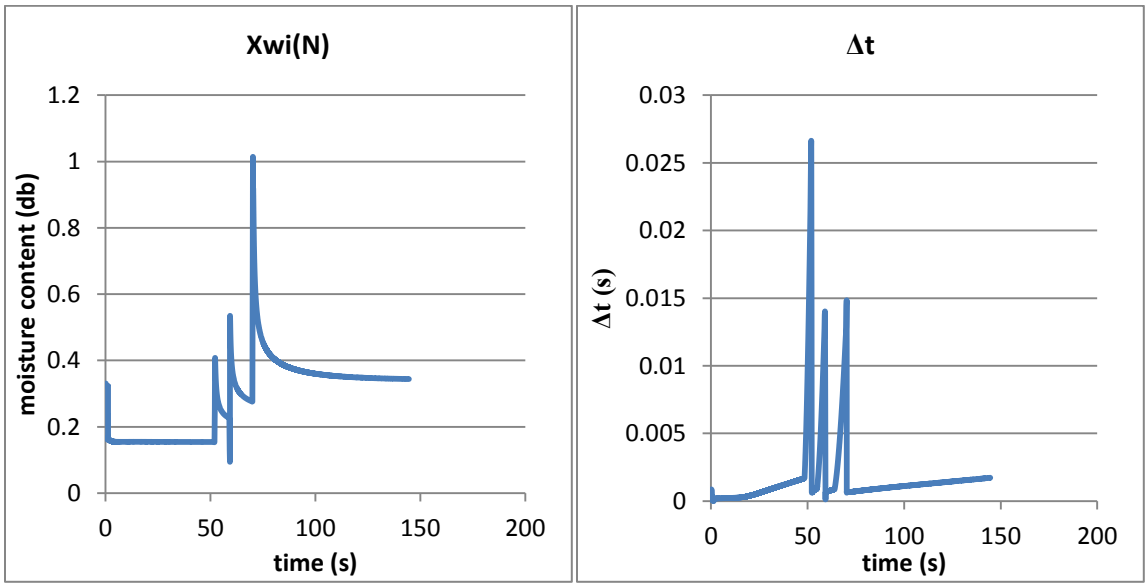

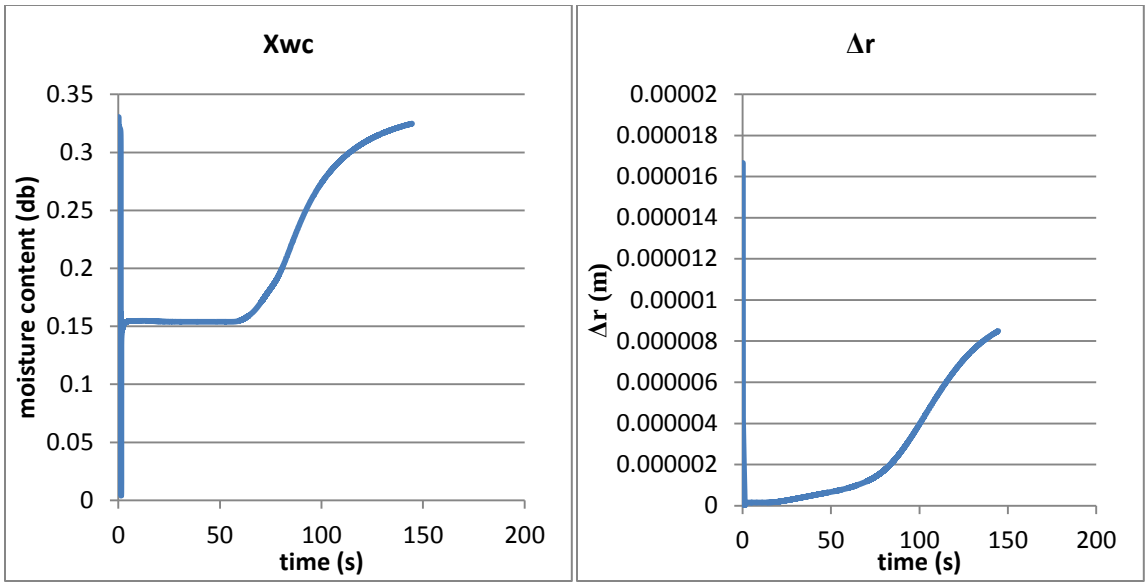

Figure A-7 Dynamics of moisture content in the (a) outermost microscopic shell, (b) Δt (c) innermost microscopic shell (d) Δr

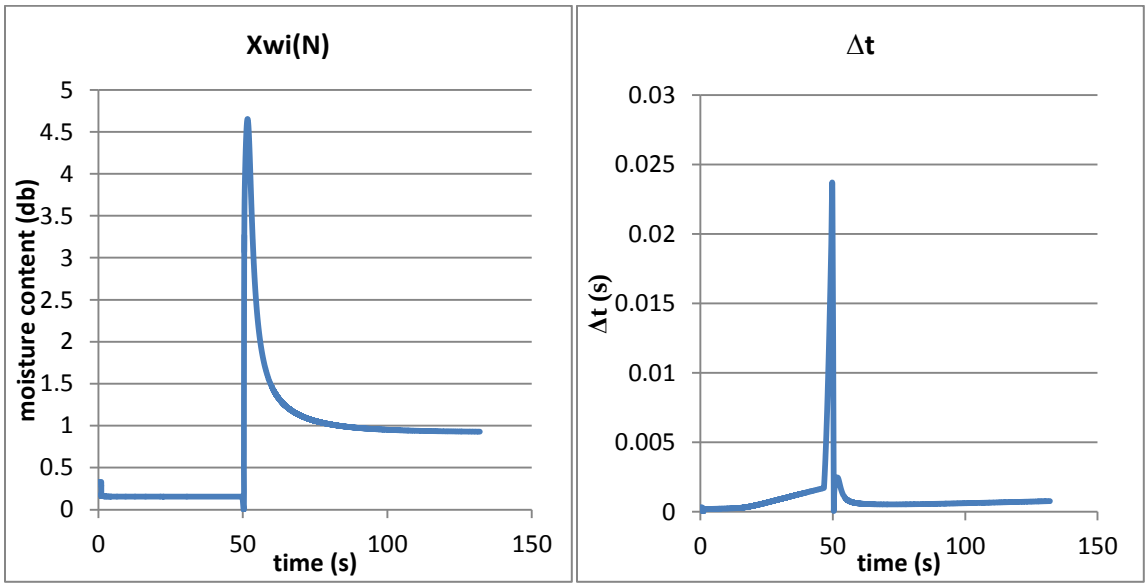

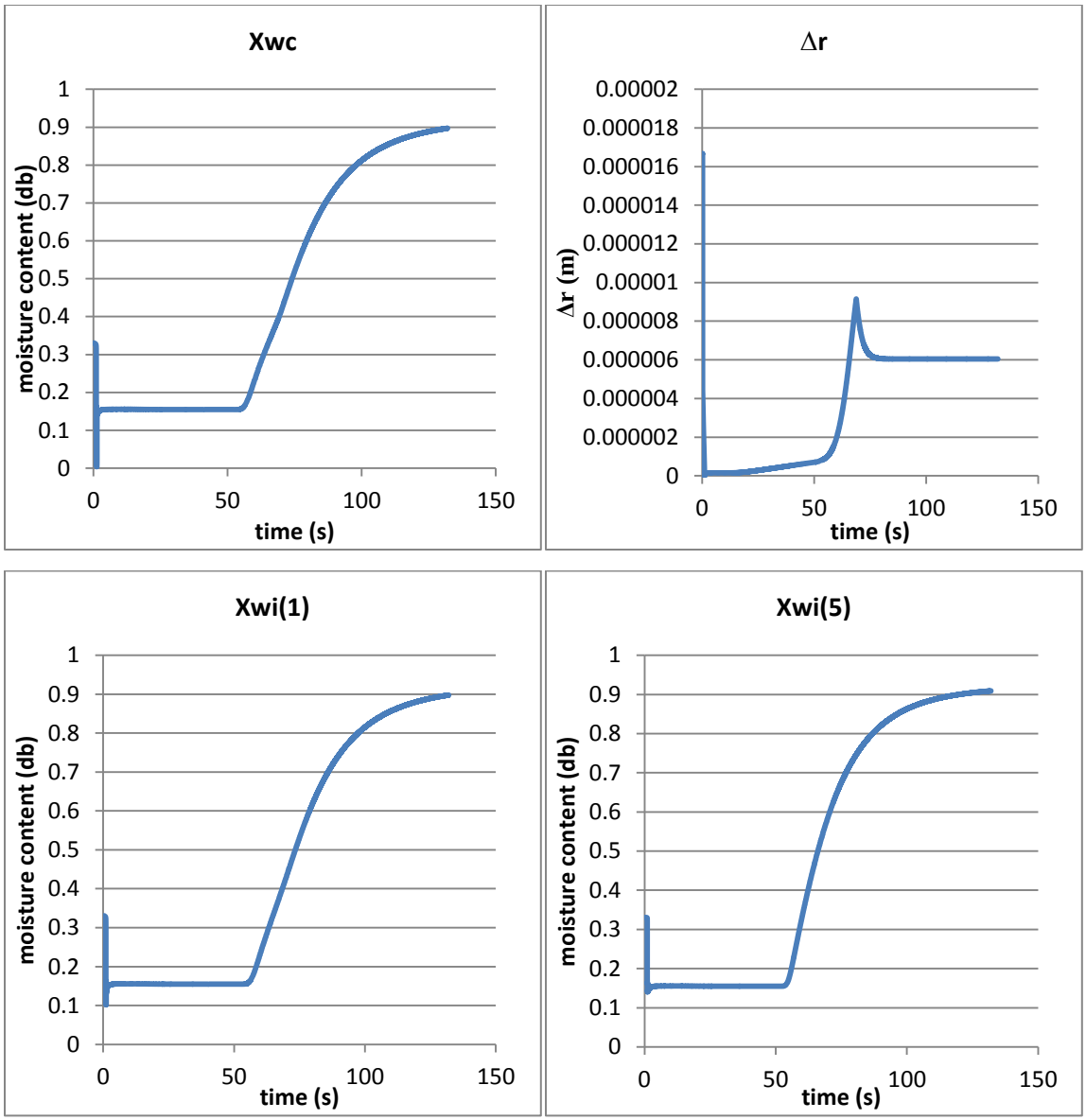

Figure A-8 Dynamics of different parameters for the mechanistic model with decoupled microscopic and macroscopic levels.

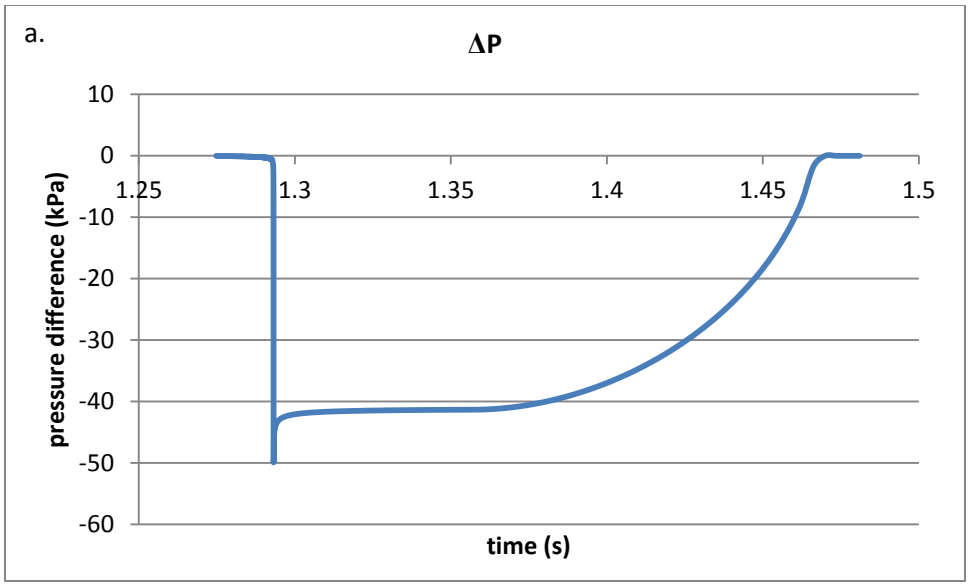
a.
ΔP
10
0
-10
-20
-30
-40
-50
-60
1.25
1.3
1.35
1.4
1.45
1.5
pressure difference (kPa)
time (s)

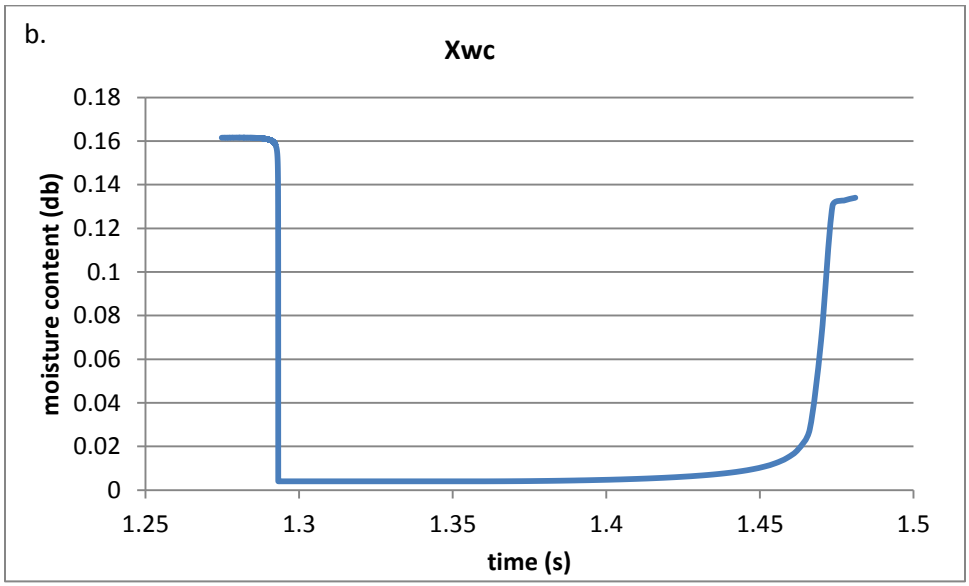
b.
Xwc
0.18
0.16
0.14
0.12
0.1
0.08
0.06
0.04
0.02
0
1.25
1.3
1.35
1.4
1.45
1.5
moisture content (db)
time (s)

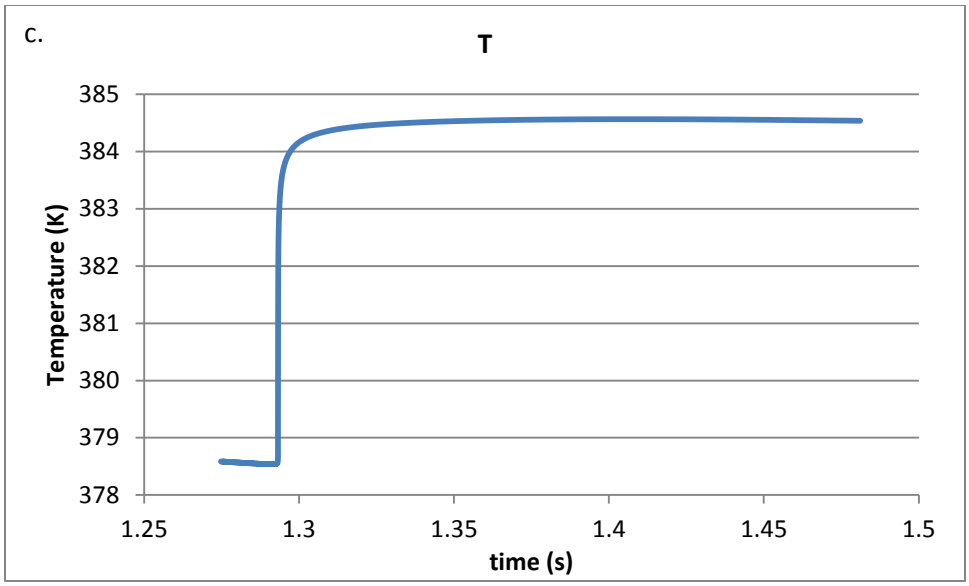

Figure A-9 Dynamics of (a) pressure difference, ΔP (b) microscopic moisture in the innermost layer and (c) temperature during the time when cycling of ΔP occurs.

Appendix B - Sample calculations supporting explanation of thermodynamic infeasibilities

Table B-1 Sample calculation for vapor pressure (as a function of temperature and moisture)

				say Xwc = 0.15		
temp	B= -0.5362 - 0.001394 * T + 2.0474 * (468.9 - T) / (477.42 - T)		temp	a_w= b * Xwc + C * Xwc / (F + Xwc)	P_{wsat} = 1002.2 * Exp(9.43699 - 3867.44 / (T - 43.37))	P_w = a_w*P_{wsat}
379	0.805635146		379	0.81478879	124.4639144	101.4118
380	0.802421819		380	0.815483003	128.7981015	105.0327
381	0.799170754		381	0.816171508	133.2561945	108.7599
				say Xwc = 0.13		
temp	C= 0.2479 + 0.001216 * T		temp	a_w= b * Xwc + C * Xwc / (F + Xwc)	P_{wsat} = 1002.2 * Exp(9.43699 - 3867.44 / (T - 43.37))	P_w = a_w*P_{wsat}
379	0.708764		379	0.796450848	124.4639144	99.12939
380	0.70998		380	0.797203407	128.7981015	102.6783
381	0.711196		381	0.797951005	133.2561945	106.3319
				say Xwc = 0.04		
temp	F= 0.002004 + 0.000003165 * T		temp	a_w= b * Xwc + C * Xwc / (F + Xwc)	P_{wsat} = 1002.2 * Exp(9.43699 - 3867.44 /	P_w = a_w*P_{wsat}

					(T - 43.37))	
379	0.003203535		379	0.396787089	124.4639144	49.38567
380	0.0032067		380	0.39727632	128.7981015	51.16844
381	0.003209865		381	0.397764959	133.2561945	53.00464

Table B-2 Sample calculations to demonstrate effect of values of N_T and T_{Nb} on T_{Nb+1}

$T_{Nb+1} = T_s * N_b * N_T / (0.5 * (2 * N_b - 1) + N_b * N_T) + T_{Nb} * 0.5 * (2 * N_b - 1) / (0.5 * (2 * N_b - 1) + N_b * N_T)$				
T_s=298K, N_b = 6				
N_T	T_{Nb+1} (when T_{Nb} =390K)	T_{Nb}	N_T	T_{Nb+1}
0.0602	384.3304	390	0.0602	384.3304
0.0601	384.3393	389.9	0.0601	384.2454
0.0600	384.3481	389.8	0.0600	384.1604
0.0599	384.357	389.7	0.0599	384.0754
0.0598	384.2719	389.6	0.0598	383.9903

Appendix C - Explanation of model algorithm and fixed input parameter values

Table C-1 The input values of the parameters that were kept constant

Parameter	Value	Unit
N_b (Number of macroscopic shells)	6	
N (Number of microscopic shells)	50	
Ps (Atmospheric pressure, fluid pressure after melt exits the die)	101.325	KPa
m_f (flow rate of the melt)	0.007292	Kg/s (wet+dry feed rate)
mc (initial value of moisture content)	0.2297	g water/ g dry matter (not constant input in stochastic model)
T_o (Initial temperature of the melt)	405.0985	K (not constant input in stochastic model)
R_o (Initial bubble radius)	5.00E-05	m
σ (Surface tension at pore-shell surface)	2.00E-06	kN/m
d_{en} (diameter at die entrance)	1.70E-02	m
d_{ex} (diameter at die exit)	4.20E-03	m
L_d (die dimension)	1.46E-02	m
L_{d1} (die dimension)	7.30E-03	m
M (=ρ_s/N_{cell})	5.80E-08	kg(mass per domain)
h (convective heat transfer coefficient)	10.00	$W/m^2.K$
n (flow behavior index)	0.4	
Ψ (spread factor in open cell fraction distribution)	0.75	
K_factor (coefficient in equation of consistency index)	1	(not constant input in the stochastic model)
D_factor (coefficient in equation of diffusivity)	1	
E_r (constant in equation of E_b)	10	kPa
τ_r (coefficient in the equation of τ_o)	0.1	kPa

β_f (coefficient in the equation of E)	17	
ρ_s (density of dry unexpanded material)	1.16E+00	g/cm^3
N_{cell} (Cell density)	2.00E+04	$cells/cm^3$
k_{xc} (Mass transfer coefficient of water in starch matrix)	1.00E-05	

For stochastic model, three selected parameters were varied, namely, temperature, initial moisture content and material constant in consistency index equation. Depending on the processing condition, up to 5% of coefficient of variation was used for each of these three input parameters to generate the distribution (set of values) for input in the mechanistic model.

Explanation of the algorithm (figure C-1)

Initially the input values were taken into the model.

"calculate pressure at the entrance of the die by backward flow"

Starting with the atmospheric pressure at the end/exit of the die, the pressure at the entrance of the die was calculated

"calculate pressure drop as the fluid proceeds through the die"

Time and distance was initialized to zero, change in distance as the melt flows through the die (dx) was calculated by multiplying ($v_x * \Delta t$) until the exit of the die.

"Calculate L, D, and K for different layers"

Parameters such as consistency index, diffusivity for the microscopic shells, domain radius etc. were calculated. Since these properties were dependent on temperature, moisture and bubble radius which did not change until die exit, there values remained same until the material exits the die.

"calculate Pw, ΔPy, Pe"

Different pressure components were calculated.

"calculate ΔP"

Pressure difference acting on the cell wall was calculated.

"check point 1" (Nucleation?)

If nucleation did not take place, there was no change in temperature, moisture, bubble radius etc. and next time step was computed. If the melt has not exited the die, pressure drop is computed again.

"check point 2" (die exit?)

Once nucleation takes place, stabilizing time step (Δt) is computed. If the melt has still not exited the die, next time step is computed and the loop goes back to calculating pressure drop. If after, increment of distance (x) in the die, the melt exits the die, then domain radius, diffusivity, consistency index, Pw, ΔPy, Pe, ΔP (change in pressure) is computed. Stabilizing time step is computed and based on all these values, change in radius and temperature is computed.

"check point 3" ($T > T_g + 30$)

If the temperature is less than ($T_g + 30$), then the process ends, since the melt solidifies. In the beginning, the temperature is higher than ($T_g + 30$) and change in moisture content of microscopic shells is computed. Other parameters such as open cell fraction, expansion ratio are also computed.

"check point 4" ($X_{wa} > 0$)

If the average moisture content of the microscopic shells is less than 0, then the process ends, otherwise, change in macroscopic moisture is calculated and new values of moisture content in different macroscopic shells is calculated by subtracting the loss in moisture content from each shell.

It should be noted that temperature used to compute the parameters in microscopic and macroscopic model is same, thereby, integrating the microscopic and macroscopic levels.

The average loss is moisture of the macroscopic shells is also computed and it is divided by number of microscopic shells (say, Xratio). Time step is incremented and new values of bubble radius (add or subtract change in radius depending on expansion or shrinkage phase), moisture in microscopic shells is calculated. For calculating the moisture in microscopic shells, first the change in moisture from each microscopic layer is subtracted from the previous value and then X ratio is subtracted to integrate the loss in moisture in the macroscopic model with the moisture in microscopic model. Hence the two levels, microscopic and macroscopic, are integrated by values of moisture and temperature.

"Check point 5" (R<0)

If bubble radius is less than 0, then the process ends, otherwise, the process is looped back to another check point.

"Check point 6" (Die exit?)

If the material has not exited the die, then pressure drop is calculated. If the material has exited the die, the fluid pressure outside the domain becomes atmospheric pressure and code is directed to calculation of properties like diffusivity, consistency index, domain radius etc. Hence, the complete simulation takes place.

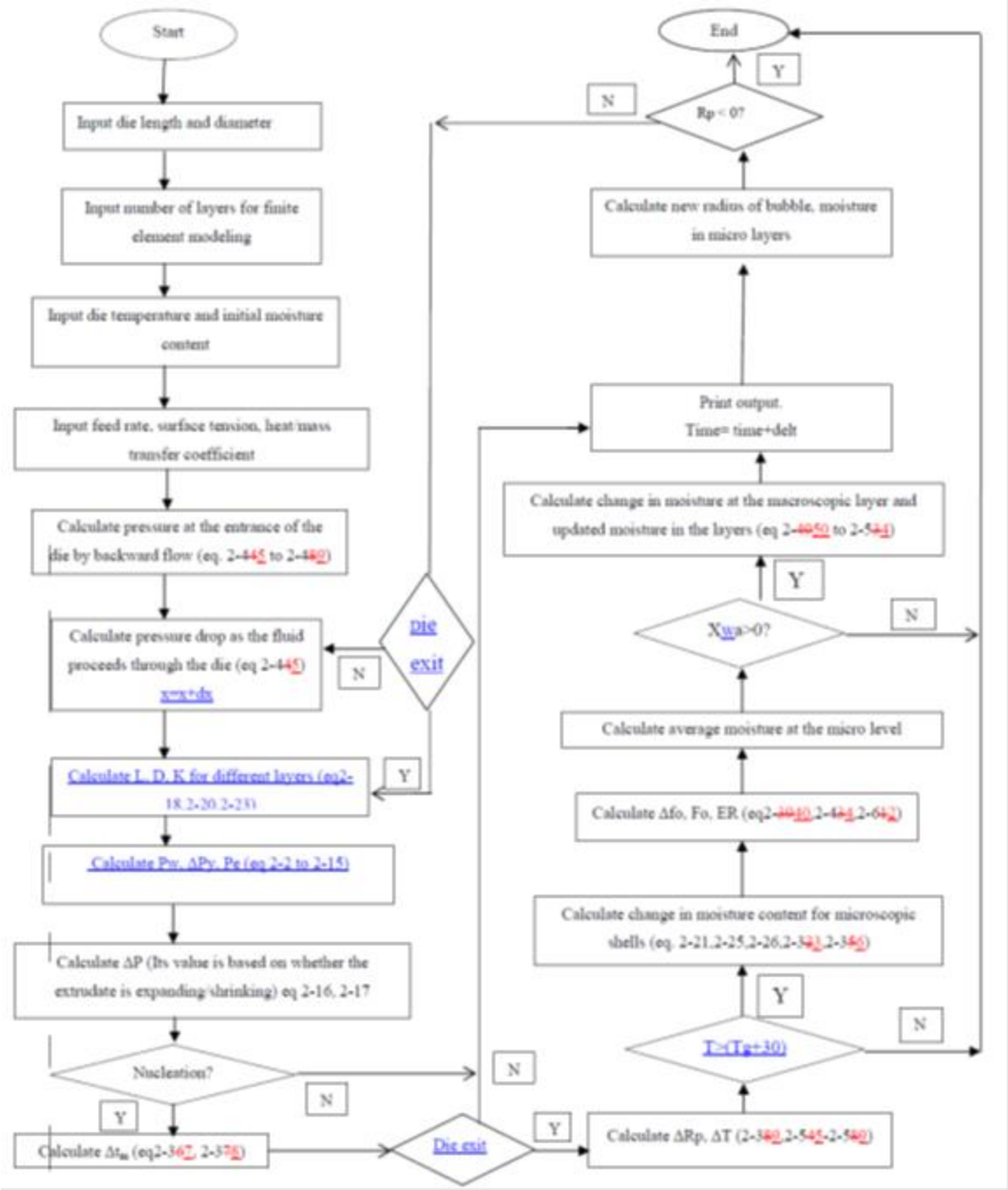

Figure C-1 Algorithm of the mechanistic model

Explanation of the stochastic algorithm

The stochastic model inputs a distribution of selected 3 inputs and generates the output as a distribution.

1) Firstly, values of die temperature and moisture content as recorded using DAQ (~400 data points) are input in the model. An average and standard deviation of these values is computed. A coefficient of variation of 2% and average value of 1 is assumed for the third parameter (material constant in consistency index equation) which results in a standard deviation of 0.02 for the third parameter.

2) Based on the average and standard deviation values of these three parameters, random numbers are generated by the code using the NORMINV function in excel. NORMINV function generates random numbers from a normal distribution which has an average and standard deviation as computed in the previous step.

3) Say, 30 random values of each of these 3 parameters is generated from the above step. First value of each of these parameters, along with the other parameters that are kept constant (as specified in the table in Appendix B) is fed into the mechanistic model and an output value for expansion ratio is simulated from the mechanistic model. Eventually, all 30 values of these 3 parameters are fed into the mechanistic model which results in 30 different outputs. Hence, the distribution of output is obtained.

Check point 1 “n input values taken?”

If the n values (30 here) are already input in the model, then the code stops. Otherwise, the code is looped back to the beginning of the mechanistic model and next set of values of the 3 parameters along with fixed parameters is input into the mechanistic model.

Sample Calculations of the mechanistic model

For moisture content = 0.2297, Initial temperature = 405.0985

1) Get all initial values and values of other parameters.

N_b = 6, N = 50, P_s = 101.325 KPa, m_f= 0.00729 kg/s, mc = 0.2297 g water/ g dry matter, T_o= 405.09K, R_o= 50 μm, $\sigma=2*10^{-6}$ kN/m, $d_{en}=1.7*10^{-2}$ m, $d_{ex}=4.2*10^{-3}$ m, $L_d=1.46*10^{-2}$ m, $L_{d1}=7.3*10^{-3}$ m, M (=ρ_s/N_{cell})= $5.8*10^{-8}$ Kg, h=10 W/m^2K, n=0.4, Ψ=0.75, k_factor = 1, Dw_factor = 1, E_r = 10 KPa, τ_r=0.1 KPa, β_f=17, ρ_s=1.16 g/cm^3, N_{cell}= 20000 cells/cm^3, $k_{xc}=10^{-5}$

Xwc = Xws = Xi(i) = mc = 0.2297

2) Calculate pressure at the entrance of the die by backward flow.

Using values of input parameters for moisture, temperature etc.

Ks = K_factor * 0.000672 * Exp(4960 / T - 12.1 * mc / (1 + mc)) = 14.57

rhow = ρ = 1000 * (1 + mc) / (0.64 + mc) = 1413.94

d2= 0.0042 (because x<Ld1)

v_x = 4 * m_f / (ρ * 3.14159 * d2 ^ 2) = 0.372

dxd = v_x * Δt = 0.0000372

dPx = dxd * Ks * 4 * ((32 * m_f / (ρ * 3.14159)) ^ n) * (((3 * n + 1) / (4 * n)) ^ n) / d2 ^ (3 * n + 1) = 8.097

P = P + dPx = 101.325+8.097 = 109.424

xd = xd + dxd = 0+0.0000372 = 0.0000372

Hence, the pressure at the entrance of the die is calculated (till xd becomes Ld)

Value of xd and time is reset to 0

3) Calculate pressure drop as the fluid proceeds through the die and calculation of other parameters such as Pw, D, and K.

First calculating the vapor pressure at given moisture and temperature

P_{wsat} = 1002.2 * Exp(9.43699 - 3867.44 / (T - 43.37)) = 285.756

B = -0.5362 - 0.001394 * T + 2.0474 * (468.9 - T) / (477.42 - T) = 0.7053

C = 0.2479 + 0.001216 * T = 0.7405

F = 0.002004 + 0.000003165 * T = 0.0033

G = 0.4561

aw = B * X_{wc} + C * X_{wc} / (F + X_{wc}) = 0.892

$P_w = P_{wsat} * a_w = 254.894$

$\upsilon = G * T / P_w - 0.01637 = 0.7084$

$D = D_{w\_factor} * 0.0000000135 * Exp(-21.61 * (548 - T) * (1.194 + 3.68 * X_{wc}) / (T * (1 + 18.98 * X_{wc}))) = 7.42 * 10^{-10}$

$D_s = D_{w\_factor} * 0.0000000135 * Exp(-21.61 * (548 - T) * (1.194 + 3.68 * X_{ws}) / (T * (1 + 18.98 * X_{ws}))) = 7.42 * 10^{-10}$

$D(i) = D_{w\_factor} * 0.0000000135 * Exp(-21.61 * (548 - T) * (1.194 + 3.68 * X_{wi}) / (T * (1 + 18.98 * X_{wi}))) = 7.42 * 10^{-10}$

$K(i) = K\_factor * 0.000672 * Exp(4960 / T - 12.1 * X_{wi} / (1 + X_{wi})) = 14.57$

$\rho(i) = 1000 / (0.64 + X_{wi}) = 1149.82$

$\epsilon = 1 - 1 / ER = 0$ (since ER = 1 at time step = 1)

$\zeta_r = 1$

$D_{eff} = Dw\_factor * (1 - \epsilon) * (1 / \zeta_r) * 0.0000000135 * Exp(-21.61 * (548 - T) * (1.194 + 3.68 * Cav) / (T * (1 + 18.98 * Cav))) = 7.42 * 10^{-10}$

$Kc = K\_factor * 0.000672 * Exp(4960 / T - 12.1 * X_{wc} / (1 + X_{wc})) = 14.57$

$Ks = K\_factor * 0.000672 * Exp(4960 / T - 12.1 * X_{ws} / (1 + X_{ws})) = 14.57$

$E_b = Er * Exp((300 - T) / 26) = 0.176$

$\tau_r = 0.1$

$E = E_b = 0.176$

$\tau_o = \tau_r = 0.1$

Pressure drop

$d2 = d_{en} - (d_{en} - d_{ex}) * xd / (L_d - L_{d1}) = 0.017$

$v_x = 4 * m_f / (rhow * 3.14159 * d2 \wedge 2) = 0.023$

$dxd = 0.023 * 0.0001 = 0.0000023$

$xd = xd + dxd = 0.0000023$

$dP_f = -dxd * Ks * 4 * ((32 * m_f / (rhow * 3.14159)) \wedge n) * (((3 * n + 1) / (4 * n)) \wedge n) / d2 \wedge (3 * n + 1) = -0.023$

$P_f = P_f + dP_f = 2045.12 - 0.023 = 2045.097$

Hence, the pressure drop is calculated until the exit of the die

4) Calculation of L

L is computed using equation 2-20 by summation of ($\Delta M/\rho_i$) for 50 microscopic shells.(not feasible to compute manually).

5) Calculation of ΔP_y, Pe, ΔP, Δt

Once the value of L is obtained, P_e and ΔP_y is obtained using equation 2-8 and 2-13.

After obtaining the components of pressure, ΔP is computed using equation 2-16..

The rest of the process is as explained in the algorithm

Calculate Δt using equation 2-37 and 2-38.

6) Calculation of ΔR and ΔT

Since all the parameters such as pressure components, Δt, Kc, Ks, R and L are calculated in previous steps, ΔR is calculated using equation 2-39

ΔT is computed using equations 2-56 to 2-61. All the parameters needed are either input values or computed in the previous steps.

If temperature is greater than Tg

7) Calculate change in moisture content of microscopic shells using equations 2-21, 2-25, 2-33 and 2-36 (using parameters computed from the above steps).

8) Calculate open cell fraction using equations 2-40 to 2-44. Calculate expansion ratio using equation 2-64.

If average moisture in microscopic shells >0 then and melt has exited the die,

9) Calculate change in moisture in macroscopic shells using equations 2-50 to 2-55 and update the existing values (by subtraction of the moisture lost).

10) Update the values of all the parameters such as bubble radius (addition or subtraction of the change in radius depending on expansion or shrinkage), moisture in microscopic shells (subtracting the loss in moisture from microscopic shells and average loss in moisture from

macroscopic shells divided by the number of layers in the microscopic shells), open cell fraction (addition of change in open cell fractions) etc.

11) Loop back to check point 6, and then either compute pressure drop first or L, D. K values with the updated values of moisture, temperature, bubble radius etc.